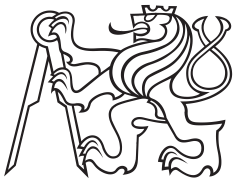

Czech
Technical
University
in Prague

F3

Faculty of Electrical Engineering
Department of Circuit Theory

Bachelor's Thesis

Optical Absorption of Colloidal Mixtures of Nanodiamonds and Metal Nanoparticles

Vendula Hrnčířová

Supervisor: **Ing. Markéta Šlapal Bařinková**
Field of study: **Medical Electronics and Bioinformatics**
Turn-in date: **May 2024**

BACHELOR‘S THESIS ASSIGNMENT

I. Personal and study details

Student's name: **Hrnčířová Vendula** Personal ID number: **507223**

Faculty / Institute: **Faculty of Electrical Engineering**

Department / Institute: **Department of Circuit Theory**

Study program: **Medical Electronics and Bioinformatics**

II. Bachelor’s thesis details

Bachelor’s thesis title in English:

Optical absorption of colloidal mixtures of nanodiamonds and metal nanoparticles

Bachelor’s thesis title in Czech:

Optická absorpce koloidních směsí nanodiamantů a kovových nanočástic

Guidelines:

Nanodiamond and metal nanoparticles are widely investigated for various biomedical applications, from sensors to therapeutics.
1. Familiarize yourself with the literature and prepare a brief summary of the findings and measurement methods for the topic of the thesis.
2. Investigate the concentration dependence of the optical absorption of nanodiamonds with oxygenated and hydrogenated surfaces. Determine the appropriate concentration for use in a mixture with metal nanoparticles.
3. Investigate the dependence of optical absorption on the concentration of metal nanoparticles in a mixture with nanodiamonds. Analyze the effect of the composition of the colloidal mixture on the change in optical absorption.
4. Investigate the dependence of optical absorption on time, discuss the stability of individual colloids and mixtures, determine the appropriate time range for studying optical phenomena.
5. Compare the results for colloidal mixtures with directly synthesized complexes of nanodiamonds with metal nanoparticles.

Bibliography / sources:

[1] Hydrogenation of HPHT nanodiamonds and their nanoscale interaction with chitosan, 10.1016/j.diamond.2023.109754.
[2] Plasmonic Nanodiamonds, 10.1021/acs.nanolett.3c01514.
[3] Nanosilver supported on inert nano-diamond as a direct plasmonic photocatalyst for degradation of methyl blue, 10.1016/j.jece.2020.104912.
[4] Ag/Nanodiamond/g-C3N4 heterostructures with enhanced visible-light photocatalytic performance, 10.1016/j.apsusc.2020.146576.
[5] Nanodiamond/gold nanorod nanocomposites with tunable light-absorptive and local plasmonic properties, 10.1016/j.jiec.2018.04.030

Name and workplace of bachelor's thesis supervisor:

Ing. Markéta Šlapal Bařinková Department of Physics FEE

Name and workplace of second bachelor's thesis supervisor or consultant:

Date of bachelor's thesis assignment: **06.02.2024** Deadline for bachelor thesis submission: **24.05.2024**

Assignment valid until: **21.09.2025**

Ing. Markéta Šlapal Bařinková Supervisor's signature	doc. Ing. Radoslav Bortel, Ph.D. Head of department's signature	prof. Mgr. Petr Páta, Ph.D. Dean's signature

III. Assignment receipt

The student acknowledges that the bachelor's thesis is an individual work. The student must produce her thesis without the assistance of others, with the exception of provided consultations. Within the bachelor's thesis, the author must state the names of consultants and include a list of references.

.	
Date of assignment receipt	Student's signature

Acknowledgements

First and foremost, I would like to thank my supervisor, Ing. Markéta Šlapal Bařinková, for her guidance and support throughout this entire work. Her patience, understanding, and kindness were invaluable. I also thank Prof. RNDr. Bohuslav Rezek, Ph.D., David Rutherford, Ph.D., and Ing. Kateřina Kolářová, Ph.D. for their help and insightful advice during this work. I am grateful to my family and loved ones for their support and the joy they bring into my life every day.

Declaration

I declare that the presented work was developed independently by me and that I have listed all used sources of information within it in accordance with the Methodical instructions for observing the ethical principles in the preparation of university theses.

In Prague, on _____

_____
Signature

Abstract

Nanodiamonds (NDs) and metal nanoparticles (NPs) are widely investigated for their diverse applications ranging from biomedicine to industry. NPs possess unique attributes compared to their bulk counterparts, including a high surface area to volume ratio, optoelectronic properties and their impact on living organisms. Further enhancements of NP properties can be achieved through creating nanocomposites containing various NP types. However, controlling their final size, distribution, and stability remains challenging. In this thesis, colloidal mixtures of 50 nm surface modified NDs (hydrogenated nanodiamonds (HNDs) and oxidized nanodiamonds (ONDs)) and 20 nm plasmonic metal NPs (silver nanoparticles (AgNPs) and gold nanoparticles (AuNPs)) were studied as an alternative to the difficult to synthesize nanocomposites. The optical properties were investigated through spectrophotometry, supplemented by zeta potential (ZP) measurements for determining stability, and dynamic light scattering (DLS) along with imaging methods including scanning electron microscopy (SEM) and transmission electron microscopy (TEM) for observing morphologies. Prior to the investigation of the colloidal mixtures, individual NP colloids of multiple concentrations were characterized to determine the appropriate ratio in the mixtures and to examine their properties, which could affect the colloidal mixture. The outcome was the determination of the location of the plasmonic peaks of metal NPs induced by localized surfaced plasmon resonance (LSPR), the poor stability of the HND colloid over time, and the undetectable colour centres in either type of ND. A concentration of 25 μg/ml of both types of NDs was chosen for use in colloidal mixtures with four concentrations of each metal NP. The optical absorption of these colloidal mixtures (AuHNDs, AgHNDs, AuONDs, and AgONDs) was studied immediately after preparation to exclude the influence of agglomeration over time. In the absorption spectrum and SEM images, the presence of nanocomplexes formed by NDs and metal NPs was manifested in all four colloidal mixtures across all concentrations. Furthermore, a phenomenon of the plasmonic peak magnitude depending on the type and concentration of metal NP in the colloidal mixtures was observed. Based on the conducted measurements, a plasmonic model for this phenomenon is presented with charge transfer between the particles, polarization of particles, and mutual interference of electromagnetic fields induced by LSPR. Colloidal mixtures were further compared with directly synthesized nanocomposites (HNDs-Chit-Ag and ONDs-PVP-Ag). This comparison showed the benefits of using colloidal mixtures over nanocomposites, particularly in controlling the size, distribution and shape of particles within nanocomplexes. The results of this thesis show the benefits of creating colloidal mixtures for tuning particle properties. Even so, more research is necessary to gain a deeper understanding of the processes taking place in these colloidal mixtures.

Keywords: surface modified nanodiamonds, plasmonic metal nanoparticles, nanocomplexes, colloidal mixtures, optical absorption

Abstrakt

Nanodiamanty a kovové nanočástice jsou široce zkoumány pro své různorodé uplatnění od biomedicíny až po průmysl. Nanočástice mají unikátní vlastnosti ve srovnání s jejich většími protějšky, včetně velkého poměru plochy k objemu, optoelektrických schopností nebo jejich vlivu na živé organismy. Dalšího vylepšení vlastností nanočástic lze dosáhnout vytvořením nanokompozitů obsahujících různé typy nanočástic. Stále však zůstává velkou výzvou kontrola jejich finální velikosti, distribuce a stability. V této práci byly zkoumány koloidní směsi 50 nm povrchově upravených nanodiamantů (hydrogenovaných (HND) a oxidovaných (OND)) a 20 nm plazmonických kovových nanočástic stříbra (AgNP) a zlata (AuNP) jako alternativa k obtížně syntetizovaným nanokompozitům. Jejich optické vlastnosti byly analyzovány pomocí spektrofotometrie, doplněné měřením zeta potenciálu (ZP) pro stanovení stability a měřením dynamického rozptylu světla (DLS), spolu se zobrazovacími metodami včetně rastrovací elektronové mikroskopie (SEM) a transmisní elektronové mikroskopie (TEM) pro pozorování morfologie. Nejdříve byly charakterizovány samotné koloidy nanočástic při různých koncentrací, aby se určil vhodný poměr ve směsi a aby se zhodnotily jejich vlastnosti, které by následně mohly ovlivnit koloidní směsi. Byla zjištěna poloha plazmonických vrcholů kovových nanočástic vyvolaných lokalizovanou povrchovou plazmonickou rezonancí (LSPR), slabá stabilita HND koloidu v čase a nedetekovatelná přítomnost barevných center v obou typech nanodiamantu. Byla zvolena koncentrace 25 μg/ml pro oba druhy nanodiamantů, které byly smíchány se čtyřmi různými koncentracemi kovových nanočástic pro vytvoření koloidních směsí. Optická absorpce těchto směsí (AuHND, AgHND, AuOND a AgOND) byla zkoumána bezprostředně po přípravě, aby se předešlo vlivu aglomerace částic. Absorpční spektra napříč koncentracemi spolu se snímky ze SEM ukázaly přítomnost nanokomplexů tvořených kovovými nanočásticemi a nanodiamanty ve všech čtyřech koloidních směsích. Dále byl pozorován jev, kdy docházelo ke změně velikosti plazmonického vrcholu v závislosti na koncentraci a typu kovových nanočástic v koloidní směsi. Na základě provedených měření, byl představen plazmonický model tohoto jevu, zahrnující přenos náboje mezi částicemi, polarizaci částic a vzájemnou interferenci elektromagnetických polí vzniklých při LSPR. Koloidní směsi byly dále porovnány s přímo syntetizovanými nanokompozity (HND-Chit-Ag a OND-PVP-Ag). Toto srovnání ukázalo výhody koloidních směsí oproti nanokompozitům, zejména při kontrole velikosti, distribuce a tvaru částic v komplexech. Výsledky této práce ukazují přínosy koloidních směsí v úpravě vlastností nanočástic. Přesto je potřeba dalšího výzkumu k lepšímu porozumnění procesům probíhajícím v těchto koloidních směsí.

Klíčová slova: povrchově upravené nanodiamanty, plazmonické kovové nanočástice, nanokomplexy, koloidní směsi, optická absorpce

Contents

Figures

Tables

Glossary

AgHND	colloidal mixture of silver nanoparticles and hydrogenated nanodiamond
AgNP	silver nanoparticle
AgOND	colloidal mixture of silver nanoparticles and oxidized nanodiamond
AuHND	colloidal mixture of gold nanoparticles and hydrogenated nanodiamond
AuNP	gold nanoparticle
AuOND	colloidal mixture of gold nanoparticles and oxidized nanodiamond
BSEs	backscattered electrons
DLS	dynamic light scattering
HND	hydrogenated nanodiamond
HNDs-Chit-Ag	hydrogenated nanodiamonds supported by chitosan and decorated with silver nanoparticles
HPHT	high pressure high temperature
LSPR	localized surfaced plasmon resonance
MSY	monocrystalline synthetic diamond powder
ND	nanodiamond
NP	nanoparticle
NV	nitrogen vacancy
OD	optical density
OND	oxidized nanodiamond
ONDs-PVP-Ag	oxidized nanodiamonds supported by polyvinylpyrrolidone and decorated with silver nanoparticles
PVP	polyvinylpyrrolidone
SEM	scanning electron microscopy
SEs	secondary electrons
TEM	transmission electron microscopy
UV	ultraviolet
VIS	visible light
ZP	zeta potential

Chapter 1
Introduction

1.1 Motivation

Today, nanodiamonds (NDs) and metal nanoparticles (NPs) are widely investigated for their diverse range of applications from biomedicine to industry. Generally, nanoparticles (NPs) possess unique properties compared to their bulk counterparts, attributed to their size and high surface area to volume ratio. Metal NPs are renowned for their plasmonic properties, while nanodiamonds (NDs) are praised for their exceptional mechanical properties, biocompatibility and fluorescent capabilities. Consequently, their great individual potential leads to an exploration of synergies between both types of nanomaterials to enhance their properties and meet the demand for new applications in the areas of biosensors, biomedicine, catalysis, space engineering, or energy harvesting. The properties of nanoparticles are influenced by many factors including nanoparticle size, shape, stability, distribution, local environment, surface chemistry, and synthesis. Nanocomposites comprising at least two NPs are synthesized through various methods. However, achieving precise control over nanoparticle size, distribution, and stability, remains a challenge, thereby impacting their properties.

1.2 Goals

The objectives of this work, following the thesis assignment, are as follows:

1. Becoming familiar with the literature and the preparation of a brief summary of the findings and measurement methods for the topic of the thesis.
2. Investigating the concentration dependence of the optical absorption of nanodiamonds with oxygenated and hydrogenated surfaces. Determining the appropriate concentration for use in a mixture with metal nanoparticles.
3. Investigating the dependence of optical absorption on the concentration of metal nanoparticles in mixtures with nanodiamonds. Analysing the effect of the composition of the colloidal mixture on the change in optical absorption.
4. Investigating the dependence of optical absorption on time, discussing the stability of individual colloids and mixtures, and determining the appropriate time range for studying optical phenomena.

5. Comparing the results for colloidal mixtures with directly synthesized composites of nanodiamonds with metal nanoparticles.

Additionally, the potential formation of nanocomplexes within the colloidal mixtures of NDs and metal NPs will be investigated through their optical absorption and supported by other characterization methods to understand possible interactions between particles.

1.3 Thesis Structure

This work is divided into three parts. Part one summarizes fundamental knowledge concerning nanodiamonds (NDs) and metal nanoparticles (NPs), along with the theory behind characterization methods used for experiments. Part two provides information on materials used for experiments and employed methodology in this work. In part three, results of the experiments are provided and discussed along with the thesis conclusion. The result part has three sections as follows:

- Characterization of Colloids of Nanodiamonds and Metal Nanoparticles
- Investigation of Colloidal Mixtures of Nanodiamonds and Metal Nanoparticles
- Comparison of Colloidal Mixtures and Directly Synthesized Nanocomposites

1.4 Authorship Contribution

This thesis was written by Vendula Hrnčířová under the supervision of Ing. Markéta Šlapal Bařinková. Vendula Hrnčířová also conducted data analysis and visualisation. The partial results were consulted with Ing. Markéta Šlapal Bařinková, prof. RNDr. Bohuslav Rezek, Ph.D., and David Rutherford, Ph.D., who offered their interpretations, proposed next steps, reviewed the thesis with suggestions for improvement, and ensured language and stylistics coherence.

The optical experiments were executed by Vendula Hrnčířová with assistance from Ing. Markéta Šlapal Bařinková. Measurements of ZP and DLS were performed by Vendula Hrnčířová at the Institute of Physics of the Czech Academy of Science under the supervision of Ing. Kateřina Kolářová, Ph.D. Doctor Kolářová also prepared the colloids of HNDs, ONDs, HNDs-Chit-Ag, and ONDs-PVP-Ag, and provided TEM images of the directly synthesized nanocomposites. The dilution series of samples and the preparation of colloidal mixtures were performed by Vendula Hrnčířová. Samples were observed through SEM by Vendula Hrnčířová and Ing. Markéta Šlapal Bařinková. Ing. Markéta Šlapal Bařinková provided the final images and did digital image processing.

Part I

Theoretical Background

This part provides fundamental information about nanoparticles (NPs) (Chapter 2), with particular emphasis on nanodiamonds (NDs) (Chapter 4), metal NPs (Chapter 3) and their interactions (Chapter 5). Methods for characterizing NPs are introduced and explained in Chapter 6, to clarify the rationale behind the experiments conducted. NP utilization, structural attributes, potential modifications and properties are discussed with a focus on optical properties, which constitute the central theme of this thesis.

Chapter 2
Nanoparticles

Nanoparticles (NPs) are materials characterized by dimensions ranging from 1 to 100 nm in size in at least two dimensions. NPs have existed naturally on our planet for millions of years. In addition to naturally occurring NPs, mankind has learned to synthesize new ones.[1] The concept of nanotechnology was introduced by Nobel laureate Richard Feynman in 1959,[2] who stated in one of his lectures that *"there is plenty of room at the bottom"*.[3] The field has since then undergone significant development and NPs are now employed in various applications. The great interest in nanotechnology has been motivated by the unique properties that emerge from the nanoscale sizes, along with the potential of NPs to revolutionize various fields.

The properties of NPs are influenced by many factors. In general, NPs boast a high surface area along with their nanoscale size, giving them unique properties in contrast to their bulk counterparts. Their characteristics can be further modified by changes in size, shape, composition or using surface modifications. These attributes can then help us classify NPs. Based on their composition, NPs can be divided into groups such as carbon-based, inorganic-based (including metal-based or metal oxide-based), organic/polymer-based or composite-based.[4] Representing the inorganic-based nanoparticles, metal NPs, are presented in Chapter 3, followed by carbon-based NDs, introduced in Chapter 4. Furthermore, NPs can be synthesized into various shapes including nanoshells, nanorods, nanoneedles, nanospheres, nanocubes or nanoplates,[5] a schematic of which can be seen in Figure 2.1.

Today, NPs are a part of everyday life, present for example in textiles, cosmetics, medicine, and consumer products.[4] However, this upswing in their use also leads to a higher release of NPs into the environment, polluting the air, water, and soil and disrupting the balance of nature. Highly hazardous are heavy metal NPs like lead or mercury, which are more stable than their bulk form, making their degradation process more difficult and causing severe damage to the environment.[2] Moreover, NPs can enter living organisms unnoticed through ingestion, inhalation or even through the skin or cellular membranes due to their size. Once inside the body, they can have

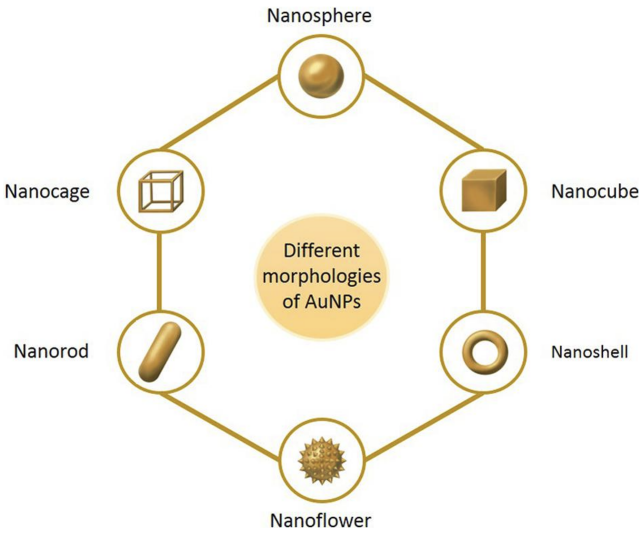

Figure 2.1: Various morphologies of NPs.[6]

unintended toxic effects such as producing oxidative stress radicals, damaging DNA or causing inflammatory responses, and even cell death. Biocompatibility and toxicity are strongly linked to size, shape, size distribution, surface area, surface chemistry, solubility, aggregation, local environment and more factors.[1,4,7] Therefore, it is crucial to master the synthesis and characterization of NPs, especially for biomedical usage. To tailor ideal NPs for specific applications, many methods of synthesis have been developed.

2.1 Nanoparticle Synthesis

Two primary approaches for NP synthesis are bottom-up and top-down, as seen in Figure 2.2. This is key, as the chosen synthesis approach and methodology influence the properties of NPs. A top-down synthesis is a destructive approach wherein bulk materials are disassembled into smaller units. This decomposition is achieved through various techniques such as mechanical milling, chemical etching, sputtering, laser ablation or electro-explosion. Bottom-up synthesis, in contrast, is based on a constructive approach, wherein NPs are formed from simpler substances such as molecules or atoms. Methods utilizing this approach include spinning, chemical vapor deposition, molecular condensation, laser pyrolysis, and sol-gel processes.[2]

Great potential lies in green synthesis which is an alternative to conventional methods for producing NPs. This approach offers many advantages such as being environmentally benign, cost-effective, energy-efficient, and relatively simple to execute. Such "green" NPs have been produced using various bio-reductants mixed with metallic salt solutions, thereby inducing a redox reaction. Both silver nanoparticles (AgNPs) and gold nanoparticles (AuNPs) can be prepared via this method. Reductants derived from yeast, fungi, bacteria, algae, and mainly plant extracts serve as reducing agents.[5] Green synthesis can also contribute to improved properties of NPs such as photocatalytic activity.[8]

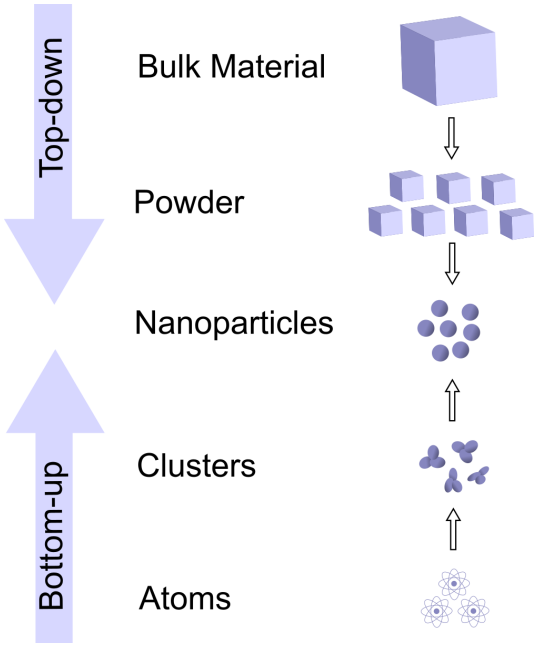

Figure 2.2: Top-down and bottom-up synthesis diagram.

2.2 Colloidal Nanoparticles

It is important to note that the properties of NPs are affected by their surroundings. For many applications, it is beneficial to have NPs in a liquid phase. For insoluble particles, such a suspension is called a colloid. The properties of colloidal nanoparticles may vary based on their local environment, and conversely, their surroundings can be influenced by the presence of the NPs. These alterations in properties, such as charge, stability or hydrophobicity, are primarily caused by surface interactions of NPs. The capacity to manipulate the characteristics of both NPs and their environment opens the way for novel innovative applications.[9]

The behaviour of NPs in colloids depends on the net interaction energy of these particles. Sufficient electrical charge causes electrostatic repulsion between particles, forcing them apart and forming a uniformly distributed colloid, while van der Waals forces counteract this repulsion. Conversely, neutrally charged NPs tend to aggregate forming large clusters under the gravitational force. To prevent aggregation, electrostatic stabilization or steric stabilization techniques can be employed.[10] Additionally, the presence of salts in the liquid phase of the colloid has aggregatory effects on nanoparticles, as it screens the charge on the surface of NPs, leading to instability.[9] Ultrasonication, employing high-frequency waves (in the kHz range), is frequently utilized to disrupt the suspended NPs and enhance colloidal stability.[11]

Chapter 3

Metal Nanoparticles

Metal nanoparticles are widely used in both biomedicine and industry. Classified as inorganic-based nanoparticles, metal NPs are made purely of metal precursors.[2] Commonly used metal NPs include aluminium, silver, gold, zinc, lead, iron, cadmium, and copper.[4] Owing to their surface chemistry, metal NPs can be modified to conjugate with various chemicals such as ligands, proteins, antibodies, and drugs. Biomedical applications, such as drug delivery, require a focus on the biocompatibility and nontoxicity of these materials.[3]

Metal NPs exhibit unique size- and shape-dependent optoelectrical properties, attributed to their localized surfaced plasmon resonance (LSPR), as discussed further in Section 3.1. Alkali and noble metals display broad absorption bands in the visible light (VIS) region of the electromagnetic spectrum. Moreover, metal NPs show potential for cancer diagnosis and therapy due to their LSPR enhanced light scattering and absorption. Additionally, metal NPs possess good thermal conductivity.[2] Leveraging their optical properties, metal NPs are employed in various imaging techniques such as magnetic resonance imaging (MRI), computed tomography (CT), positron emission tomography (PET), surface-enhanced Raman spectroscopy (SERS), and ultrasound as imaging probes.[3] Moreover, metal NPs are present in electronics, sensors, and photonic materials.[2] Possible catalytic usage of metal NPs has been investigated in recent years as well.[10]

Silver nanoparticles (AgNPs) and gold nanoparticles (AuNPs) are widely applied in the biomedical field. Therefore, they have been selected for our experiments and they will be discussed in the following Sections 3.2 and 3.3, respectively.

3.1 Localized Surface Plasmon Resonance

As previously mentioned, noble metal NPs, such as AgNPs and AgNPs, exhibit a distinct UV-VIS extinction band, that is not present in the absorption spectrum of their bulk counterparts. This phenomenon occurs when the frequency of an interacting light particle, photon, aligns with the collective excitation of the conduction electrons of the NPs, known as localized surfaced plasmon resonance (LSPR),[2,12] as illustrated in Figure 3.1. The displacement of the electrons relative to their nuclei induces a Coulombic restoring force, causing oscillation of the electron cloud (as shown in Figure 3.1 in violet) within the nuclear framework.[12] LSPR oscillations are characterized by coherent and collective spatial behaviour.[7] LSPR excitation leads to the selective absorption of a certain wavelength and amplifies local

electromagnetic fields near the surface of NPs.[2] The extinction cross-section, which can dramatically exceed the geometrical size of particles, is primarily influenced by absorption for small particles, smaller than 30 nm, while scattering becomes predominant for larger particles.[13]

The peak wavelength is dependent on the size, shape, distribution, surface functionalization, aggregation state, dielectric properties of NPs, and properties of local environment.[2,7,13] Due to the sensitivity of the LSPR frequency and near-field enhancement, LSPR is widely employed for detecting molecular interactions near the surface of the NPs.

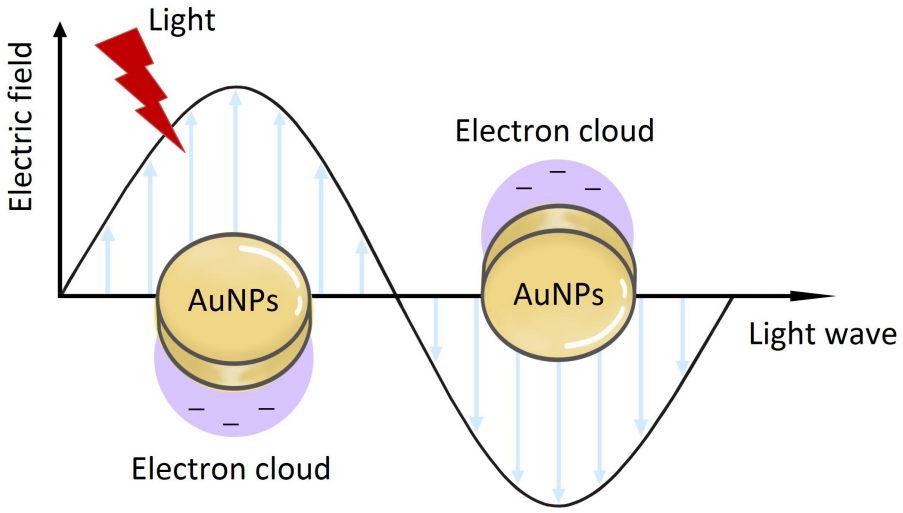

Figure 3.1: Localized surface plasmon resonance (LSPR) principle[6]

The electron oscillation has finite lifetimes, followed by excited plasmon decay, which can be either radiative or nonradiative. The mechanism of LSPR relaxation is illustrated in Figure 3.2.[14] LSPR spectroscopy can thus provide thermodynamic and real-time kinetic data of binding processes.[7] Enhancement of the local electromagnetic field strengthens Raman scattering, infrared absorption, and the local refractive index. Hot electron transfer from non-radiative relaxation enables charge carriers with sufficient energy to initiate external chemical processes, such as enzyme-like activity and radiosensing. Plasmons can convert absorbed light into heat by generating hot electrons, which subsequently relax and increase the temperature of the medium. This phenomenon is utilized in photothermal therapy and wound healing. Plasmonic NPs can act as electron donors to molecular oxygen, leading to the formation of radicals. Radicals can contribute to cell death, which shows the antimicrobial potential of plasmonic NPs. Plasmon resonance energy transfer (PRET) involves non-radiative decay, where the resonant energy is transferred from the metal to the adjacent fluorophores, affecting their optical properties. The remarkable properties of plasmonic metal NPs make them extensively researched and employed in imaging, sensing, labelling, drug delivery and tissue engineering.[14]

In addition to LSPR, propagation surface plasmon resonance (PSPR) also exists, occurring on metal thin films and propagating along the metal surface for distances up to hundreds of micrometres.[14]

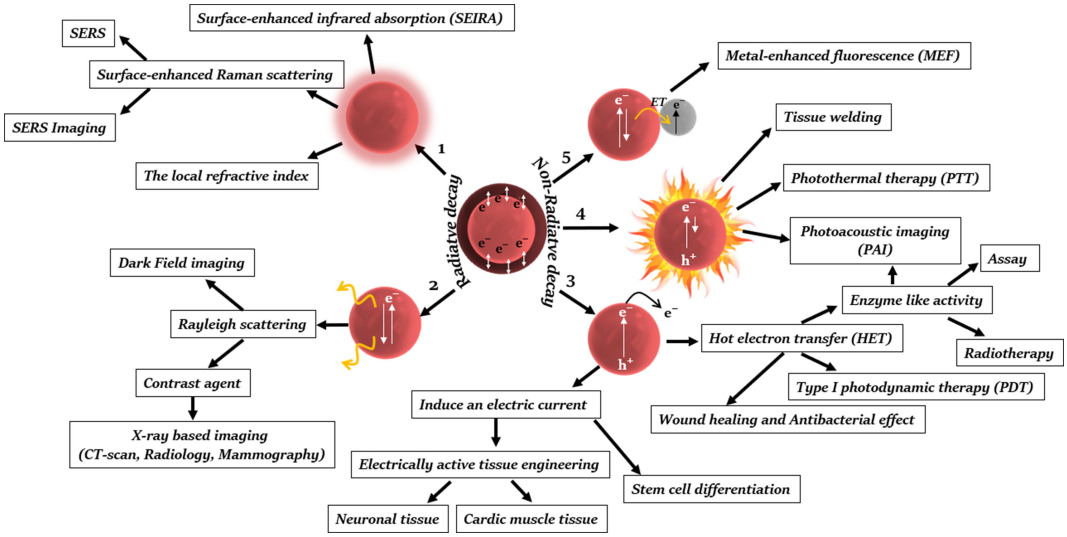

Figure 3.2: Mechanisms of localized surfaced plasmon resonance (LSPR) relaxation. (1) radiative decay by electromagnetic-field enhancement, (2) radiative decay by light scattering, (3) non-radiative decay by hole-hot electron pair, (4) non-radiative decay by plasmonic heating, and (5) non-radiative decay by plasmon resonance energy transfer (PRET).[14]

3.2 Silver Nanoparticles

In recent years, silver nanoparticles (AgNPs) have emerged as one of the most used metallic nanoparticles across various fields, including device coating, optical sensors, cosmetics, drug delivery, cancer therapy, food industry, textiles, antibacterial applications, and many more. AgNPs can be synthesized using conventional physical, chemical, and biological methods. The chosen method of synthesis influences the particle properties.[7] Typically, AgNPs are synthesized through the reduction of a silver salt with a reducing agent in the presence of a colloid stabilizer such as polyvinyl alcohol, citrate or cellulose.[3]

AgNPs possess plasmonic properties with a plasmonic peak around 400 nm.[15] The biological activity of AgNPs is influenced by several factors including size, shape, and surface charge, which can render them both beneficial and dangerous. Smaller particles, with their larger surface area to volume ratio, may exhibit increased toxicity compared to larger ones. Additionally, positively surface charged AgNPs have been observed to remain in the bloodstream longer than negatively charged ones. Due to their antibacterial activity, AgNPs are being explored as an alternative to antibiotics,[7] as AgNPs may cause denaturation of RNA and DNA replication leading to cell death. However, bacteria resistant against AgNPs have been reported in recent years.[15] Apart from their antibacterial effects, AgNPs demonstrate antifungal, antiviral, anti-inflammatory, anti-cancer, and anti-angiogenic properties.[7,15] Moreover, studies suggest that AgNPs may be effective in treating wounds. With their plasmonic properties and large effective scattering cross-section, AgNPs are also good candidates for molecular labelling.[3]

3.3 Gold Nanoparticles

Another widely used metal NP is gold (AuNPs). Its plasmonic peak is usually located around 520 nm in the absorption spectrum, within the VIS region. The synthesis of AuNPs typically involves the chemical reduction of gold salts using reducing agents such as citrate,[3] but they can also be prepared via environmentally sustainable green synthesis methods.[16]

AuNPs are considered the most stable among noble NPs and can be prepared in various shapes and sizes, which influences their properties. Their high chemical and physical stability renders them highly biocompatible.[6] Similar to AgNPs, AuNPs possess a high surface area to volume ratio, allowing for the conjugation of their surface with ligands such as oligonucleotides, proteins, drugs, dyes and antibodies containing functional groups, making them promising agents for drug and gene delivery.[3,6] Due to their optical properties, AuNPs find applications in biological imaging, electronics, photothermal therapy, and material science.[3] AuNPs are capable of converting light energy into heat, inducing cellular apoptosis and thus showing potential in cancer treatment.[17] Additionally, AuNPs exhibit antimicrobial, antioxidant, and anticancer activities.[6] However, they also demonstrate some toxicity attributed to their physiochemical properties, which may be decreased by introducing functional groups to their surface.[6,17]

Chapter 4

Nanodiamonds

Nanodiamonds (NDs) are carbon-based nanoparticles derived from a crystal allotrope of carbon, alongside other carbon nanomaterials like fullerene, graphene, and carbon nanotubes or fibres.[18] Despite their common carbon base, each type possesses distinct properties and is thus fit for diverse applications. NDs inherit some of the properties of diamond bulk form and gain new unique attributes stemming from their nanoscale dimensions and large surface area. Notably, they demonstrate exceptional mechanical properties, high biocompatibility, stable fluorescence, and low toxicity.[19] As a result, NDs find use across many fields such as electronics, photovoltaics, energy storage, electrochemical sensors, automotive industry, beauty products, biomedicine, and for serving diagnostic and therapeutic purposes.[20]

Given their versatility, extensive research explores their properties, especially their usage in combination with other substances, looking for a synergy of materials. Various synthesis methods yield NDs with diverse morphologies, sizes, polarity, electric conductivity, and surface chemistry, further expanding their potential applications.

4.1 Nanodiamond Structure

In the core, carbon atoms are mostly sp^3 hybridized, akin to bulk diamonds, forming a rigid structure with tetrahedral symmetry, where each carbon atom is covalently bound to four others.[21,22] A high chemical inertness, extreme hardness and possible formation of nitrogen vacancy (NV) centres are attributed to the core structure.[21]

The surface of the NDs is still not fully explored, with several potential models. Due to the need to terminate the bonds, the surface of NDs enables broad surface chemistry modification. Termination can be achieved by various molecules such as hydrogen, oxygen or sp^2 carbon (or other types of carbon phases), or functional groups, which can be utilized to control colloidal and optoelectric properties.[21–23] For example, the stability of NDs is significantly influenced by presence of sp^2 carbon.[24] An example of an ND surface with various functional groups can be seen in Figure 4.1. More information about surface modifications is provided in Section 4.3. Additionally, the doping of NDs with elements such as boron, nitrogen, or tritium can further alter their properties, enhancing features like electrical conductivity or photoluminescence.[20] The shape and size of NDs vary depending on the synthesis method and the specific conditions under which they are formed.

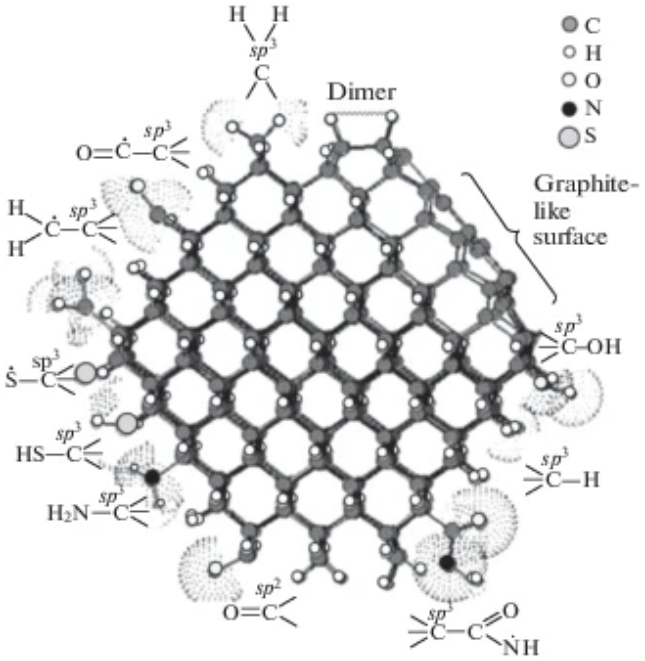

Figure 4.1: The surface of a ND with various functional groups.[25]

4.2 Nanodiamond Synthesis

Diamonds can be formed naturally when high pressure and temperature are applied to carbon-containing fluids deep within the Earth for millions of years or during massive explosions such as volcanic activity or meteorite impact. Alternatively, diamonds can be produced artificially through various synthesis methods, each of which can influence their final properties. Common methods include detonation synthesis, laser ablation, high pressure high temperature (HPHT) synthesis, and chemical vapour deposition.[20] These methods may be seen in the carbon phase diagram in Figure 4.2. The first NDs were discovered in the 1960s in the USSR using detonation techniques and since then the technology of synthesis has developed to better control the shape and size of NDs.[24] For the experiments conducted in this thesis, NDs were prepared using the HPHT method. A brief description of this technique follows.

The HPHT method mirrors the natural processes of ND formation by simulating the high-pressure, high-temperature conditions found deep within the Earth, where the carbon lattice is constructed from pristine carbon precursors. The type, purity and crystallinity of these carbon precursors influence the properties of the resulting NDs.[19]

Today, the HPHT method with a top-down approach typically involves pressures around 5-6 GPa and temperatures ranging from 1300-1500°C, although specific values may vary and directly impact the properties of NDs.[19] Microcrystals produced through the HPHT method are mechanically ground to achieve nanoscale particles, typically through ball milling. However, this process may introduce some impurities

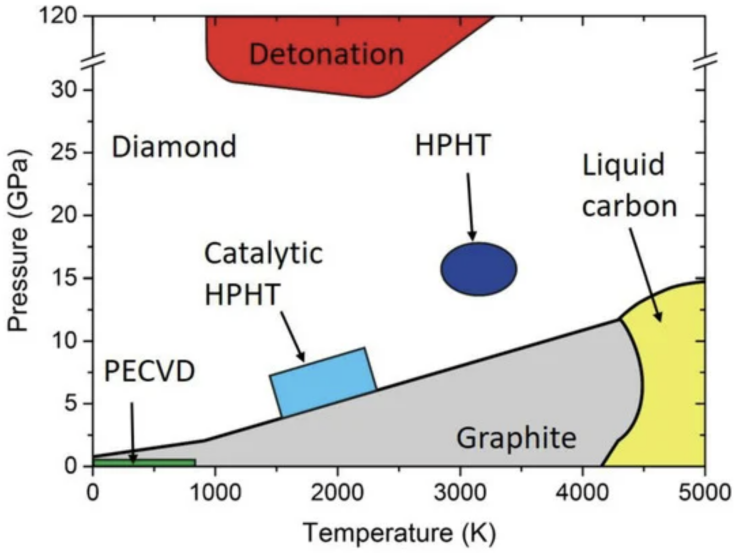

Figure 4.2: Carbon phase diagram with ND synthesis examples.[26] Displayed carbon phases are graphite (grey), liquid (yellow), and diamond (white). Presented synthesis methods are detonation (red), high pressure high temperature (HPHT) and catalytic HPHT (blue and azure, respectively), and plasma enhanced chemical vapour deposition (PECVD) (green).

to the NDs, necessitating subsequent cleaning steps.[27] The bottom-up approach for HPHT NDs requires different pressure and temperature conditions, as well as different precursors, such as halogenated adamantane.[28]

Advances in HPHT synthesis have led to NDs with enhanced toughness, wear-resistence and thermal stability.[19] One of their main advantages over detonation NDs is the uniform structure with a low concentration of lattice defects such as dislocations or twinning.[27,29] Moreover, for their monocrystalline structure and large size, HPHT NDs can be nearly completely purified from the sp^2-C bonds.[30]

The size of NDs strongly influences their properties. However, there is currently a lack of precise size control during HPHT synthesis and size separation, leading to wide size distributions.[27] Commercial HPHT ND powders can contain particles as small as 10 nm. In contrast, detonation NDs typically have a narrower size distribution with their minimum size being even smaller.[21] Ongoing developments primarily focus on producing particles with sizes smaller than 5 nm and controlling aggregation, surface chemistry, size distribution and the presence of optical centres.[21,24]

4.3 Surface Modifications of Nanodiamonds

Modification of ND surfaces can enhance their properties and tailor them for specific applications. Prior to implementing more complex chemical functionalities, it is often advantageous to modify the surface through processes of hydrogenation or oxidation, which can adjust many properties. Precise control over surface chemistry can be achieved when even one type of functional group is present on the surface.[24]

Further surface alterations involve the introduction of chemical groups such as the

amino group, carboxyl group, sulfur group, ester group, anhydride group, or hydroxyl group,[19] organometallics, polymers, drugs, DNA, RNA, proteins, peptides, and many others.[13] Functionalizing the surface enables the covalent linkage of biological macromolecules or other nanoparticles to form nanocomposites.[19] Additionally, the presence of functional groups also affects the stability of NDs.[18] A schema of typical surface modifications can be seen in Figure 4.3.

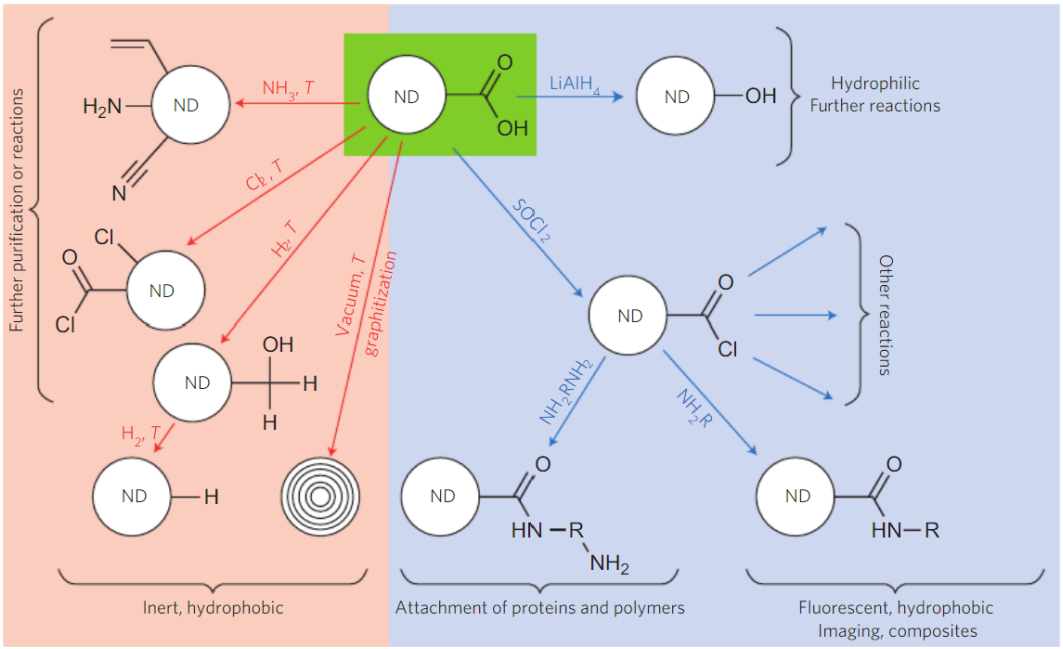

Figure 4.3: Surface chemistry of NDs with resulting properties. The starting material for surface modification is often ND with carboxylic groups (green), the red region represents modifications by high-temperature gas treatment, while the blue one contains modifications by ambient-temperature wet chemistry.[24]

4.3.1 Hydrogenated Nanodiamonds

HPHT hydrogenated nanodiamonds (HNDs) are NDs with hydrogen atoms bound to their surface, resulting in modified surface properties, chemical reactivity and interactions with other materials. The hydrogenation of HPHT NDs involves the removal of non-diamond carbon, the elimination of oxygen groups, and the stabilization of C-H terminations at the ND surface. This can be achieved by two main methods: plasma-assisted hydrogenation or annealing under hydrogen flow.[31]

HNDs offer homogeneous surface chemistry, making them suitable for subsequent functionalization. They exhibit surface conductivity, improved biocompatibility, negative electron affinity, a hydrophobic nature, and a positive ZP. However, they have a tendency to aggregate.[28,30,31] Additionally, negative electron affinity can enhance field emission and photoemission from the ND surface.[13]

4.3.2 Oxidized Nanodiamonds

Similar to HNDs, oxidized nanodiamonds (ONDs) exhibit properties that make them more suitable for biomedical applications. After synthesis via the HPHT method, the surface of NDs is typically covered by sp^2 graphitic carbon. This layer can be removed through oxidization, the process of binding functional groups containing oxygen on the ND surface.[29] However, the surface of ONDs cannot be considered homogeneous like in the case of HNDs, as multiple types of chemical groups containing oxygen are typically present. Common oxidation methods include air annealing, acid treatment, and UV exposure.[31]

The oxidation of NDs results in improved biocompatibility, increased cellular uptake of various pharmaceuticals, minimized potential oxidative stress and facilitated surface functionalization.[32] Oxidized surfaces are commonly used for derivatization through techniques such as silanization, esterification, or amidation.[31] In contrast to HNDs, ONDs exhibit positive electron affinity, hydrophilicity, and negative ZP. Overall, ONDs possess good colloidal stability.[30,31] Moreover, ONDs are electrically resistive compared to electrically conductive HNDs.[30]

4.4 Nanodiamond Properties

NDs exhibit chemical stability, biocompatibility, and fluorescence.[24] HPHT NDs are generally optical transparent over a broad range of wavelengths, with a high refractive index in their core and strong absorptive properties towards UV light.[19]

NDs can contain colour centres, such as a nitrogen vacancy (NV), silicon vacancy, or germanium vacancy, which impart unique optical properties to them.[19] HPHT NDs specifically may contain nitrogen in concentrations ranging from 100 to 300 parts per million (ppm).[22] When subjected to high-energy irradiation, NDs undergo structural damage, resulting in the formation of vacancies. Subsequent thermal annealing causes these vacancies to migrate towards nitrogen centres, forming NV colour defect centres responsible for fluorescence emission.[22,24] Detonation NDs can also host NV centres but are not able to exhibit stable fluorescence because the vacancies are too near the surface, allowing non-radiative decay.[13] Fluorescence makes NDs useful as single-photon sources or for bioluminescence labeling.[19] NV centres in fluorescent NDs are illustrated in Figure 4.4.

Biocompatibility is crucial to biomedical applications, and NDs are shown to endure biological processes while maintaining stable biological properties.[19] Moreover, ND layers show resistance to bacteria colonization, making them an ideal coating material for biomedical implants.[33] While NDs are generally nontoxic, their cytotoxicity depends on sufficient purification from sp^2 carbon and the type of the cell in question.[29] Therefore, toxicity must be evaluated for each application and ND type due to surface modifications and impurities.

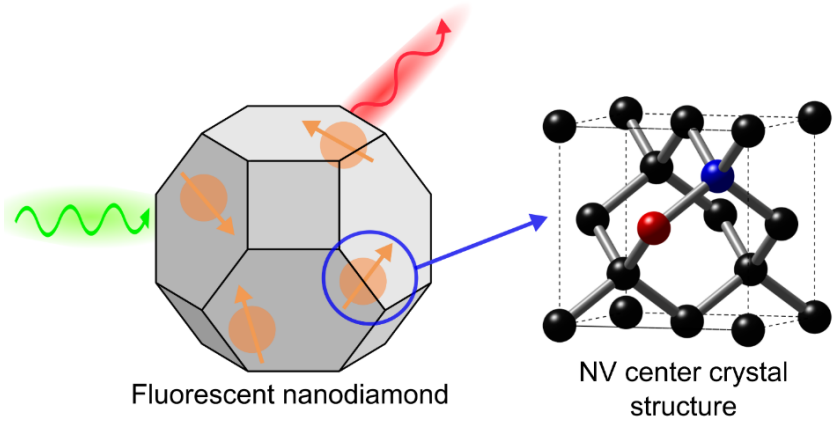

Figure 4.4: NV centres in fluorescent NDs. The crustal structure of the NV centres contains a nitrogen atom (red) and a vacancy (blue) in the lattice. An incident light beam (green) interacting with the fluorescent ND can induce fluorescent emission (red).[26]

4.5 Nanodiamond Applications

NDs have found applications across a diverse range of fields. In biomedicine, NDs have gained attention due to their chemical inertness and lack of cytotoxicity, making them suitable for example for bioimaging, drug delivery, heat therapy, biosensors,[19] surgical implants, and nanocomposites or as a tissue scaffold.[24]

The nitrogen-vacancy centres in NDs can be used for cellular tracking, temperature sensing, magnetic and electric field measurements, as well as the measurement of pressure, pH and nuclear magnetic resonance spectra.[32] NDs are perfect for bioimaging due to their small size, stable and bright fluorescence, and high biocompatibility. Most of the emission lies in the near-infrared spectrum which generates high-resolution imaging for diagnostic purposes.[19] Moreover, NDs enhance the performance of biosensing devices by improving durability, chemical resistance, biocompatibility, fluorescence, and catalytic structures.[20]

Surface modified NDs can be functionalized with various groups for the delivery of drugs, DNA, proteins, hormones, and antibodies,[19] both intracellularly and extracellularly.[18] Furthermore, surface modified NDs demonstrate antimicrobial and antibacterial effects against both gram-positive and gram-negative bacteria.[18] NDs have been also used in beauty products due to their high skin absorption rate, aiding in the delivery of active chemicals and promoting tissue healing.[20]

There are many more applications of NDs nowadays and many more are in the process of investigation, testing, and awaiting future implementation.

Chapter 5

Metal Nanoparticle-Nanodiamond Nanocomposites

The multifunctionality of materials, especially in biomedicine, is a desired goal.[13] By combining different types of NPs, new materials (nanocomposites) are formed, exhibiting enhanced properties compared to their pristine forms and tailored to specific applications. Nanocomposites, heterogeneous materials still keeping the nanometric scale, combine two or more different NPs to highlight their unique properties arising from their small size, large surface, and interfacial interaction between phases.[34] The properties of nanocomposites depend not only on the types of substances involved but also on their ratio of representation, the final size and shape of the composite, and their mutual interaction.

Nanocomposites of metal NPs and NDs find wide use as imaging agents, sensors, and catalysts[13] due to the unique and useful properties of both components. Metal NPs such as AgNPs and AuNPs possess plasmonic effects, granting them unique optoelectrical properties discussed in Section 3.1. NDs, prized for their mechanical and thermal properties, chemical stability, biocompatibility and rich surface chemistry often serve as ideal filler materials in nanocomposites.[24] They also exhibit energy absorption upon laser irradiation due to their low heat diffusivity[35] and can contain NV centres used for photoluminescence (as discussed in Chapter 4).[36]

NP-ND nanocomposite preparation typically involves the direct synthesis of metal NPs in a ND dispersion or the post-synthesis attachment of metal NPs onto the surface of NDs through covalent or non-covalent bonds. Direct synthesis can be done by reducing metal ions or salts on ND surfaces using reducing agents. However, the post-synthesis approach offers more control over the shape and size distribution of the metal NPs since the metal NPs have been already synthesized before being attached to NDs. Synthesis conditions, such as pH and temperature, influence the resulting properties of nanocomposites.[13] Surface modifications of NDs, like hydrogenation or oxidization, and coating with materials such as chitosan or PVP, can improve bonding with metal NPs, colloidal stability, dispersibility, or biocompatibility.[23,29]

5.1 Silver Naoparticle-Nanodiamond Nanocomposites

The efficacy of AgNP properties such as their plasmonic properites[15] and strong antibacterial effects.[7] can be decreased due to aggregation. Incorporating inert NDs enhances stability and thereby helps to maintain their properties.[37] Moreover, newly attained nanocomposites may enhance antimicrobial activity towards both Gram-negative and Gram-positive bacteria and at the same time lower toxicity to human cells.[23] This outcome exhibits great potential for new biomedical applications.

Furthermore, AgNP-ND nanocomposites enhance AgNP properties for surface-enhanced Raman spectroscopy (SERS) and NV centre sensing. Moreover, the increased light absorption in the visible region caused by the plasmonic properties of the AgNPs could potentially increase the photocatalytic properties of H-terminated nanodiamond surfaces since pure diamond does not absorb visible light.[23] It was observed, that AgNP-ND nanocomposite exhibits excellent multi-solvent dispersibility and enhanced photocatalysis under VIS irradiation via LSPR. Furthermore, this AgNP-ND photocatalyst can be recovered and reused with stable activity.[37] For example, nanocomposites of AgNPs, NDs, and g-C_3N_4 (a metal-free graphite phased carbon nitride) displayed enhanced photocatalytic performance shown in water dissociation to produce H_2, attributed to the light scattering effect of NDs, LSPR of AgNPs, and efficient charge transfer channels.[38]

5.2 Gold Naoparticle-Nanodiamond Nanocomposites

Plasmonic AuNPs are exceptionally stable,[6] however, the presence of NDs can help to prevent AuNPs from degrading during use, for example in photoacoustic imaging and transmission electron microscopy (TEM).[36] Moreover, a charge transfer process from AuNPs to the sp^2 bonds on ND surfaces enhances their catalytic and sensing capacities, including temperature detection.[36] NDs also improve heat energy transfer from AuNPs to the medium, increasing resistance to dissolution under strong irradiation. AuNP-ND nanocomposites also show an enhancement of photoacoustic and scattering signals.[13]

The RING (Resonance Indicator of Nanodiamond and Gold) represents a successful implementation of a metal NP-ND nanocomposite, comprising a closed plasmonic nanocavity formed by clusters of AuNPs enclosing a single nanodiamond through DNA self-assembly hybridization. This unique structure exhibits maximal interaction between plasmonic resonance and NV centres, thereby modulating the transition dynamics of the enclosed NV centres and increasing fluorescence. Interestingly, the fastest excitation and radiative decay rate were observed for RINGs containing smaller NDs and larger AuNPs attributed to the higher local density of optical states within smaller nanocavities. These RING nanocomposites find applications in biological sensing, monitoring dynamic intracellular pH or temperature and serve as solid-state single-photon emitters.[39] The RING structure is presented in Figure 5.1.

Additionally, a study focusing on tunable light-absorption of nanocomposite of NDs and gold nanorods demonstrated enhanced photo-responsive reactivity, facilitated electron mobility, and larger contact area, compared to spherical AuNPs, which underscores the shape-dependence properties of NPs even in nanocomposites.[35]

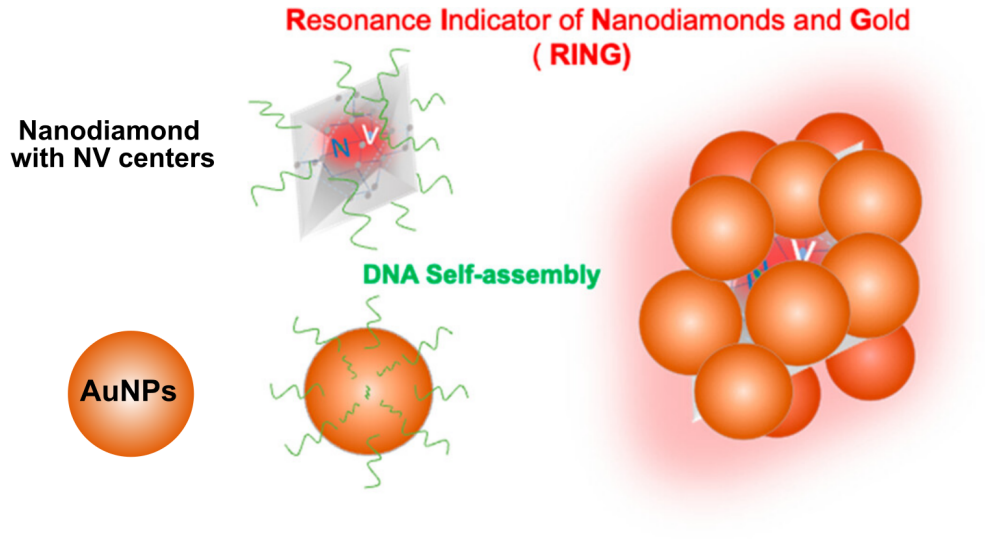

Figure 5.1: The RING (Resonance Indicator of Nanodiamond and Gold) structure represents a nanocomposite formed by a ND with NV centres and AuNPs. Adopted[39] and adjusted.

Chapter 6

Characterization Methods Principles

Diverse techniques are employed to analyze a broad range of relevant NP properties. Modern technologies allow us to investigate nanoparticle morphology using techniques such as scanning electron microscopy (SEM), polarized optical microscopy (POM) or transmission electron microscopy (TEM). Structural characterization involves studying the composition, size and bonding nature of materials, which can be observed through techniques like zeta potential (ZP) determination, dynamic light scattering (DLS), Raman spectroscopy, infra-red spectroscopy, or X-ray diffraction. Surface area can be analyzed by the Brunauer-Emmett-Teller (BET) method. Optical properties such as absorption, reflectance, luminescence and phosphorescence can be investigated through methods like spectrophotometry, diffuse reflectance spectrometry (DRS) or spectroscopic ellipsometry.[2] For better comprehension of our experiments, a description of characterization methods employed in this thesis is presented.

6.1 Optical Absorption

When an electromagnetic wave interacts with a material, it can undergo various phenomena including reflection, absorption, transmission, scattering or refraction at the molecular level, shown in Figure 6.1. Optical absorption describes the process by which a material absorbs electromagnetic radiation in the form of light, which is converted into heat and is evaluated using the reflection loss value or transmission energy relative to the incident wave energy.[40] On the other hand, the absorbance of a material indicates how much of the incident light is lost during the interaction, which can occur through all of the above-mentioned processes. It is often represented as a spectrum (function of wavelength)[41] and is commonly expressed using optical density (OD), which represents the absorbance of the sample at a given wavelength per unit distance.

According to Lambert-Beer Law, absorbance (A) is determined by the molar absorbance coefficient (ϵ), the length of the light path through the sample (b), and the concentration of absorber (c):

$$A = \epsilon \times b \times c$$

A key insight from this law is that absorbance is directly proportional to concentration.[42] Moreover, absorption is influenced by factors such as particle size, production technology, presence of impurities, dielectric medium, and chemical surroundings.[7,43]

Certain particles, such as AgNPs and AuNPs, exhibit unique optical properties that lead to strong interactions with specific wavelengths of light, LSPR, and projected in high absorbance at the specific wavelengths, creating an absorption band.[7] More about this phenomena was explained in Section 3.1. The LSPR peak wavelength position and intensity are frequently utilized for sample analysis.

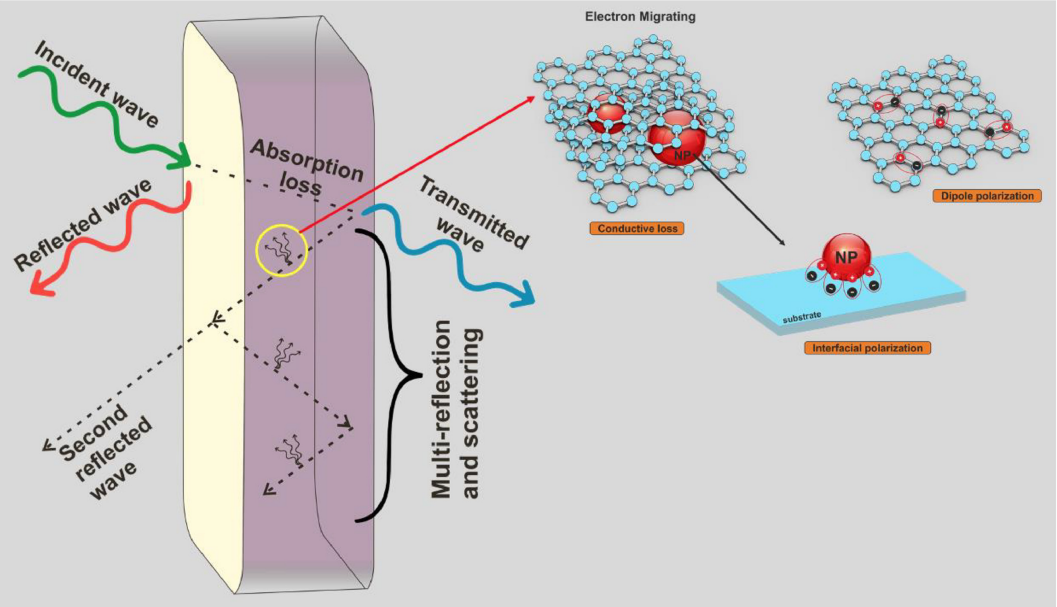

Figure 6.1: Interaction of materials with electromagnetic waves.[40]

6.1.1 Spectrophotometry

Spectrophotometry is a simple, sensitive, reliable, and cost-effective method[7,42] used for measuring light absorbance of colloidal suspensions, enabling analysis of their concentration, size, and aggregation state.[41] A microplate reader is often employed to maximize the number of samples while minimizing the volume of each sample and the time required for measurements. It allows thermostatic control and sample shaking before analysis.[42]

The spectrophotometer consists of a light source, monochromator and detectors. Measured samples are exposed to light spanning a specific range of wavelengths (created by the monochromator), typically selected from the UV or VIS spectrum, as most samples absorb in this range.[42] The device measures the intensity of light at each wavelength after it passes through the sample. A simple schema of spectrophotometer can be seen in Figure 6.2. From the knowledge of light intensity before and after interaction with the sample, OD can be determined, and a spectral graph can be generated.

It is important to be aware of the fact that highly concentrated solutions can exhibit high absorptivities and scattering, both affecting the measurements. Consequently, it becomes challenging to entirely discern the spectra into absorption and scattering components.[43]

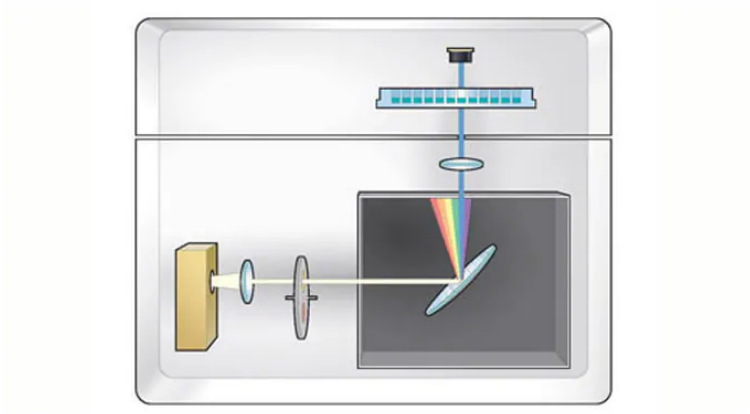

Figure 6.2: Schema of a spectrophotometer containing a light source, monochromator, and detector.[44]

6.2 Zeta Potential

Surface charge is one of the factors responsible for the range of NP properties, including their toxicity and dispersion behaviour. Zeta potential (ZP) serves as an indicator of surface charge, representing the electrokinetic potential at the slipping plane, the interface between particles and the medium.[45]

Upon dispersion in a colloidal medium, an electric double layer (EDL) forms on the surface of the NPs, resulting from an increased concentration of ions with charges opposite to that of the particles. This double layer consists of the inner Stern layer, composed of tightly bound immobile ions, and the outer diffuse layer, containing both negative and positive ions that are less firmly attached (Figure 6.3).[45,46] Measurements of ZP are typically conducted from electrophoretic mobility of charged particles induced by an electric field, employing methods such as electrophoretic light scattering or the electroacoustic phenomenon.[45]

Under an applied electric field, charged particles move, along with the ions bound within the hypothetical boundary, the slipping plane (where ZP is defined), contrary to those beyond the boundary.[46,47] The composition and width of the diffuse layer, and thus the ZP, is influenced by factors such as pH, ionic strength and concentration.[45] Electrophoretic light scattering utilizes two laser beams. One is scattered by the moving particles in the colloid, while the second one serves as a reference. The intensity of scattered light fluctuates over time proportionally to the speed of the particles, whose movement was induced by the electric field. This fluctuation is caused by the Doppler shift.[45,46]

ZP can be used to determine the stability of colloids. Particles with a large ZP tend to repel each other and have no tendency to aggregate. Solutions with absolute ZP values of > 30 mV are generally considered stable.[46] However, ZP

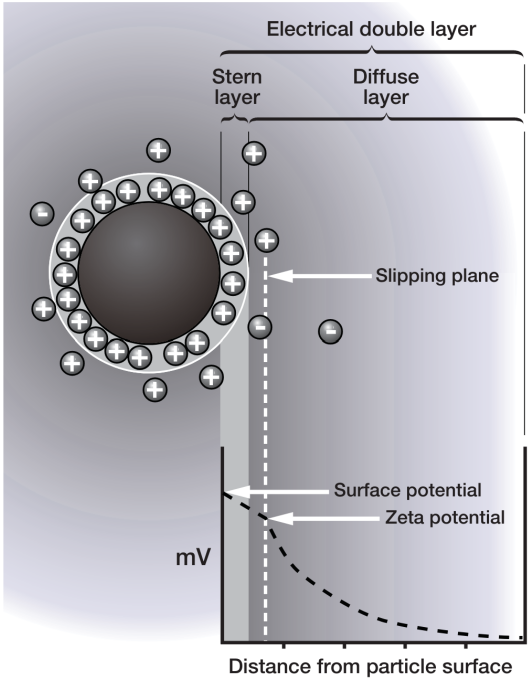

Figure 6.3: Schematic representation of ZP.[46]

provides information solely on electrostatic repulsion, disregarding the impact of van der Waals forces and steric interactions, which can also affect colloidal stability. Consequently, colloids with low ZP may appear stable, and vice versa. Neither the charge nor the charge density on particles themselves can be estimated from ZP.[45]

Simultaneously with ZP measurements, dynamic light scattering (DLS) measurements are often performed, as the same instruments may often be utilized for both techniques. However, while a cuvette with electrodes is needed for measuring electrophoretic mobility (and therefore ZP), it can, but does not have to, be used for DLS. Such a cuvette with electrodes can be seen in Figure 6.4.

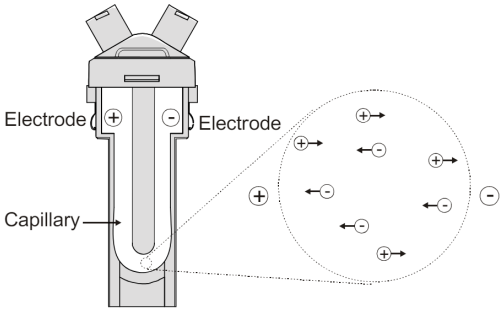

Figure 6.4: A cuvette with electrodes for ZP measurements.[46]

6.3 Dynamic Light Scattering

As previously noted, the morphology of nanoparticles can significantly affect their properties. Dynamic light scattering (DLS) is a nondestructive method for particle size estimation in colloidal systems performed by measuring their Brownian motion.[7,45]

The size of particles is determined by analyzing the scattering of light from a laser passing through the colloid, induced by the natural movement of particles.[7,46] The fluctuation in intensity over time, caused by the constructive and destructive phases of scattered light from moving particles[45,46] is illustrated in Figure 6.5. In short, smaller particles typically exhibit faster movement, leading to greater intensity fluctuations, and vice versa.[41]

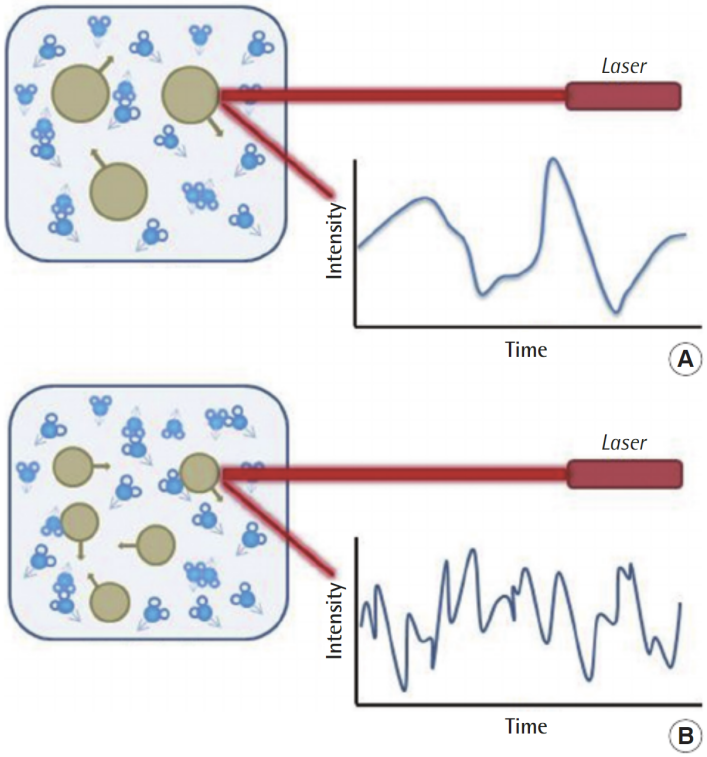

Figure 6.5: Size dependence of the fluctuation of scattered light for (A) large particles and (B) small particles.[41]

Although DLS measurements can provide valuable information, there are parameters we need to be aware of to provide correct interpretation. The results from DLS may be visualized through intensity, volume or number distributions, each offering distinct valuable information. Additionally, higher sample concentrations may lead to multi-scattering, where light scattered from one particle interacts with others before reaching the detector, resulting in reduced intensity. Conversely, low concentrations may not generate sufficient scattered light for analysis. Hence, it is important to determine the optimal concentration for DLS measurements.[45]

The shape of NPs within a colloid can also vary, and is seldom purely spherical. DLS, however, provides the hydrodynamic radius (R_H), which represents the radius of a hypothetical hard sphere moving at the same velocity as the nonspherical NPs within dispersion.[45] This consideration is important when interpreting DLS results, as particles of distinctly non-spherical shapes will give results distorted by the different dimensions of the particle. Therefore, to comprehensively understand the morphology of particles, imaging methods are beneficial in the characterization of particles as an addition to DLS measurements.

6.4 Imaging Methods

Microscopic analyses yield valuable information regarding the morphology of particles including their elemental composition and shape. Since NPs are invisible to the naked eye and often undetectable with a light microscope, electron microscopes are commonly employed to visualize the nanoworld with high resolution.

Producing high-quality images from electron microscopes often requires demanding sample preparation, which can pose challenges in obtaining representative shape, size and distribution results. This difficulty arises because the volume of the analyzed sample is typically very limited.[41] Additionally, samples for electron microscopy must typically be dried before imaging, which leads to a loss of information concerning the state of particles in suspension. For this reason, microscopy is a suitable complement to other measurements such as DLS.

6.4.1 Scanning Electron Microscopy

Scanning electron microscopy (SEM) is a surface imaging technique that focuses a beam of highly energetic electrons towards the sample under investigation. It is capable of visualising particles below 10 nm in size.[7] The electron beam in SEM scans the surface of a given sample, where it interacts with surface molecules through elastic and inelastic scattering.[48]

Due to these different interactions, various types of signal may be measured, with secondary electrons (SEs) and backscattered electrons (BSEs) being utilized in this thesis (Figure 6.6). SEs are emitted near the surface of the sample through inelastic scattering, providing information about its three-dimensional surface topography and electrical properties. BSEs are created through elastic scattering, possess more energy, and can escape from deeper regions of the sample. The number of emitted BSEs is dependent on the mean atomic number of the specimen, thereby offering information about its composition[49] and crystallographic orientation.[48]

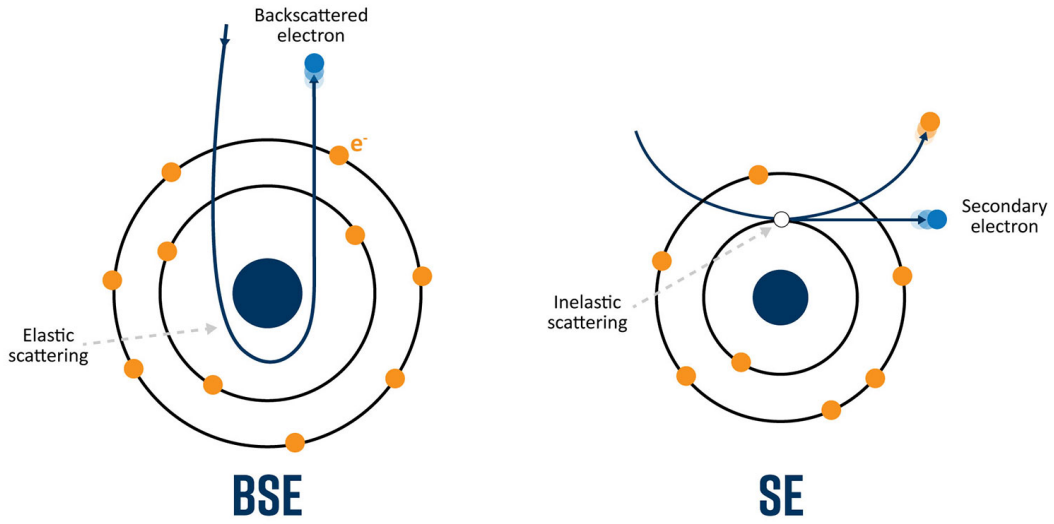

Figure 6.6: Schematic representation of BSEs and SEs.[50]

6.4.2 Transmission Electron Microscopy

Transmission electron microscopy (TEM) is another microscopy method that utilizes an electron beam to characterize the morphology and provides information about the volume of the material. TEM can distinguish between different materials within the sample based on electron interactions. Additionally, this method provides information about layered materials.[2] In TEM electrons are transmitted through an ultra-thin specimen and interact with it, allowing for detailed imaging and analysis. TEM can achieve a remarkable resolution down to 0.07 nm.[41] This superior spatial resolution is an advantage of TEM over SEM, allowing more detailed imaging of nanoscale structures. However, TEM requires a more specific working environment including high vacuum conditions. Furthermore, the quality of sample preparation is demanding, requiring precise thinning of the sample to achieve optimal imaging results.[7]

Part II

Materials and Methods

In this part, a description of employed materials (Chapter 7) and methods (Chapter 8) is given. All experiments took place in a sterile environment, flowbox or lab, and using protective equipment. The equipment was sterilized either by autoclaving or UV sterilization, or it was delivered sterile from the manufacturer.

Chapter 7
Materials

For our experiments, hydrogenated nanodiamonds (HNDs) and oxidized nanodiamonds (ONDs) were used as representatives of nanodiamonds (NDs). These surface modified NDs were chosen for the experiments due to recent successful investigations into their bonding with silver nanoparticles (AgNPs).[23,29] For metal nanoparticles (NPs), AgNPs and gold nanoparticles (AuNPs) were selected as they both exhibit plasmonic behaviour. Colloids of those four particle types were characterized before and after mixing them to get colloidal mixtures. Subsequently, the colloidal mixtures containing AgNPs were compared with directly synthesized nanocomposites of NDs and AgNPs.

7.1 Nanodiamonds

The employed nanodiamonds, HNDs and ONDs, were provided by Ing. Kateřina Kolářová, Ph.D., from the Institute of Physics of the Czech Academy of Science. More information about HNDs and ONDs is presented in Section 4.3.1 and 4.3.2, respectively. Commercially available high pressure high temperature (HPHT) monocrystalline synthetic diamond powder (MSY) (Pureon) was used for the experiments. Per the manufacturer's specification, NDs in powder form should have a regular, blocky shape and high reproducibility. The powder contained particles with a reported average size of 50 nm. The method description for preparing HNDs and ONDs was provided by Ing. Kateřina Kolářová, Ph.D. as follows:

- The nanodiamond powder was oxidized/baked in an oven at 450°C for 5 hours to produce ONDs.
- To prepare HNDs, the nanodiamond powder was activated for 6 hours in a hydrogen atmosphere at 800°C.

Both suspensions were finalized by mixing each with demineralized water for a final concentration of 1 mg of nanodiamond powder per 1 ml of water. Subsequently, the solutions were sonicated for 1 hour on an ultrasonic tip to create a dispersed suspension. Both solutions have a greyish cloudy colour, with HNDs appearing darker than ONDs, as seen in Figure 7.1.

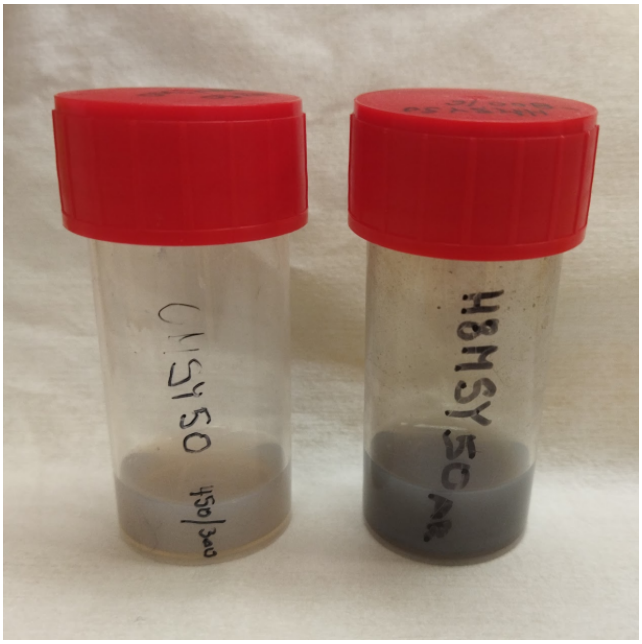

Figure 7.1: Photos of ND colloids - ONDs (left) and HNDs (right)

Over time, some HND particles sedimented in the colloid (see Figure 7.2), but were redispersed prior to experiments by sonication. Neither solution requires storage at low temperatures or protection from light to keep their properties.

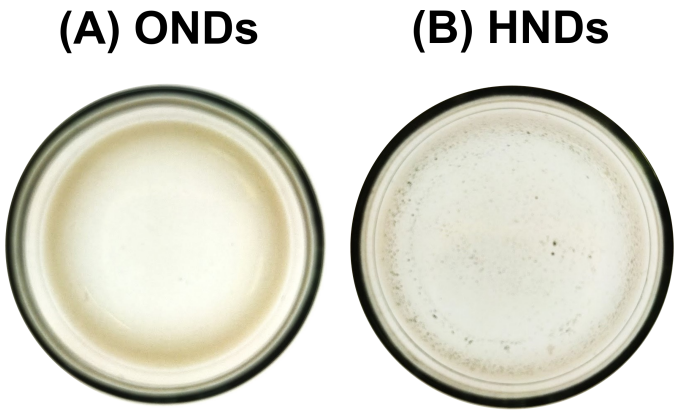

Figure 7.2: Photos of ND colloids with detail of sedimented particles - (A) ONDs and (B) HNDs.

For this work, two batches of each ND colloid were utilized. The batch prepared on 27.7.2023 was used initially in our analyses. The directly synthesized nanocomposites were made from the batch prepared on 9.1.2023. Severe degradation of optical absorbance was observed in the old batch of HNDs compared to the new one as seen in Figure D.3 in Appendix D. Therefore, the colloidal mixtures were prepared from the new batch and analysed again.

7.2 Metal Nanoparticles

In Table 7.1 below, specifications for the two types of metal NPs, AuNPs and AgNPs, are given.

Property	AuNPs	AgNPs
Manufacturer	BBI Solution	Sigma
Concentration [μg/ml]	50	20
Stabilizer	NONE	Citrate
Storage	4 °C	4 °C
Sensitivity	NONE	air and light
Color	Pink	Yellow
Size [nm]	20	20
Shape	spherical	spherical
Plasmonic Peak Wavelength [nm]	around 520	around 400

Table 7.1: Specifications of the employed metal nanoparticles - AuNPs and AgNPs.

7.3 Directly Synthesized Nanocomposites

Directly synthesized nanocomposites were provided by Ing. Kateřina Kolářová, Ph.D., from the Institute of Physics of the Czech Academy of Science. She prepared a suspension of HNDs and ONDs decorated with silver. For these nanocomposites, she used NDs from the second batch discussed in Section 7.1. Both nanocomposites were functionalized using either chitosan (for HNDs) or polyvinylpyrrolidone (PVP) (for ONDs) to better anchor silver to the ND surface. Ing. Kateřina Kolářová, Ph.D. provided a description of her synthesis process as follows:

7.3.1 Hydrogenated Nanodiamonds Decorated with Silver

To prepare the nanocomposite of hydrogenated nanodiamonds supported by chitosan and decorated with silver nanoparticles (HNDs-Chit-Ag):

1. 6 mg of HNDs dispersed in 6 ml of demineralized water were mixed with 18 ml of a chitosan solution prepared by mixing 40 mg of chitosan, 0.03 ml of HCl (35%, p.a) and 20 ml of dH_2O.
2. The mixture was heated for 3 hours at 60 °C with constant stirring.
3. The mixture was then centrifugated twice at 15,000 rpm for 10 minutes and the supernatant was replaced with dH_2O to a final volume of 6 ml of HND-chitosan.
4. 6 ml of HND-chitosan was heated to 100°C under constant stirring and 0.04 g of $AgNO_3$ dissolved in 0.5 ml of dH_2O were slowly added.

5. After ten minutes, 6 ml of 0.01% Polyethyleneimine (PEI) were added and the mixture was heated for another 40 minutes.

6. The resulting suspension of HNDs-Chit-Ag was centrifugated twice at 15,000 rpm for 10 minutes and the supernatant was replaced with dH_2O for a final volume of 6 ml of suspension.

The colloid of the HNDs-Chit-Ag has a grey cloudy colour. The photo of the colloid can be seen in Figure 7.3 on the right side.

7.3.2 Oxidized Nanodiamonds Decorated with Silver

To prepare the nanocomposite of oxidized nanodiamonds supported by polyvinylpyrrolidone and decorated with silver nanoparticles (ONDs-PVP-Ag):

1. 6 mg of ONDs dispersed in 6 ml of demineralized water were mixed with 25 ml of a PVP25 solution. The PVP25 solution contains 0.5 g of PVP dissolved in 25 ml of H_2O.

2. The mixture was heated for 3 hours on a hot plate to 60 °C with constant stirring.

3. The mixture was then centrifugated twice at 15,000 rpm for 10 minutes and the supernatant was replaced with dH_2O to a final volume of 6 ml of a solution of OND-PVP.

4. 6 ml of OND-PVP were heated to 60°C and 0.4 g of PVP25 dissolved in 24 ml 96% ethanol were added and stirred for 20 minutes.

5. 0.04 g of $AgNO_3$ dissolved in 0.5 ml of dH_2O were added drop by drop. The mixture was constantly stirred for 2 hours at 60°C.

6. Finally, the resulting mixture was centrifugated twice at 15,000 rpm for 10 minutes and the supernatant was replaced with dH_2O to a final volume of a 6 ml ONDs-PVP-Ag suspension.

The colour of the colloid of ONDs-PVP-Ag is dark yellow and the solution is not translucent. The yellow colour is attributed to the presence of AgNPs. The photo of the colloid can be seen in Figure 7.3 on the left side.

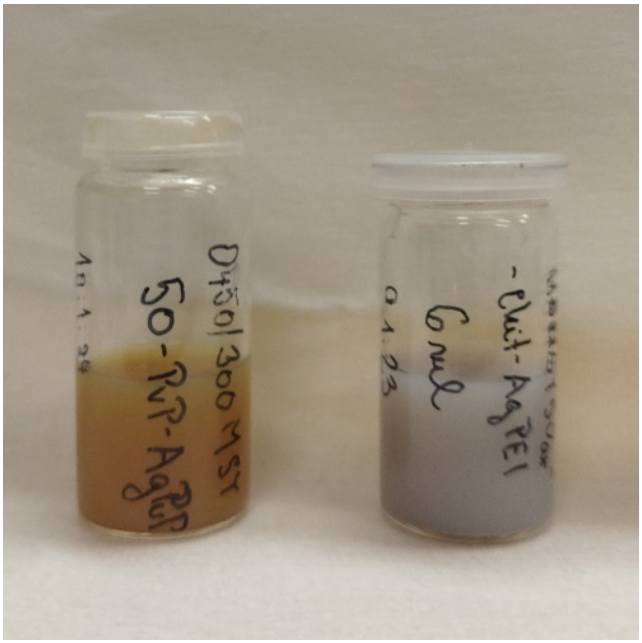

Figure 7.3: ONDs-PVP-Ag (left) and HNDs-Chit-Ag (right)

For the directly synthesized nanocomposites, it was difficult to obtain the exact ratio of constituents. Therefore, the concentration of present NDs was assumed to be 1 mg/ml based on the concentration of the stock 50 nm ND colloid used for decoration.

Chapter 8
Methods

In the course of our experiments, several methods were employed to investigate the optical absorption, stability, and morphology of samples. This chapter describes the procedures that were applied during this work.

8.1 Dilution Series

As the dependence on concentration was investigated many times throughout the experiments, a brief description of the steps of a dilution series (used to get specific dilutions of a sample) is presented. A two-fold dilution series was chosen, as it provides results over a useful span of concentrations, which is more densely sampled than other dilution alternatives (e.g. a 10-fold dilution series).

However, sometimes to obtain the starting concentration for the two-fold dilution series, 4-fold or 10-fold dilution (with similar steps as for two-fold dilution) had to be performed beforehand.

The process of creating a two-fold dilution series included the following steps:

1. Before each experiment, NDs were sonicated at 35 kHz for 10 minutes in a sonication bath to resuspend NDs which had fallen out of suspension.
2. 2 ml Eppendorf tubes were used for 1.5 ml sample dilutions. HPLC grade water was used as the diluting agent and pipetted in the required volume into the Eppendorf tubes prior to the addition of the colloids.
3. The stock colloid of a desired volume was added to the first Eppendorf tube to obtain the starting concentration and properly mixed to assure equal distribution in the sample.
4. After that, half of the volume (0.75 ml) was pipetted and added into the following Eppendorf tube (holding 0.75 ml of HPLC water) and mixed again. By repeating these steps we obtained the desired sample set.

8.2 Colloidal Mixtures

Colloidal mixtures were prepared in two sets, one with a fixed concentration of NDs at 25 μg/ml and one at 6.25 μg/ml. The concentration of the added metal NPs varied and it is listed in Table 8.1.

Sample	AuNPs [μg/ml]	AgNPs [μg/ml]
1	45	18
2	22.5	9
3	11.25	4.5
4	5.625	2.25

Table 8.1: Concentration of metal NPs in colloidal mixtures.

Creating colloidal mixtures of NDs and metal NPs involved the following steps.

1. NDs were sonicated at 35 kHz for 10 minutes in a sonication bath.
2. A dilution series of NDs was performed to obtain concentration 250 or 62.5 μg/ml, as the ND colloids will be mixed with the metal NPs in a 1:9 ratio afterwards for a final concentration of 25 μg/ml and 6.25 μg/ml, respectively.
3. A four-step two-fold dilution series of metal NPs provided four solutions of AgNPs (20, 10, 5, 2.5 μg/ml) and four solutions of AuNPs (50, 25, 12.5, 6.25 μg/ml), with the first concentration in the series being the full stock concentration of the given NP.
4. Sixteen Eppendorf tubes were prepared and filled with 200 µl of the diluted NDs (25 or 6.25 μg/ml).
5. Then, 1.8 ml of each concentration of the metal NPs prepared in step 3, was pipetted into the Eppendorf tube with NDs, giving us the final colloidal mixture.
6. Finally, all the colloidal mixtures underwent proper agitation by hand.

By this procedure, four colloidal mixtures (AuHNDs, AgHNDs, AuONDs, and AgONDs) of four concentrations of present metal NPs each were created for a fixed ND concentration of either 25 or 6.25 μg/ml. A new set of colloidal mixtures was prepared for each experiment to avoid faulty results due to the potential instability of the samples.

8.3 Spectrophotometry

In this work, absorbance spectra were used for the investigation of plasmonic peaks, the stability of substances and the interactions in colloidal mixtures.

Spectrophotometer Specification

The Epoch2 microplate reader from BioTek was used for these experiments. This spectrophotometer can operate with 6- to 384-well microplates. For our experiments, 96-well UV black body microplates were used to allow measurements in the UV spectrum. The plate has 12 numbered columns (1-12) and 8 letter-marked rows (A-H). Based on the manufacturer's description, the spectrophotometer has a monochromator wavelength selection system and compares light from the xenon lamp with light transmitted through the samples. It measures at wavelengths from 200 to 999 nm in 1 nm increments and offers endpoint, kinetic and spectral scanning and linear, orbital, or double-orbital shaking. Additionally, it provides control of temperature from 4 °C to 65 °C and condensation control. The measurement range is from 0.000 to 4.000 optical density (OD) with a resolution of 0.0001 OD. The spectrophotometer OD accuracy is ±0.010 OD, and wavelength accuracy and precision of ±2 nm and 0.2 nm, respectively. The theory behind optical absorption, OD estimation, and spectrophotometry is provided in Chapter 6.1.

The spectrophotometry experiments took place in the Microbiology Laboratory of the Department of Physics of the Faculty of Electrical Engineering of CTU. The spectrophotometer was set to 37 °C to mimic the temperature of the human body and the gradient was set to 0°C. Before each measurement, a 10 second orbital shake at 282 cpm (cycles per minute) was done. The settings of the spectrophotometer were set for wavelengths in the range of 200 to 900 nm with a 2 nm increment. A plastic lid was not used during measurements, as the plastic would alter the UV spectrum (see Figure D.2 in Appendix D).

8.3.1 Concentration Analysis

The concentration dependence of optical absorption was examined on NP colloids, the colloidal mixtures and the directly synthesized nanocomposites. Firstly, the dilution series was analyzed for each colloid.

- For colloids of metal NPs and NDs, a seven-step two-fold dilution series generated 28 samples listed in Table 8.2. The starting concentration of NDs was set to 200 μg/ml. Higher concentrations caused overflow as the spectrophotometer measurement range is 0 to 4 optical density (OD). Starting concentrations of metal NPs were the respective stock concentrations of each purchased colloid (50 μg/ml for AuNPs and 20 μg/ml for AgNPs) as these concentrations are already quite low and no benefit can be gained from further diluting the stock for an initial sample.

- Colloidal mixtures were prepared according to the procedure described in Section 8.2 in two sets, one with the concentration of NDs fixed at 25 μg/ml and one at 6.25 μg/ml. The concentration of metal NPs present in each colloidal mixture is listed in Table 8.1.

- Directly synthesized nanocomposites were prepared by a four-step two-fold dilution series giving 4 samples of each type listed in Table 8.2.

Step	HNDs [μg/ml]	ONDs [μg/ml]	AuNPs [μg/ml]	AgNPs [μg/ml]	HNDs-Chit-Ag [μg/ml]	ONDs-PVP-Ag [μg/ml]
1	200	200	50	20	100	100
2	100	100	25	10	50	50
3	50	50	12.5	5	25	25
4	25	25	6.25	2.5	12.5	12.5
5	12.5	12.5	3.125	1.25	-	-
6	6.25	6.25	1.5625	0.625	-	-
7	3.125	3.125	0.78125	0.3125	-	-

Table 8.2: Concentrations of samples of NP colloids and directly synthesized nanocomposites analyzed through Spectrophotometry.

Once the samples were prepared and properly mixed, 200 μl of each sample were pipetted into the microplate. Three adjacent columns were dedicated to each sample with the concentration of samples descending over seven rows. Each sample was pipetted and measured in triplicate to enable post-process averaging and obtain more accurate results. The last row, "H", was filled with HPLC grade water as a blank sample used in data post-processing for the blank correction of OD. An example of the microwell arrangement used for the measurement of pristine NPs can be seen in Figure 8.1.

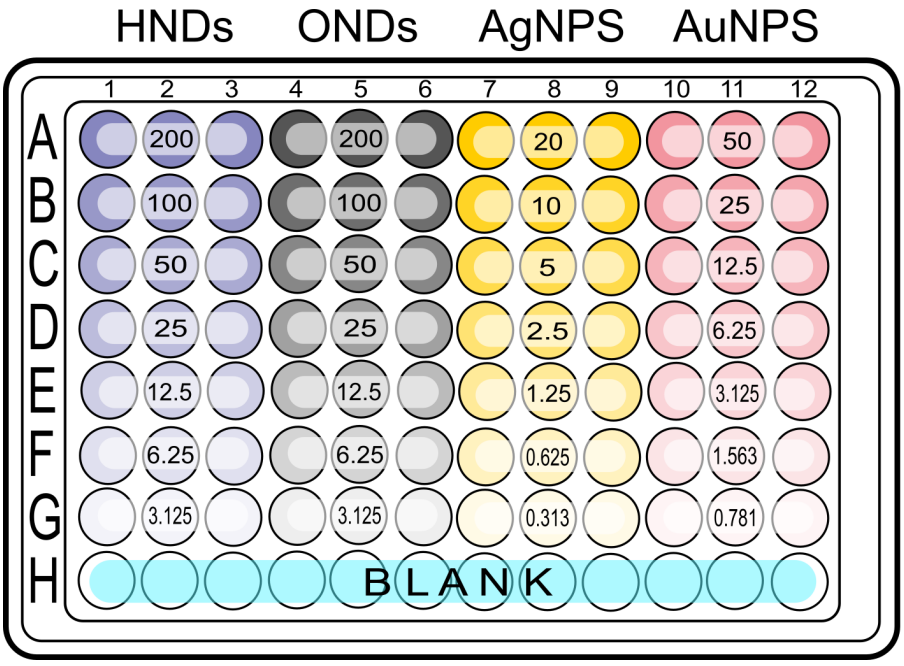

Figure 8.1: Dilution series of individual ND and metal NP colloid arrangement for spectrophotometry using 96 well UV black body microplate with listed concentration in μg/ml. Each cell represents three successive columns containing the same sample. Row "H" contains blank samples of HPLC grade water used in data post processing for the blank correction of OD.

Data Analysis

The data from spectrophotometry was analyzed in the Gen5 software for microplate data collection and analysis and by Matlab using and altering a script provided by the supervisor. The average and standard deviation of OD were computed from values of three replicates of each sample. All values were blank corrected by the subtraction OD values of pure water from the OD of colloids to obtain undistorted data. The mean and standard deviation from the analyzed data are presented in spectral graphs as curves and see-through planes, respectively. Peaks in graphs were identified using the Matlab findpeaks() function, which marks points with higher values than their two neighbouring samples from both sides. Once the peaks or points of interest were found, their coordinates were transferred into Microsoft Excel, and projected in a dot plot, so peak analysis could be performed. Peak analysis was complemented by a linear trend line computed by Excel using the ordinary least squares method.

Colloidal Mixtures Analysis

To see differences in the optical absorbance of colloidal mixtures, the OD of the pristine ND colloid was subtracted from the OD of the colloidal mixtures and the ubtracted spectrum was displayed. Comparing the subtracted spectrum of colloidal mixtures with the spectrum of metal NPs, potential interactions between the NDs and metal NPs manifested into their absorption spectrum could be analysed more clearly.

Lambert-Beer Law Verification

Additionally, the verification of Lambert-Beer law was performed investigating linearity of OD at a 450 nm wavelength for each concentration and each sample. The 450 nm wavelength was chosen as it is in the VIS region and between the plasmonic peaks of both metal NPs. To evaluate the linearity of the obtained data, a linear trend line was computed.

8.3.2 Stability Analysis

Stability analysis through spectrophotometry directly followed the concentration analysis (Section 8.3.1) so the same samples were used. The stability of samples was analysed by comparing spectra of colloids at time zero up to 24h. However, keeping solutions in the spectrophotometer at 37 °C for up to 24 hours caused evaporation seen in Figure D.1 in Appendix D. Lowering the temperature to 18 °C still caused noticeable evaporation after a few hours and putting transparent foil over the plate altered the spectrum in the UV region significantly as seen in Figure D.2 in Appendix D. Therefore, samples were stored with a lid in the incubator at 37 °C between measurements and manually inserted into the spectrophotometer at each desired timepoint to prevent evaporation. However, some evaporation could still influence the measurement, because one measurement step took over an hour in the spectrophotometer at 37 °C.

- OD of NP colloids was measured at time zero, 2, 4, 8, 6, 8 and 24 hours for one concentration of each colloid - 100 μg/ml of both NDs, 10 μg/ml of AgNPs, and 25 μg/ml of AuNPs. One concentration was picked with the assumption of no significant differences across the concentrations and in order to make the experiment feasible, as each step took around an hour to measure.
- Colloidal mixtures and directly synthesized nanocomposites were analyzed at time zero and 24 hours for each prepared concentration.

Sedimented Nanoparticles

As some particles were observed to sediment in the colloid, especially in the case of HNDs, after measuring the stability through spectrophotometry, photos of the colloids were taken. Samples were illuminated from below using a transillumination panel with a white, evenly distributed light source and photographed on a mobile phone.

Data Analysis

Stability was determined by computing the standard deviation of OD at each point of the spectrum between time zero and all subsequent timepoints. The sum of the standard deviations divided by the number of measured wavelengths gave the average standard deviation. The stability limit was set at the average standard deviation of 0.05. This value was estimated considering the spectrophotometer accuracy, which is $\pm$0.010 OD and possible evaporation during the measurements, therefore a difference of up to 0.05 was considered stable. In the case of stability evaluation based on multiple concentrations, we are talking about the total average standard deviation, calculated as the average of the average standard deviations.

8.4 Zeta Potential and Dynamic Light Scattering Measurements

Zeta potential (ZP) and dynamic light scattering (DLS) (the theory behind these methods is provided in Sections 6.2 and 6.3, respectively) were measured at the Institute of Physics of the Czech Academy of Science at the Department of Semiconductors under the supervision of Ing. Kateřina Kolářová, Ph.D., using the Zetasizer Nano from Malvern with a helium-neon laser (633 nm) and a scattering angle of 173°.

Measurement Procedure

Each sample was diluted and pipetted into a disposable folded capillary cell equipped with electrodes. Before measuring, the measurement workflow was set in the Malvern software. Prior to measuring, the samples underwent a 1-minute stabilization period. Measurements of both ZP and DLS were performed in triplicate, where the specific number of measurement components was analyzed by the machine itself, based on the differences between measurements and sample quality (the number

of sub-measurements fluctuates between 12 and 100). For accurate computation, the type of solution was provided to the software.

The concentration of the measured samples was chosen based on the quality report from Zetasizer. After a few tests, samples with concentrations listed in Table 8.3 were used for ZP and DLS measurements.

Sample	HNDs	ONDs	AuNPs	AgNPs	AuHNDs
μg/ml	25	25	6.25	2.5	5.625 /25

Sample	AgHNDs	AuONDs	AgONDs	HNDs-Chit-Ag	ONDs-PVP-Ag
μg/ml	2.25/25	5.625/25	2.25/25	25	25

Table 8.3: Concentration of samples used for ZP and DLS measurements. For colloidal mixtures, the number before the slash sign gives the concentration of the present metal NP, and the number after the slash sign gives the concentration of the present ND. Concentrations listed for directly synthesized nanocomposites, HNDs-Chit-Ag, and ONDs-PVP-Ag, are the assumed concentrations of NDs.

pH Measurements

As ZP is susceptible to changes in the pH of the substance, the pH of each sample was measured using the Malvern MPT-2 Multipurpose Autotitrator at the time of ZP measurements. The samples were measured at the room temperature. Apart from pH, temperature, and ion concentration can alter a value of ZP.

Data Analysis

ZP and DLS measurements were analyzed first for quality by the Zetasizer software. Further analysis was done in Matlab using a script provided by the supervisor. As measurements of ZP were performed in triplicate, their mean ZP value was calculated and used in this thesis.

Data from DLS could be displayed in three distinct ways - by number, volume, or intensity distribution. Intensity distribution is directly obtained from a DLS measurements and number and volume distributions are generated from it. The number distribution gives us information about the amount of particles of a specific size, while the volume distribution can point to the presence of larger particles in the solution even though their amount is too low to be noticeable in number distribution. Graphs for each sample consist of three distributions as DLS was measured in triplicate.

8.5 Scanning Electron Microscopy

For this work, the Zeiss EVO 10 scanning electron microscope was used to observe samples and obtain images of NPs. The measurements took place in the Corelative SEM-AFM Microscopy Laboratory of the Physics Department of the Faculty of Electrical Engineering of CTU under the supervision of Ing. Markéta Šlapal Bařinková.

Samples were drop-cast onto a silicon wafer substrate and left to air-dry at room temperature. Images for the NPs were obtained at an EHT of 17 kV, probe current of 5 pA and at a working distance of approximately 8.5 mm. The brightness and contrast settings were kept the same overall measurements in order to allow for the comparison of the signal between samples. Images were created using the signal from BSEs and SEs.

Digital Image Processing

Ing. Bařinková provided images of the measured SE and BSE signal processed in Gwyddion[51] and Matlab. The brightness of all images was increased so that the individual structures of the NPs could be better observed and that the printed version of this thesis met the standards. Additionally, metal NPs in the BSEs images were highlighted in red and separated from their background. Briefly, the BSE images were thresholded to distinguish metal NPs from NDs. From this, a mask was created and coloured red, which was subsequently overlaid onto the SEs image of the same structure to enhance the recognition of the materials in the sample.

8.6 Transmission Electron Microscopy

Additional images of HNDs-Chit-Ag and ONDs-PVP-Ag form transmission electron microscopy (TEM) were provided by Ing. Kateřina Kolářová, Ph.D., from the Institute of Physics of the Czech Academy of Science and this technique is briefly introduced in Section 6.4.2. Doctor Kolářová acquired images using Tecnai G2 20 (FEI).

Part III

Result and Discussion

Chapter 9

Results and Discussions

In this chapter, the obtained experimental results are presented and discussed. While experiments involved many additional steps to achieve suitable results, they are not all presented in this part; some are instead provided in Appendix D for reference. The experiments are divided into three sections - characterization of ND and metal NP colloids, investigation of their colloidal mixtures, and comparison of those colloidal mixtures with directly synthesised nanocomposites. The main goal was to investigate the colloidal mixtures from the point of view of their plasmonic optical absorption.

9.1 Characterization of Colloids of Nanodiamonds and Metal Nanoparticles

Firstly, experiments were conducted with individual colloids of nanodiamonds (NDs) and metal nanoparticles (NPs) to characterize them and determine the optimal ratios of substances for the colloidal mixtures. The objective was to highlight their properties and promote potential synergy. The characterization will later help elucidate the factors behind observed plasmonic effects in the colloidal mixtures.

9.1.1 The Concentration Dependence of Optical Absorption

For the optical absorption analysis, a concentration series of each colloid diluted in HPLC grade water was prepared for each of the four colloids - hydrogenated nanodiamonds (HNDs), oxidized nanodiamonds (ONDs), gold nanoparticles (AuNPs) and silver nanoparticles (AgNPs). The procedure is described in Section 8.3.1. The concentration dependence of optical absorption spectra of NDs is shown in Figure 9.1. The presented data curves are an average of triplicate samples. The standard deviation of these triplicates was computed and for all samples is too small to see in the graphs, meaning the measurement value is relatively constant across the samples. As expected, the optical density (OD) of NDs declines with the decrease of concentration. NDs have high optical absorption in the UV region, where ONDs have a steeper decline than HNDs. The OD for both types of NDs in the infra-red region is minimal. Therefore, the presence of NV centres or other colour centres in the NDs is negligible since they are not projected in the absorption spectrum. However, this does not rule out the presence of NV centres

completely.

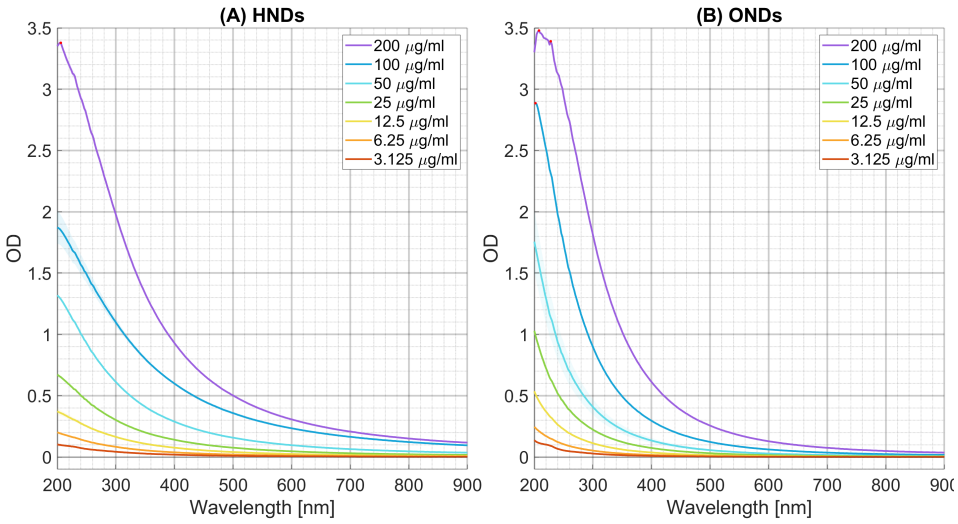

Figure 9.1: The concentration dependence of the optical absorption of NDs - (A) HNDs and (B) ONDs. The data curves are averages from triplicate, blank-corrected samples. Standard deviations from the triplicates are displayed as see-through planes.

In Figure 9.2, the concentration dependence of optical absorption of metal NPs is shown. Just as with NDs, absorption decreases with a decrease in concentration. The triplicates appear stable with a virtually undetectable standard deviation. In addition to high optical absorption in the UV region, two distinct peaks are also visible in both spectra - a smaller peak around 260 nm and a larger peak in the VIS area. As there is no documented characteristic peak around 260 nm for either metal NP, these peaks were probably caused by organic contamination. Peaks in the VIS region were evaluated as plasmonic peaks, characteristic for these metal NPs as discussed in Section 3.1.

The high prominent peaks were identified using the Matlab findpeaks() function explained in Section 8.3.1 and marked by a red dot. The plasmonic peaks of AgNPs and AuNPs are located around 398 nm and 526 nm, respectively. The peak location and OD value for the plasmonic peak of the metal NPs are listed in Table 9.1. Plasmonic peaks of higher concentrations are found at a relatively stable wavelength. However, the spectra of lower concentrations exhibit unexpected shifts probably due to their weak absorption compared to the local environment. Furthermore, the lowest values of OD are close to the resolution of the spectrophotometer - 0.0001 OD. Changes of 2 nm in the experiment are not considered significant because the wavelength accuracy of the spectrophotometer is ±2 nm and the spectrophotometer itself was set with a 2 nm step increment. Overall, the plasmonic peak location remains relatively the same over all concentrations studied in this thesis. Based on these results, we can expect no aggregation of metal NPs dependent on concentration in the individual colloids. In the case of aggregation of metal NPs, shifts in the plasmonic peaks would be observed, as the size affects their location.

To test the validity of Lambert-Beer Law, discussed in Chapter 6.1, which states that optical absorption is linearly dependent on concentration, the OD values

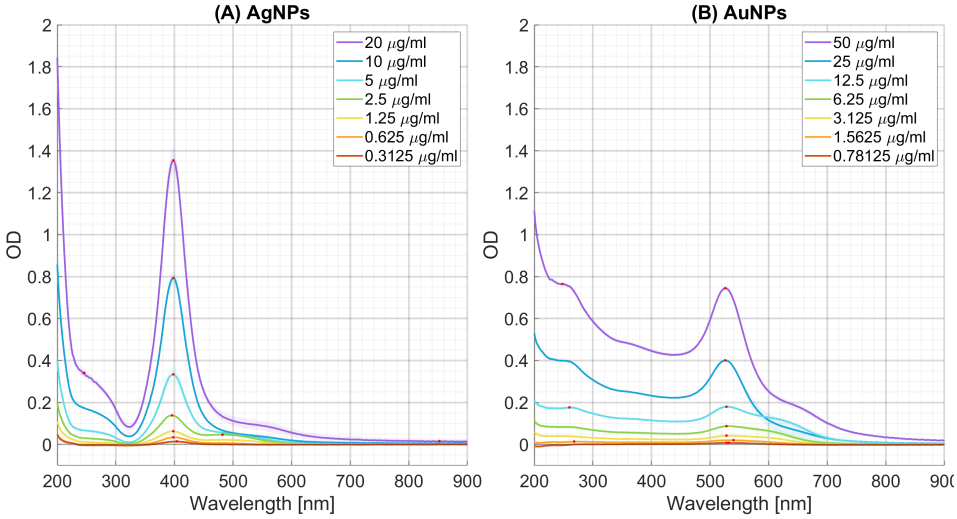

Figure 9.2: The concentration dependence of the optical absorption of metal NP - (A) AgNP and (B) AuNP. The data curves are averages from triplicate, blank-corrected samples. Standard deviations from the triplicates are displayed as see-through planes.

NPs:	AgNPs			AuNPs		
Step	c [μg/ml]	OD	λ [nm]	c [μg/ml]	OD	λ [nm]
A	20	1.354	398	50	0.744	526
B	10	0.793	398	25	0.400	526
C	5	0.334	398	12.5	0.179	528
D	2.5	0.138	396	6.25	0.089	528
E	1.25	0.063	398	3.125	0.045	528
F	0.625	0.034	398	1.5625	0.020	(540)
G	0.313	0.015	(404)	0.781	0.011	528

Table 9.1: Plasmonic peak analysis of metal NPs listing the concentration (c) of the colloids, and the OD and wavelength (λ) of the detected plasmonic peaks

at 450 nm (see Section 8.3.1) were plotted over concentrations and are displayed in Figure 9.3. The expected linearity is noticeable for ONDs, AgNPs and AuNPs. The optical absorption seems to be linear for HNDs at lower concentrations as well. However, higher concentrations of HNDs are no longer consistent with the linear trend. This may be due to a higher rate of agglomeration in HND samples of higher concentrations.

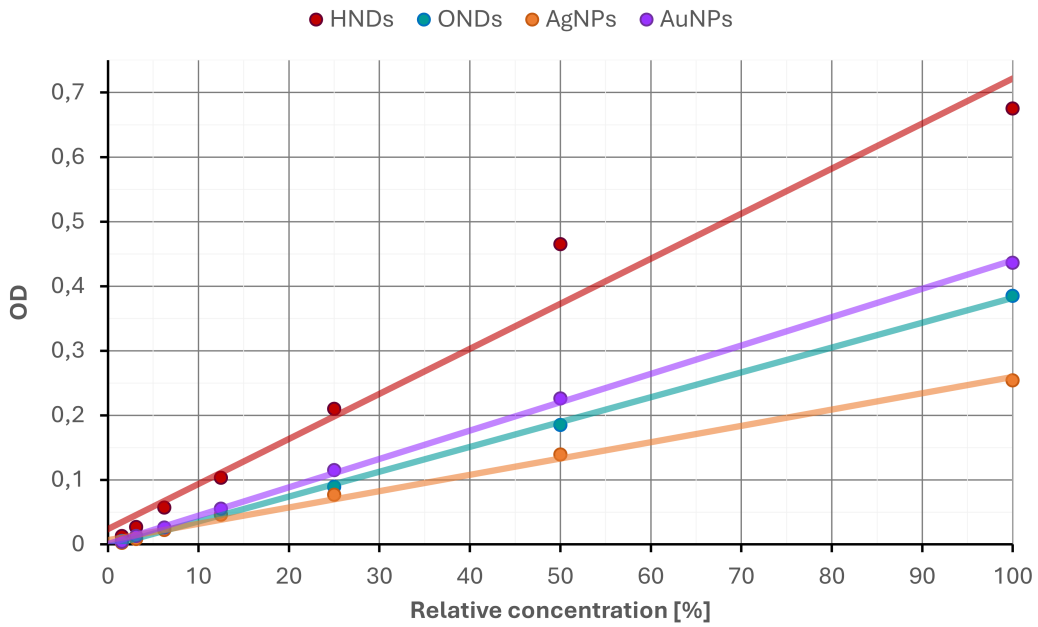

Figure 9.3: Lambert-Beer law verification on the individual colloids (HNDs, ONDs, AgNPs, and AuNPs) with OD measured at a wavelength of 450 nm and blank corrected. The horizontal axis is expressed as a percentage of the starting concentration of the stock solution. Data points represent measured samples and full lines are linear trend lines of the corresponding colloids.

9.1.2 Stability of Colloids

Along with measuring the concentration dependence of optical absorption, the stability of colloids was investigated and analysed at 6 time-points - at time zero and 2 hours, 4 hours, 6 hours, 8 hours, and 24 hours after dilution - with the primary assumption of no significant differences across the concentrations. This measurement was done without the lid, as the plastic in the lid absorbs strongly in the UV region similar to foil that we tested to prevent evaporation as seen in Figure D.2 in Appendix. The results of the stability measurements of individual colloids may be seen in Figure 9.4 for NDs and Figure 9.5 for NPs. As explained in Section 8.3.2, the stability level over time of each colloid was determined by computing the average standard deviation (the sum of standard deviations at each measured wavelength divided by the number of wavelengths) of OD at each point of the spectrum between time zero and all subsequent timepoints. The threshold for determining stability was set at 0.05 considering spectrophotometer accuracy and possible evaporation.

For NDs (Figure 9.4), spectra from concentrations of 100 μg/ml HNDs (A) and 100 μg/ml ONDs (B) are presented. For ONDs, data showed no visible instability and its spectra remained fairly stable even after 24 hours. This is supported by the average standard deviation, which drifts slightly but does not change drastically. In the HND graph, a significant increase in OD of HNDs across the spectrum after 24 hours is observed. This was accompanied by visible HND particles aggregating

at the bottom of the microwell plate at the end of the experiment and a measurement overflow in the UV region. The aggregation of HND particles in the colloid was probably due to their weak bond with water molecules. Generally, undispersed particles have higher absorbance than dispersed ones. This indicates that HNDs are less stable than their oxygenated counterparts, which is supported by the deviation curve in the corner of the HND graph. Its difference values cross the set 0.05 limit after the 5-hour mark and continue to grow for the duration of the experiment.

During the process of experiments, another batch of HNDs and ONDs was made available, which was primarily intended for the synthesis of decorated nanocomposites. The second batch was analysed as well and the differences in spectra of NDs compared to the first batch can be seen in D.3 in Appendix D. The first batch was first measured approximately 4 months after it was prepared and the second one within a few days of preparation. Assuming that the quality of the colloids after synthesis was the same (since both batches were made by the same methodology and from the same MSY powder), we can clearly see that the stability of HNDs is very low over time. Contrarily, the spectra of ONDs do not change much, indicating stability. The following experiments with colloidal mixtures were conducted with the new "fresh" batches of NDs.

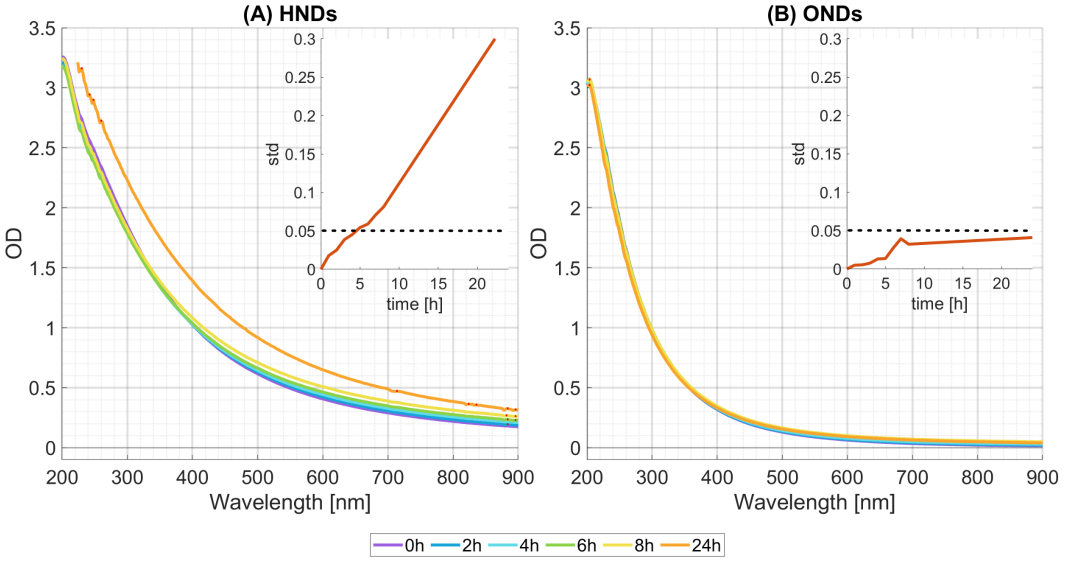

Figure 9.4: Stability of ND colloids with average OD standard deviation. OD dependence on time of (A) HND spectra, (B) OND spectra, with concentrations of 100 μg/ml for both NDs. Mean values OD of triplicates are blank corrected. Insets in each graph show the average standard deviation of OD values in relation to time zero across the spectrum.

Figure 9.5 shows the stability of metal NPs. The spectra of 10 μg/ml AgNPs and 25 μg/ml AuNPs were measured up to 24 hours in the time-points listed above and their OD difference over time did not exceed the 0.05 stability limit of average standard deviation. Therefore, they are both considered stable. Looking closely, the plasmonic peaks do not change their positions over time, which indicates no significant changes in the size of particles caused by agglomeration.

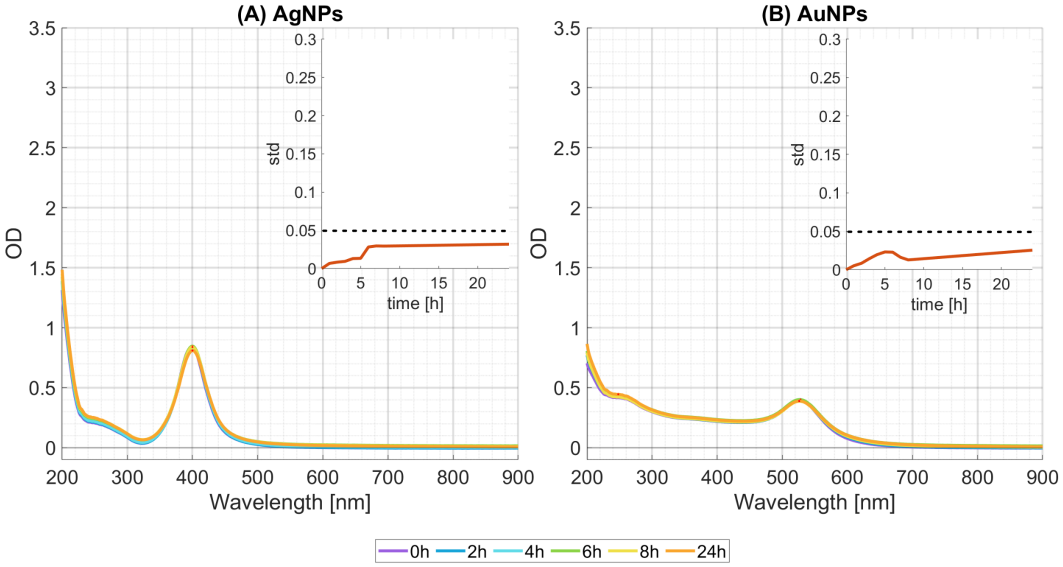

Figure 9.5: Stability of NP colloids with average OD standard deviation. OD dependence on time of (A) AgNPs, (B) AuNPs, with concentrations of 10 μg/ml and 25 μg/ml, respectively. Mean values OD of triplicates are blank corrected. Insets in each graph show the average standard deviation of OD values in relation to time zero across the spectrum.

Zeta potential

Following the spectrophotometry stability measurement, the zeta potential (ZP) of one concentration of each colloid was measured using the workflow described in Section 8.4. Based on the quality evaluation from the Zetasizer software, concentrations of colloids were selected to ensure accurate results. For both NDs, a concentration of 25 μg/ml was chosen and the concentration of AuNPs and AgNPs was 6.25 μg/ml and 2.5 μg/ml, respectively. Because ZP is pH dependent on the colloid, pH values of colloids are listed along with ZP in Table 9.2.

Colloid	c [μg/ml]	ZP [mV]	pH
HNDs	25	23	6.6
ONDs	25	-55	5.6
AuNPs	6.25	-41	6.5
AgNPs	2.5	-36	7.1

Table 9.2: ZP and pH of ND and metal NP colloids with their concentrations.

ZP values of AuNPs, AgNPs and ONDs are all negative and their absolute values are safely above the 30 mV limit of stability according to Section 6.2. Based on ZP, the OND colloid is the most stable with ZP = -55 mV. The HND colloid, on the other hand, is the only one with a positive ZP. Additionally, the low ZP of the HND colloid (ZP = 23 mV), whose absolute value is under 30 mV, points to its instability and corroborates the results from the spectrophotometric measurements.

The pH values of the colloids indicate that all samples apart from AgNPs are slightly acidic with values under 7. Even so, the pH values of HNDs and AuNPs are

only slightly below 7 and therefore slightly acidic. AgNPs have pH = 7.1 so it can be considered neutral.

9.1.3 Structure of Colloids

As the properties of NPs are influenced by their shapes and sizes, the colloids were further investigated using dynamic light scattering (DLS) and scanning electron microscopy (SEM) to elucidate the structural dynamics of the colloidal systems.

DLS

Dynamic light scattering (DLS) was used to more closely investigate the sizes and potential aggregation of nanoparticles in colloids. The steps taken in these measurements are provided in Section 8.4. Figure 9.6 shows the volume distribution of NDs and metal NPs showing the total volume of particles in different size ranges. This distribution was chosen as it indicates larger, agglomerated, particles even though their number is low. The number distribution can be seen in Figure D.4 in Appendix D.

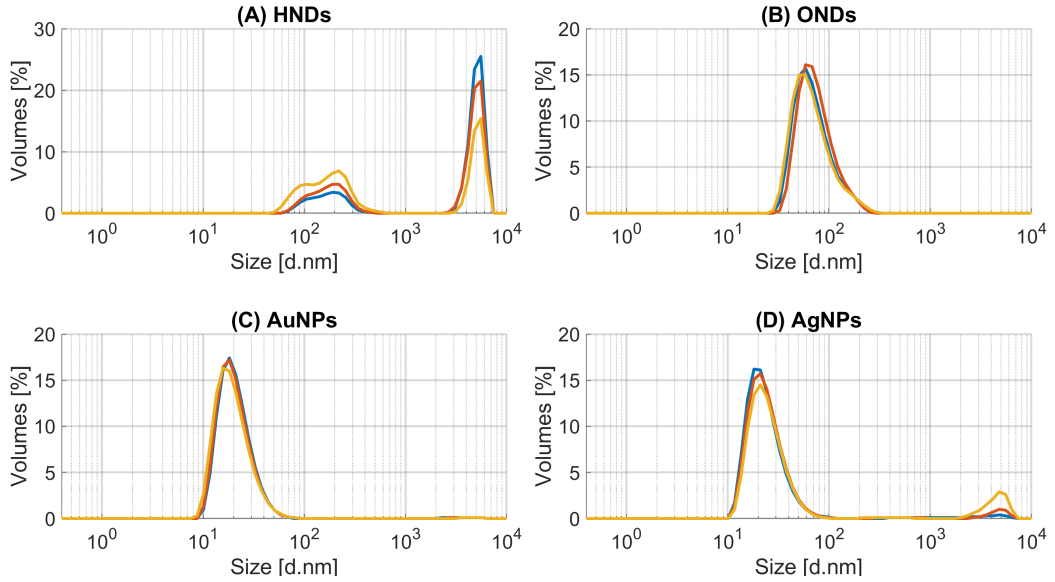

Figure 9.6: Volume distribution of colloids of (A) HND (25 μg/ml), (B) OND (25 μg/ml), (C) AuNP (6.25 μg/ml), (D) AgNP (2.5 μg/ml) from DLS measurements

According to Figure D.4, the mean size of metal NPs was slightly smaller than reported by the provided data sheets, around 15 nm. In Figure 9.6, the little prominence in the volume distribution of AgNPs around 4500 nm can be caused by agglomeration as well as contamination of the sample during preparation. However, the number of particles of this size is so small that it is not projected in the number distribution shown in Figure D.4.

NDs were purchased as powder nanoparticles with a mean reported size of 50 nm. However, they were surfaced modified by hydrogenation (HNDs) and by oxidation (ONDs). These treatments, while aimed at tuning the surface properties of the NDs,

should not change their size. However, they could change their aggregation tendency. OND particles remained around 50 nm in size as seen in their number distribution in Figure D.4 and without larger particles indicating agglomeration according to the volume distribution in Figure 9.6. However, the HND colloid seems to contain much larger particles around 5500 nm in size, which can be seen in the volume distribution in Figure 9.6. In the number distribution, Figure D.4, these bigger particles are not projected and the mean size is determined to be 90 nm. The larger units of HNDs were presumably formed by agglomeration which once again supports the instability of the HND colloid observed by the previous experiments, given mostly by its hydrophobic nature and low ZP.

SEM

To visualise the actual shapes of NPs, scanning electron microscopy (SEM) was performed (see Section 8.5 for more information about the workflow). Images of samples were obtained using secondary electrons (SEs) showing the topography of particle surfaces.

Figure 9.7 shows SEM images of NDs and metal NPs. Both types of NDs have a crystalline shape typical for NPs synthesised by the HPHT method. Based on the images, HNDs (A) seem to form large spatial structures which point to agglomeration. However, some separate particles are still visible. OND (B) particles agglomerate together on the surface of the silicon substrate as well, but the units are smaller and there are more separate particles. This observed agglomeration on the substrate, may be due to sample preparation (drop casting) and will not give us much additional information on the stability of the NDs or their dispersion in the colloid. Metal NPs are shown with their typical spherical shape. AgNPs (D) are nicely distributed with a minimum of merged units. AuNPs (C) seem to form some clusters and their brightness in the images varies.

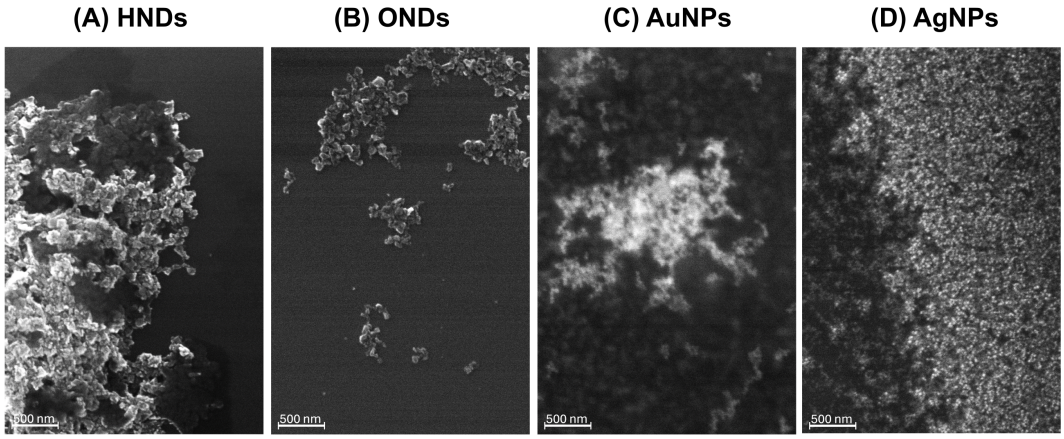

Figure 9.7: Images of NDs and metal NPs from SEM using the signal from SEs. (A) HNDs, (B) ONDs, (C) AuNPs, and (D) AgNPs.

9.1.4 Discussion

The absorption spectra of the colloids gave us important data for subsequent experiments. As expected, plasmonic bands of metal NP colloids with prominent peaks were visible in the VIS region of their spectra. From the absorption spectra, metal NPs seem to be stable, which is supported by their ZP. The size of the metal NPs agrees with the sizes stated by the manufacturers (around 20 nm).

NDs exhibit high absorption in the UV region, which gradually decreases as the wavelength increases. The potential presence of NV centres or any other colour centres is negligible. The most crucial piece of information from the consequent measurements was the instability of HNDs, which needs to be taken into consideration. Due to the sedimentation of NPs in the HND colloid, the appropriate time for studying its optical absorption is right after the sonication of the colloids, ideally within the first 5 hours. The low ZP of HNDs indicates that this colloid can be imperilled by aggregation in the long run. The OND colloid, on the other hand, indicates good stability and based on its number distribution from DLS measurements, their mean size remained 50 nm as the reported mean size of the original MSY particles. Based on DLS measurements, the HND colloid contains particles with a mean size of 90 nm with some larger aggregates present.

Based on the data obtained from the optical absorbance analysis, subsequent analyses were conducted using a concentration of 25 μg/ml for both HNDs and ONDs. This concentration was chosen as its OD values were both lower than plasmonic peak values of both metal NPs and comparable to the overall OD spectra values. This ratio enables the plasmonic peaks of metal NPs to still be detectable in colloidal mixtures and not overshadowed by the NDs. The OD of the NP plasmonic peaks in concentrations below the fourth dilution (2.25 μg/ml for AgNP and 5.625 μg/ml for AuNPs) were poorly detectable with uncertain information. Therefore, to completely cover all acceptable options, each ND colloid with the concentration of 25 μg/ml was mixed with the four highest concentrations of each metal NP. Those colloidal mixtures were further investigated and the results of the measurements performed on these mixtures are presented in the following section.

9.2 Investigation of Colloidal Mixtures of Nanodiamonds and Metal Nanoparticles

The core part of this thesis was to investigate the colloidal mixtures of nanodiamond (ND) and metal nanoparticle (NP). Initially, it was hypothesized that metal NPs might exhibit different behaviour in the presence of HNDs compared to the colloidal mixture with ONDs, owing to the different surface modifications of the NDs. On the other hand, it was anticipated that both AgNPs and AuNPs should behave similarly, given their plasmonic properties and similar surface characteristics.

The colloidal mixtures were prepared through a straightforward procedure of combining two dilutions of colloids and mixing them properly as described in Section 8.2. Due to the instability of HNDs previously observed in Section 9.1, the NDs were sonicated before mixing as a precautionary measure.

The established approach for creating colloidal mixtures involved combining the four highest concentrations of colloids of metal NPs with NDs with the ND concentration fixed at 25 μg/ml. Subsequently, the optical absorption of the newly prepared colloidal mixtures, namely AuHNDs, AgHNDs, AuONDs, AgONDs, was analysed.

9.2.1 The Optical Absorbance of Colloidal Mixtures

The optical absorbance of colloidal mixtures was examined using a spectrophotometer (see Section 8.3.1). The resulting spectra are depicted in Figure 9.8 and the curves are averaged from triplicates. Standard deviations, displayed as see-through planes, are almost undetectable showing the uniformity of the triplicates.

There are visible contributions of both particle types - the ND constituent is manifested by a higher optical absorption in the UV region and the plasmonic band is characteristic for metal NPs. In the near-infrared and infrared spectra, none of the colloidal mixtures have a higher absorbance. Emphasis was placed on observing shifts in plasmonic peak locations and changes in values of their optical absorption, as such changes typically signify interactions between particles or changes of size.

Additionally, all four colloidal mixtures meet the Lambert-Beer theorem stating that their OD is linearly dependent on their concentration as seen in Figure D.8 in Appendix D.

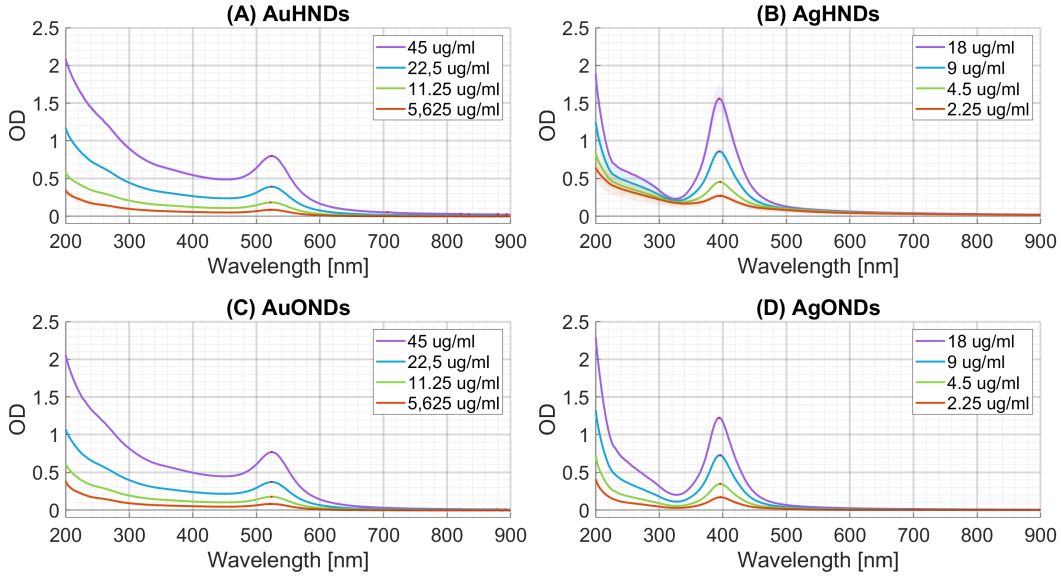

Figure 9.8: Optical absorption of colloidal mixtures of metal NPs and NDs: (A) AuHNDs, (B) AgHNDs, (C) AuONDs, (D) AgONDs. The concentrations of NDs are fixed at 25 μg/ml, the concentration of metal NPs are provided in the legends. Mean OD values are blank corrected and the standard deviation is displayed as a see-through plane.

To highlight the spectral differences, the previously measured OD values of the corresponding NDs were subtracted and are represented by dashed lines in Figures 9.9 and 9.10 focusing specifically on the plasmonic peak regions. Additionally, in these graphs, the spectra of metal NPs themselves are represented by dotted lines. Theoretically, if the colloids were to mix without any interactions between the nanoparticles, the subtracted spectrum (spectrum of the colloidal mixture without the spectrum of its corresponding ND) would align with the spectrum of the corresponding metal NP. This expectation arises because the OD of NDs and metal NPs would simply add up in the absence of interactions.

Figure 9.9 illustrates the spectra of the colloidal mixtures with AuNPs. In graph (A), the spectrum of the colloidal mixture of gold nanoparticles and hydrogenated nanodiamonds (AuHNDs) exhibits notable changes in the OD. At first glance, it appears that HNDs contribute to a reduction of the OD of the AuNP plasmonic peak. It is noteworthy that the subtracted spectrum of the lowest investigated concentration exhibits a negative OD. Conversely, in the graph (B), the colloidal mixture of gold nanoparticles and oxidized nanodiamonds (AuONDs) appear to be more consistent with the spectrum of the AuNP colloid itself.

Figure 9.10 depicts the spectra of colloidal mixtures with AgNPs. The differences between the optical absorbance between the pristine AgNP colloid and the subtracted signal are visible for both, the colloidal mixture of silver nanoparticles and hydrogenated nanodiamonds (AgHNDs) in graph (A) and the colloidal mixture of silver nanoparticles and oxidized nanodiamonds (AgONDs) in graph (B). To further elucidate the behaviour of colloidal mixtures, their plasmonic peaks will be thoroughly examined in the following section.

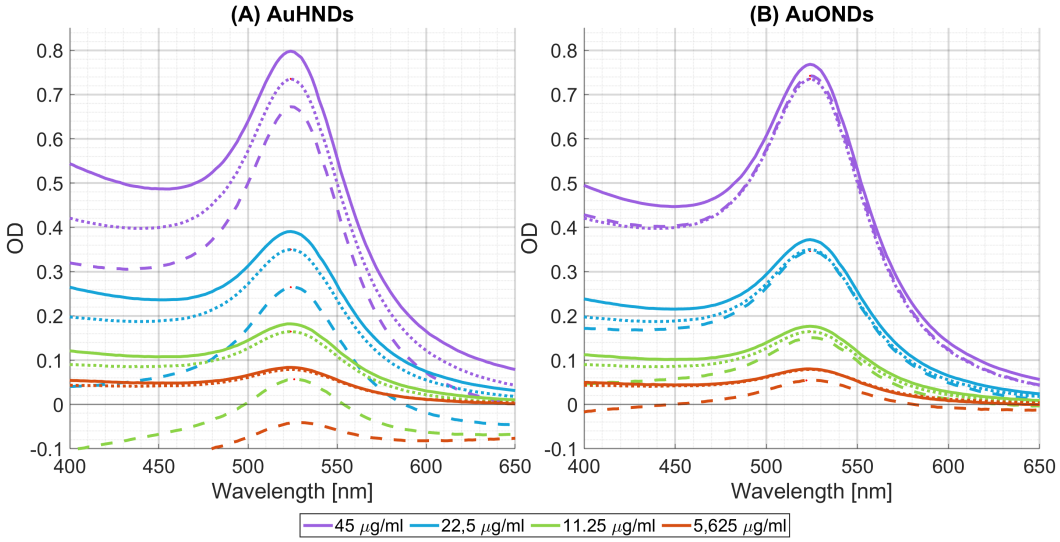

Figure 9.9: Optical absorption of colloidal mixtures of AuNPs with NDs (25 μg/ml) compared with the optical absorption of AuNPs once blank corrected. (A) AuHNDs, (B) AuONDs. Full lines represent the optical spectrum of the colloidal mixtures, dashed lines the colloidal mixture spectrum with subtracted ND spectra and the dotted lines are the spectrum of the metal NPs.

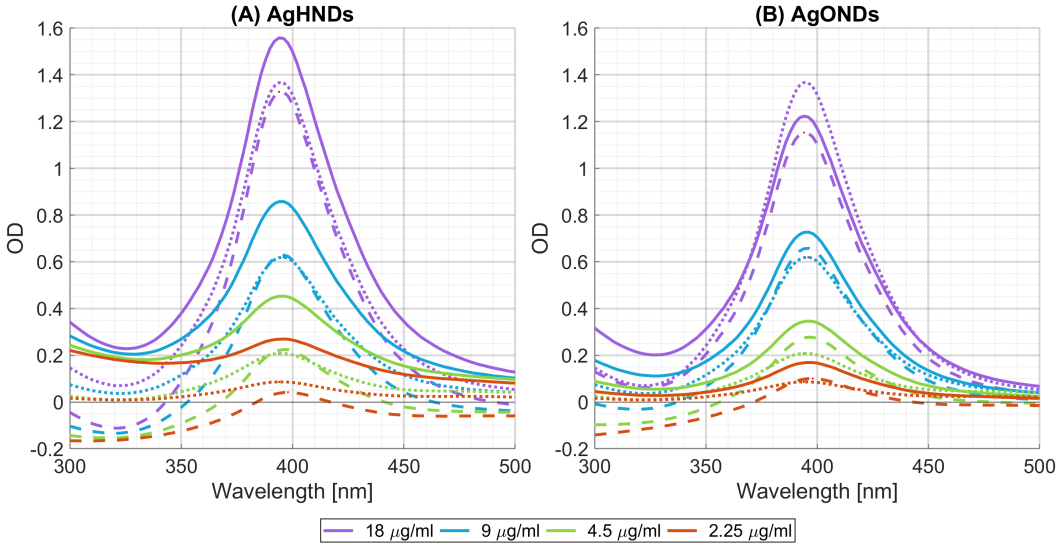

Figure 9.10: Optical absorption of colloidal mixtures of AgNPs with NDs (25 μg/ml) compared with the optical absorption of AgNPs once blank corrected. (A) AgHNDs, (B) AgONDs. Full lines represent the optical spectrum of the colloidal mixtures, dashed lines the colloidal mixture spectrum with subtracted ND spectra and the dotted lines are the spectra of the metal NPs.

Plasmonic Peak Analysis of Colloidal Mixtures

Figure 9.11 shows the dependence of peak location on the concentration of metal NPs. As mentioned previously, changes in plasmonic peak location typically indicate variations in particle size, such as agglomeration. In this case, we would see agglomeration attributed to the presence of NDs, as no relevant peak shifts were present in the pristine metal NP colloids in time and at different concentrations investigated in Section 9.1. In Figure 9.11, the lower concentrations of colloidal mixtures exhibit a more scattered peak location compared to the pristine metal NPs. However, a 2 nm shift cannot be considered conclusive evidence of a different size range, as the wavelength accuracy of the spectrophotometer is ±2 nm. Even if the shifts were due to an increase in particle sizes, only shifts to the higher wavelength would be observed. Moreover, the 2 nm shifts would signify a minimal increase in dimensions compared to the overall size of the particle. Therefore, the agglomeration of particles due to the interaction of NDs and metal NPs in the colloidal mixture is not substantiated by this data.

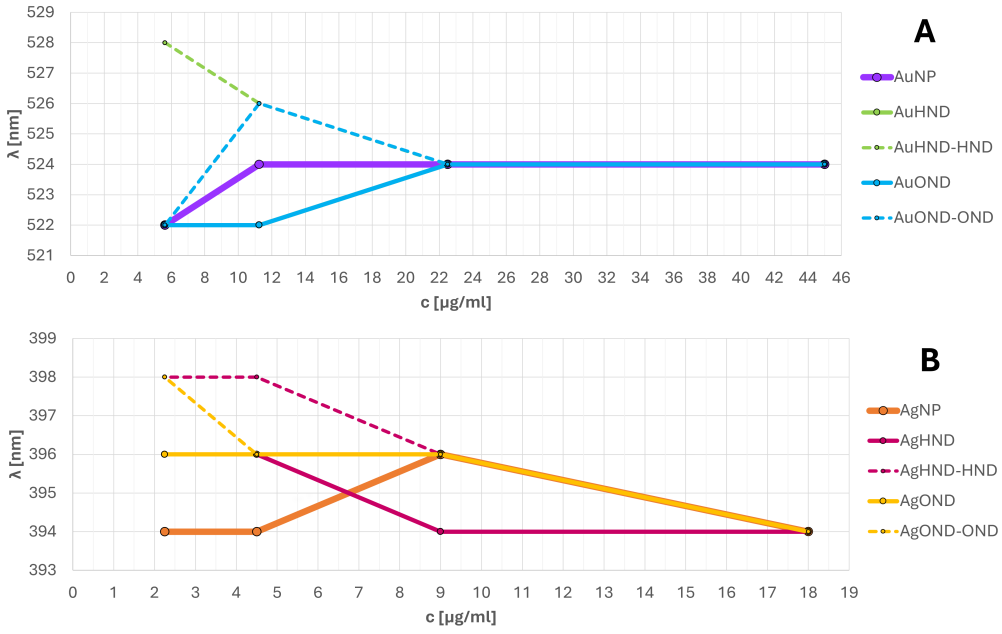

Figure 9.11: Dependence of plasmonic peak location of colloidal mixture on the concentration of metal NPs with ND concentration fixed at 25 μg/ml. (A) colloidal mixture containing AuNPs, and (B) AgNPs. The dashed lines represent values of colloidal mixtures after subtraction of ND spectra.

In Figure 9.12, the dependence of optical absorbance on the concentration of metal NPs is evaluated for colloidal mixtures. All colloidal mixtures contain 25 μg/ml of corresponding NDs and only the concentration of metal NPs differs. There is an obvious difference between the two metal NPs.

The behaviour of the plasmonic peak OD in colloidal mixtures of AgNPs after subtracting the OD of NDs seems to vary. At lower concentrations, the presence of NDs appears to enhance the OD of the AgNP plasmonic peak. However, once

a threshold concentration is reached (in this experiment approximately at 10 μg/ml) the NDs tend to lower the OD of the peak. Notably, ONDs exhibit a steeper decline in the AgNP curve compared to HNDs, where the subtracted curve tends to loosely follow the AgNP curve initially and then gradually cross it.

The colloidal mixtures of AuNPs exhibit the opposite trend. Their subtracted OD is initially lower than the OD of the pristine AuNP colloid and gradually tends to approach it. AuONDs with the highest concentration (45 μg/ml) even surpassed the pristine NP OD once a concentration of 34 μg/ml was reached. It is possible that if the curves continued along this trend, they would eventually surpass the OD of the AuNPs. It was assumed, that this would require either a higher concentration of AuNPs or a lower concentration of NDs. However, results from the next experiment (Figure 9.14) showed that more NDs are needed in the colloidal mixture to observe this effect. Overall, the interaction of AuNPs with HNDs changed the OD more than with ONDs.

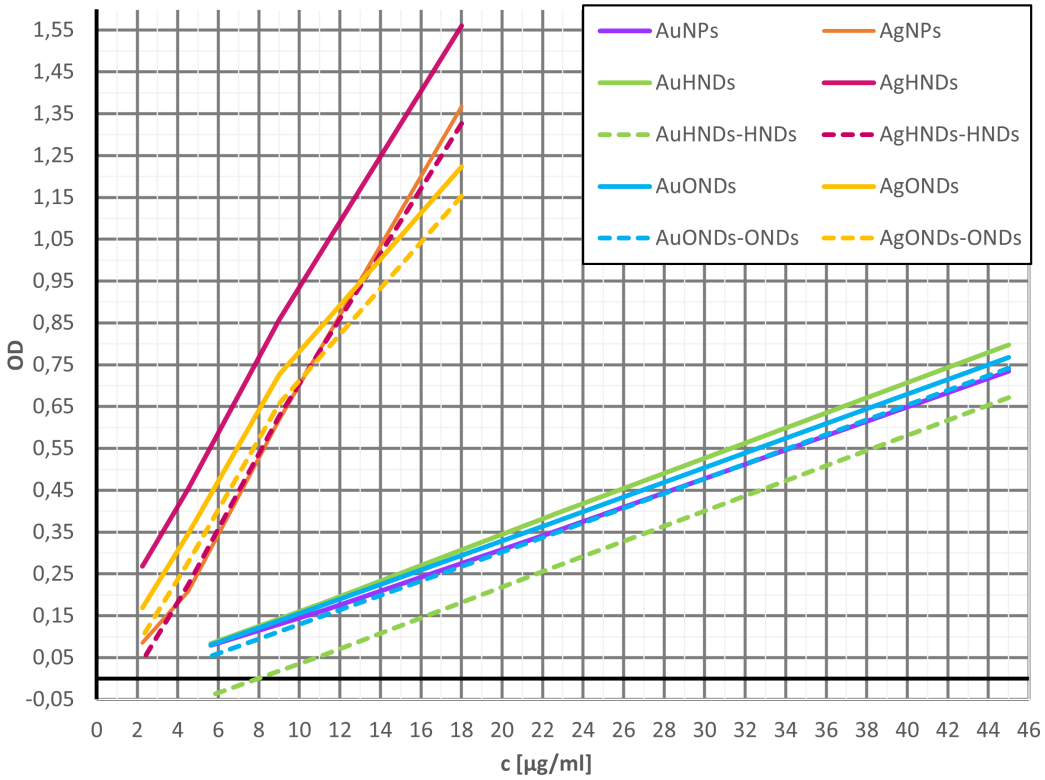

Figure 9.12: Dependence of plasmonic peak OD on the concentration of metal NPs in the colloidal mixtures with 25 μg/ml concentration of NDs. Full lines represent data for colloidal mixtures, while dashed lines depict colloidal mixtures with subtracted ND spectra.

Figure 9.13 displays deviations of the ODs of colloidal mixtures (with subtracted OD of ND 25 μg/ml) from the ODs of metal ND colloids dependent on the relative concentration of metal NPs.

These observations suggest a change in the optical absorption of colloidal mixtures in the presence of a specific combination and concentration of NDs and metal NPs.

To prove the difference in the behaviour of AgNPs and AuNPs, the experiment was repeated. The concentrations of metal NPs remained the same, but the concentration of NDs was lowered to 6.25 μg/ml (one-fourth of the previous value). That means that there will be more metal NPs for each ND particle.

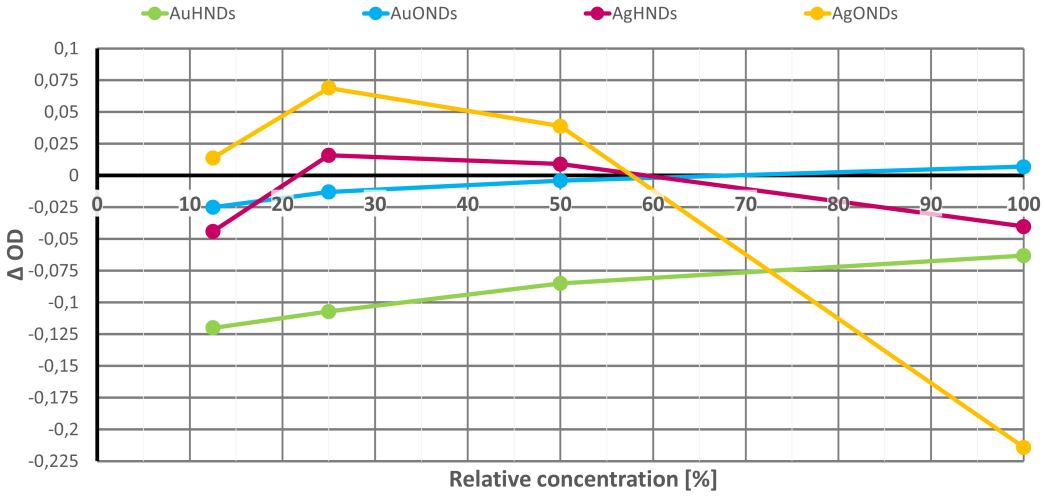

Figure 9.13: Deviations of plasmonic peak OD of colloidal mixtures with subtracted NDs (25 μg/ml) from the OD of pristine metal NP colloids dependent on the relative concentration of metal NPs expressed as a percentage.

Figure 9.14 illustrates the dependency of the plasmonic peak OD on the concentration of metal NPs in colloidal mixtures with NDs at a concentration of 6.25 μg/ml. The entire spectrum can be seen in Figure D.5 in Appendix D. The trend of colloidal mixtures of AgNPs mirrors that of Figure 9.12. The region of the curve crossing is zoomed in to provide a clearer depiction of this transition. The crossing of the AgNP linear trend lines, took place at approximately 6 μg/ml for both AgHND and AgOND in the presence of 6.25 μg/ml of NDs.

Conversely, the subtracted curves of colloidal mixtures with AuNPs commenced below the pristine AuNP colloid's OD curve and gradually approached it, but neither curve crossed. Mixtures with both types of NDs ran parallel along the AuNP line after the concentration of 11 μg/ml was reached. A comparison with the previous results in Figure 9.12 indicates that to surpass AuNPs OD more NDs are needed in the colloidal mixture.

The deviations of plasmonic peak ODs of colloidal mixtures with subtracted OD of ND (6.25 μg/ml) are presented in Figure D.6 along with the dependence of their peak location in Figure D.7 in Appendix D.

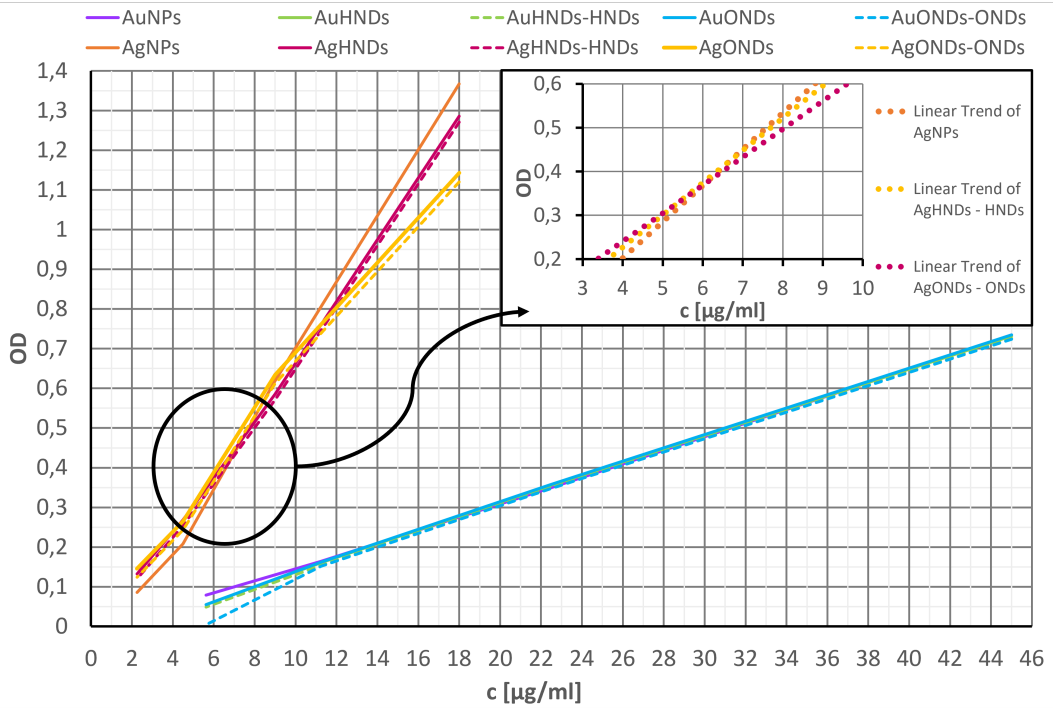

Figure 9.14: Dependence of plasmonic peak OD on the concentration of metal NPs with a 6.25 μg/ml concentration of NDs. Full lines represent data for colloidal mixtures, while dashed lines depict colloidal mixtures with subtracted ND spectra.

The contrasting behaviour observed in the colloidal mixtures containing AgNPs and AuNPs prompts new questions regarding the potential interactions of particles within the colloidal mixture. To formulate possible hypotheses, it is essential to investigate the possible effects of their stability and structure. Exploring these aspects will provide deeper insights into the underlying mechanism driving the observed phenomena.

9.2.2 Stability of the Colloidal Mixtures

The stability of all colloidal mixtures was evaluated by spectrophotometry, with the micro-well plate left in an incubator set at 37 °C overnight between measurements as described in Section 8.3.2. The OD values are an average from triplicate samples. Figure 9.15 presents a comparison of spectra of colloidal mixtures with the concentration of NDs at 25 μg/ml at time zero and after 24 hours, represented by a full line and a dashed line, respectively. Colloidal mixtures with AuNPs demonstrate consistent stability across the spectrum, with a total average standard deviation (the average of all average standard deviations) from all concentrations around 0.014 and 0.016 in OD for AuHNDs and AuONDs across concentrations and the spectrum, respectively.

HNDs appear to cause a more pronounced decrease in OD in (B) AgHNDs, indicating agglomeration. Its total average standard deviation of OD of all concentrations is 0.12, with the largest difference observed for the highest

concentration (average standard deviation 0.212). Assuming that the colloid is considered stable if the average standard deviation is under 0.05, the colloidal mixture AgHNDs is unstable. The AgOND colloid remained stable with a total average standard deviation of 0.026. However, the highest concentration of AgONDs was beyond the stability limit (average standard deviation 0.066). The average standard deviation of OD across the spectrum for each colloidal mixture and metal NP concentration is listed in Table 9.3.

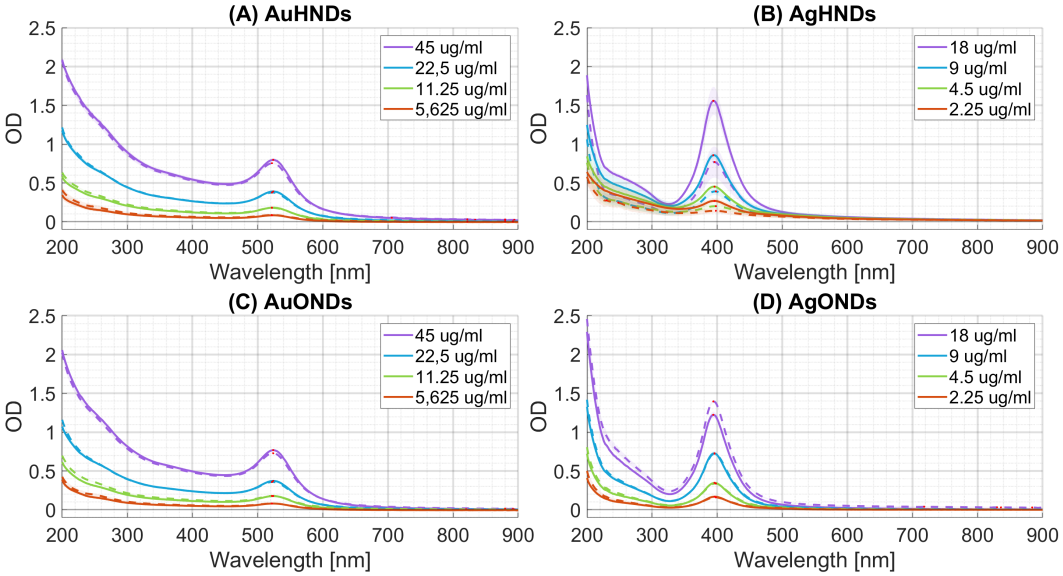

Figure 9.15: The stability of colloidal mixtures of metal NP and ND at time zero and after 24 hours. (A) AuHNDs, (B) AgHNDs, (C) AuONDs, (D) AgONDs, full lines represent spectra at time zero and dashed lines represent spectra after 24 hours. Spectra are blank corrected. The standard deviation of triplicates is projected as a see-through plane. The concentration of NDs in the colloidal mixture is 25 μg/ml. Concentrations of metal NPs are listed in legends.

concentration [μg/ml]	AuHNDs	AgHNDs	AuONDs	AgONDs
45	0.019	-	0.022	-
22.5	0.008	-	0.012	-
18	-	0.212	-	0.066
11.25	0.014	-	0.020	-
9	-	0.139	-	0.013
5.625	0.015	-	0.012	-
4.5	-	0.077	-	0.013
2.25	-	0.054	-	0.012

Table 9.3: The change of the OD of colloidal mixtures after 24 hours formulated as average standard deviation across the spectrum for each concentration. The concentration of NDs was 25 μg/ml and the concentration of metal NPs is provided in the table.

In the colloidal mixtures with AuNPs, the plasmonic peak appears to shift towards larger wavelengths on average by approximately + 2 nm. While this shift may seem insignificant considering the spectrophotometer's accuracy of ±2 nm, it still provides interesting insights, especially comparing it with the behaviour of the colloidal mixtures with AgNPs, which exhibit a plasmonic peak shift towards smaller wavelengths on average by approximately - 2 nm.

After 24 hours, small dark seeds appeared at the bottom of the wells with the highest concentrations of AgHNDs as observed in Figure 9.16. The sedimentation of particles affected the OD since the absorption is measured by the transmission of light. To corroborate these spectrophotometry results, the ZP of colloidal mixtures was measured as well.

Figure 9.16: Photos of micro-well plates at (A) time zero and (B) after 24 hours with wells, where black seeds occurred, marked in red.

Zeta potential

ZP was measured alongside pH for the colloidal mixtures to evaluate their stability (steps of the procedure are given in Section 8.4). Data listed in Table 9.4 confirm the hypothesis that colloidal mixtures containing HNDs are unstable, as their absolute ZP values are below 30 mV. Surprisingly, AuHNDs exhibit higher instability of the two HND mixtures with ZP = -10 mV, contradicting the results from the spectrophotometry stability experiment, where the AgHND spectrum changed the most. However, its ZP value is higher (-25 mV). The ZP of AuONDs and AgONDs is -39 mV and -37 mV, respectively, indicating stability. Notably, the ZP of all colloidal mixtures is negative. The discrepancies between ZP values and optical absorption measurements over time may arise because ZP is only a sign, not the only condition determining stability. All of the samples are slightly acidic based on their pH values.

Colloids	c [μg/ml]	ZP [mV]	pH
AuHNDs	5.625	-10	6.5
AuONDs	5.625	-39	5.6
AgHNDs	2.25	-25	6.8
AgONDs	2.25	-37	6.8

Table 9.4: ZP and pH of colloidal mixtures. The concentration listed in the table is the concentration of the metal NPs in the colloidal mixture. The concentration of NDs was 25 μg/ml.

9.2.3 Structure of Colloidal Mixtures

Based on data obtained from spectrophotometry and ZP measurements, questions arise regarding the structural properties of the colloidal mixtures. The observed phenomena of the dependency of colloidal mixtures' OD on the type of metal NPs and their concentration may be due to structural changes of particles. The fundamental question revolves around understanding how the particles interact physically and whether they form complexes when combined. More information about these aspects can be gained from DLS analysis of particle size and from SEM imaging.

DLS

The volume distribution of the colloidal mixtures' particle size is graphically depicted in Figure 9.17 and their number distribution is presented in Figure 9.18. The DLS measurements were conducted approximately 3 hours after the preparation of colloidal mixtures according to Section 8.4.

Table 9.5 shows the mean values of particle sizes in colloidal mixtures obtained from DLS measurements and the mean sizes of individual colloids studied in Section 9.1.3. It is assumed, that if the ND attach to the metal NP, the complexes should be at least 70 nm in size.

In the number distribution (Figure 9.18) of AuHNDs, graph (A), a significant percentage of 20 nm AuNPs is observed. However, the volume distribution, Figure 9.17 (A), shows a high peak at 5000 nm, possibly indicating a few agglomerated particles comprising merged units of HNDs and AuNPs. In graph (B) of the number distribution of AgHNDs, the mean size of particles is estimated at around 70 nm. Once again, a significant percentage of 5500 nm particles in the volume distribution suggests agglomeration. AuHNDs seem to form fewer complexes and more AuNP particles remain alone compared to AgHNDs. Based on the measurement of the optical absorption of the colloidal mixtures (Section 9.2.1), agglomeration concerns mainly NDs, as it does not manifest itself in the plasmonic peak shift of metal NPs.

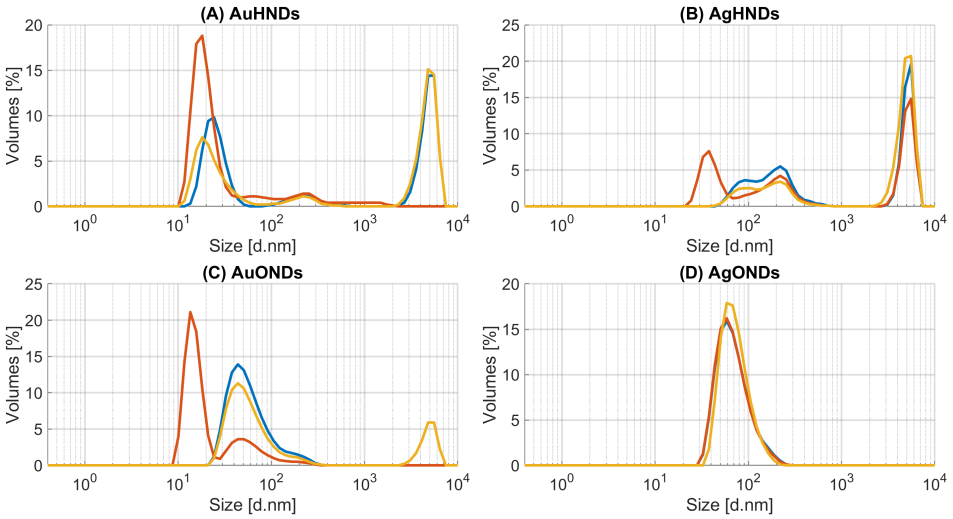

Figure 9.17: Volume distribution of colloidal mixtures from DLS. (A) AuHNDs (6.25 μg/ml), (B) AgHNDs (2.5 μg/ml), (C) AuONDs (6.25 μg/ml), (D) AgONDs (6.25 μg/ml), where the given concentration is that of the metal NPs in the colloidal mixture. The concentration of NDs for all four mixtures was 25 μg/ml.

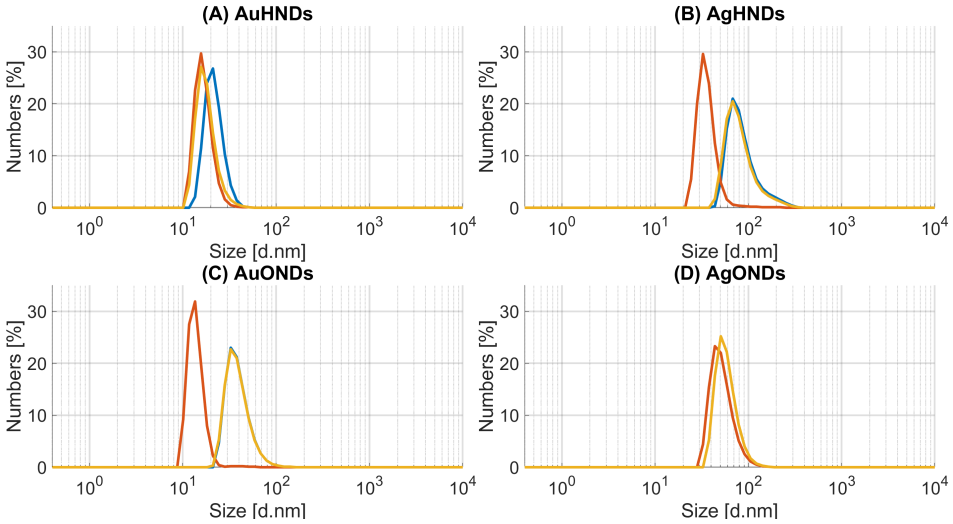

Figure 9.18: Number distribution of DLS particle sizes in the colloid of (A) AuHND (6.25 μg/ml) , (B) AgHND (2.5 μg/ml), (C) AuOND (6.25 μg/ml), (D) AgOND (6.25 μg/ml), where the concentration of ND in the colloidal mixtures is 25 μg/ml.

In colloidal mixtures with ONDs (graphs (C) and (D) of volume distribution (Figure 9.17)), there is no significant evidence of agglomerated particles. In the number distribution, Figure 9.18, AuONDs particles with a mean size of 32 nm are present and AgONDs display a peak at 50 nm. Consequently, complexes may possibly exist in both types of colloidal mixtures AuONDs and AgONDs since there is the presence of particles with sizes above 70 nm. Particles in both colloidal mixtures containing ONDs appear to not agglomerate at least in the short term.

Colloids	c [μg/ml]	mean size [nm]
HNDs	25	90
ONDs	25	50
AuNPs	6.25	15
AgNPs	2.5	15
AuHNDs	5.625/25	20
AuONDs	5.625/25	32
AgHNDs	2.25/25	70
AgONDs	2.25/25	50

Table 9.5: Mean Particle sizes of colloidal mixtures and individual colloids with their concentration listed. In the case of the concentration of colloidal mixtures, the number before the slash gives metal NP concentration and the number after the slash gives ND concentration.

SEM

SEM images of colloidal mixtures (Figures 9.19 and 9.20) were taken, according to the procedure from Section 8.5, to investigate the morphology of the particles in the colloidal mixtures. These visualisations were created by combining images obtained from SEs and BSEs by Ing. Markéta Šlapal Bařinková. The background is an SE image with the signal showing the structures in the colloidal mixture. A mask from the BSEs with metal NPs marked red is overlaid, for better distinction of NDs and metal NPs.

As depicted in Figure 9.19 (A) showing AuHNDs, HNDs form mostly large clusters with unevenly distributed AuNPs on the surface. Conversely, image (B) AuONDs shows that the ONDs do not tend to form clusters as tightly packed as those of AuHNDs and the AuNPs are more evenly spread out with only a few groupings on the surfaces of ONDs.

Figure 9.20 shows colloidal mixtures containing AgNPs. Both NDs formed larger clusters and red-coloured AgNPs are evenly distributed on their surfaces. Defined complexes have been formed in AgONDs and the presence of free AgNPs outside the ND structure is minimal. Conversely, AgHNDs formed a bulky structure and there is evidence of free AgNPs outside the surface.

The large cluster formation is more likely due to the preparation process (drop-casting) of samples for SEM imaging since data from DLS measurement (Section 9.2.3) does not show the presence of such a large number of particles of this size in any of the colloidal mixtures. In all sample images, there are just a few metal NPs in the mixture that are not on the ND surface. Therefore, it is assumed, that metal NPs were bound to the surface of NDs before the colloidal mixtures were drop-cast, rather than merely settling on the surface during evaporation. This is evidence of nanocomplex formation in the colloidal mixtures.

These SEM images complement our findings that there are more interactions between particles in AuHNDs than in AuONDs. On the other hand, AgOND particles are more active in forming nanocomplexes than AgHNDs.

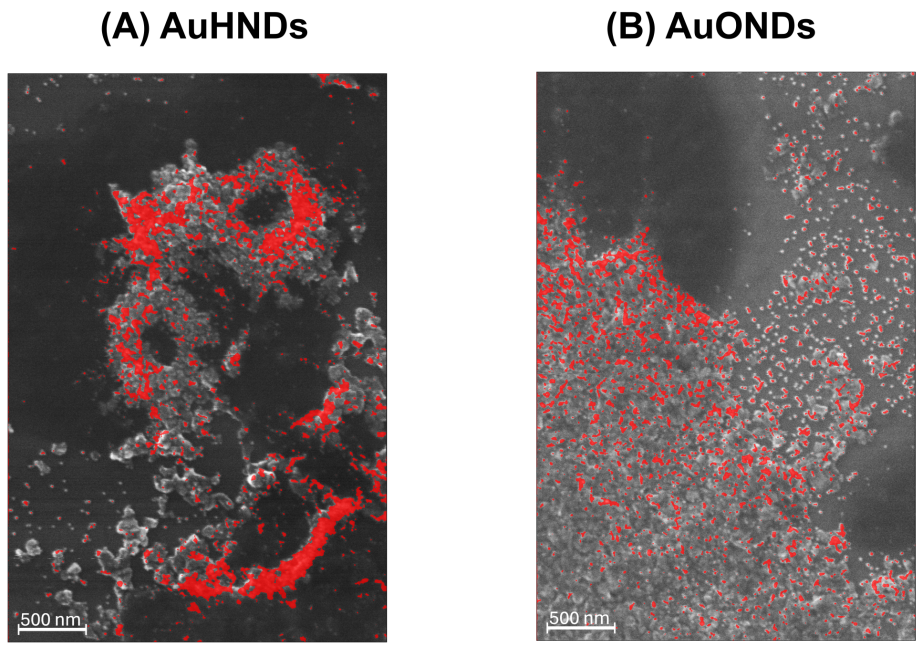

Figure 9.19: Images of colloidal mixtures containing AuNPs from SEM. The background was obtained from SEs and red-marked areas are AuNPs from BSEs. (A) AuHNDs, (B) AuONDs

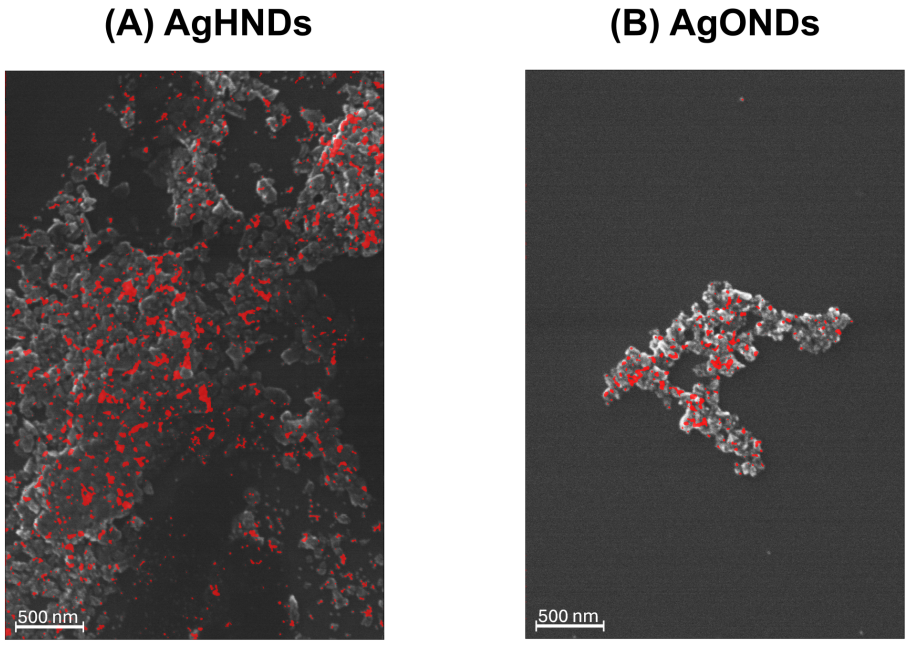

Figure 9.20: Images of colloidal mixtures containing AgNPs from SEM. The background was obtained from SEs and red-marked areas are AgNPs from BSEs. (A) AgHNDs, (B) AgONDs

9.2.4 Discussion

The optical absorbance experiment revealed complex phenomena regarding the behaviour of different metal NPs in the colloidal mixture. In colloidal mixtures containing AgNPs (AgHNDs and AgONDs), the presence of NDs led to an increase in the absorption of plasmonic peaks at lower concentrations of the metal NP. As the concentration of AgNPs in the mixture increased, the distance between the lines decreased. Eventually, the OD of the subtracted colloidal mixture decreased under that of the AgNPs alone and the distance between the OD curves began to increase.

The colloidal mixtures containing AuNPs exhibited the opposite effect. In these mixtures, the presence of NDs initially resulted in a decrease in the absorption of the plasmonic peak, compared to the pristine AuNP colloid. As the concentration of the AuNPs in the mixture increased, the distance between the OD of the subtracted colloidal mixture and AuNPs alone started to decrease. However, the surpass of the pristine AuNPs was observed only for AuONDs with a concentration of 25 μg/ml of ONDs and was very slight. For other colloidal mixtures with AuNPs, it is assumed that the behaviour would be the same if the concentration of NDs were higher.

The type of NDs in the colloidal mixture also affects optical properties. HNDs in a mixture with AuNPs change the OD more than ONDs. Contrarily, the presence of ONDs leads to more significant changes in OD in the mixture with AgNPs than the presence of HNDs.

Outside the plasmonic peak region, all investigated colloidal mixtures followed the Lambert-Beer law. Moreover, there was no immediate indication of the agglomeration of metal NPs when colloids of AgNPs and AuNPs were mixed with ND colloids. However, the AgHNDs exhibited a significant decrease in stability after 24 hours. All four colloidal mixtures had negative ZP values. The absolute values of ZP of colloidal mixtures with HNDs (AgHNDs and AuHNDs) were lower than 30 mV, which may predict the instability. On the other hand, both mixtures containing ONDs presented negative ZP, with absolute values 30 mV, pointing to their stability. Based on these results and data from stability measurements of individual colloids (Section 9.1.2), it is most appropriate to examine the optical properties of the colloidal mixtures immediately after their preparation or within 5 hours, especially for HND mixtures.

The DLS analysis of the colloidal mixtures reveals significant differences in particle size distribution and agglomeration dynamics across different combinations of metal NPs and NDs. The presence of agglomerated particles is particularly evident in colloidal mixtures containing HNDs, although it is not consistently reflected in the absorption spectra through the plasmonic peak shift. Therefore, the agglomerate particles are most likely only formed by NDs, or metal NPs within them remain separate. Based on the number distribution, more complexes seem to be formed in colloidal mixtures with AgNPs than with AuNPs, especially in the case of AgHNDs, which have a mean particle size of 70 nm. The presence of these formations of nanocomplexes is further supported by SEM images, which depict the presence of metal NPs adhering to the surfaces of NDs. Since there is

a minimum of metal NPs seen unattached to ND surfaces, the localization of NPs is not solely due to the sedimentation of particles during the drop-casting. The formation of nanocomplexes of metal NPs and HNDs can be induced electrostatically since HNDs have a positive ZP, while the ZP of metal NPs is negative. However, the ZP of ONDs is negative therefore chemical effects or other forces must be working against electrostatic repulsion in the complexes containing ONDs. Some light can be shed on the properties of colloidal mixtures and the formation of their nanocomplexes by comparing them with directly synthesised nanocomposites prepared by Ing. Kateřina Kolářová, Ph.D. The outcome of this comparative analysis is presented in Section 9.3. Before that, a few possible factors of the observed optical phenomenon in the colloidal mixtures are proposed.

Plasmonic Model

There is no obvious explanation of the different crossing phenomena of the curves of metal NPs in colloid with NDs. There is no significant peak shift in the spectra of colloidal mixtures compared to spectra of colloids of pristine metal NPs, implying the consistent size of metal NPs in all measured colloids. Therefore, the agglomeration of metal NPs is not considered the potential cause of the crossing phenomena. Given the uncertainty surrounding the presence and concentration of NV centres (or any other colour centres) in the NDs, it is also unlikely that NV centres play a role in these phenomena.

The main difference between the behaviour of the two metal nanoparticles in this model would be caused by the differences in their ionisation energies. AuNPs, which possess a higher ionisation energy compared to AgNPs, may tend to bind their electrons more tightly. This implies that AgNPs may have more free electrons than AuNPs to participate in LSPR processes. This also means the possibility of electrons being more readily released from AgNPs. In complexes with NDs, the metal NPs would then act differently, as explained below.

At a lower AgNP concentration on the ND surface, mutual synergy can occur due to the contribution of electrons from the ND to the LSPR oscillation of electrons of AgNP, possibly leading to an increase of overall OD of the plasmonic peak. NDs only have a finite number of available electrons and have to distribute them between the interacting metal NPs. The more particles are on the surface of ND, the fewer electrons each of them will receive, resulting in a smaller ND contribution to the LSPR. As the concentration of AgNPs increases, the surface of the ND may become saturated and the ability of ND to increase the LSPR effect of AgNPs may fade. When AgNPs are even more densely accumulated on the ND surfaces, the electron oscillation caused by LSPR may be disturbed by destructive interference of AgNPs and their total OD may thus decrease.

Conversely, at a lower concentration of AuNPs, NDs may suppress the plasmonic effect of the AuNPs on their surfaces by blocking electrons that might otherwise participate in LSPR. Once the ND is saturated, its restraining influence may decrease. With increasing concentrations of AuNPs, their mutual proximity may then amplify their LSPR, increasing the OD of the plasmonic peak. The constructive interference of densely accumulated AuNPs, as opposed to the destructive interference of densely

packed AgNPs, may be given by their low number of free electrons and the overall stability of their plasmons.

Constructive and destructive interferences of plasmonic metal NP local fields had been studied using optical simulation conducted by Hiroki Gonome[52] from Yamagata University - Japan, in 2019, using the COMSOL and the Wave Optics module. Electric field vectors in 3D assemblies of plasmonic particles were simulated to explore the resonance effect and the rotation of the electric field. The simulations revealed that the interference effect and radiative properties of the particles are influenced by factors such as their distance, diameter, material, number, and background refractive index. Analysis of the vector mapping of local fields indicated that silver particles may exhibit weaker field compared to gold particles, attributed to the field scattering,[52] which corresponds with the results we have seen.

This model can be explained in mixtures containing HNDs, which are electrically conductive, and therefore more favourable for charge transfer. In the case of electrically resistive ONDs, charge transfer is less likely, but the polarization of particles can help explain the model. Polarization may facilitate electric interactions by creating dipoles and a local electromagnetic field, which can transfer charges even though ONDs do not have free electrons.

To validate this hypothesis, a more comprehensive investigation is necessary. More concentration ratios of NDs and metal NPs should be examined. Due to the influence of concentration ratios on optical properties, all colloidal mixtures of these ratios should undergo scrutiny for their stability, ZP, and structure. Additionally, capturing the morphology of nanocomplexes via TEM would be beneficial. Further information could be gained by assessing the strength of bonds between NDs and metal NPs using techniques like atomic force microscopy (AFM) or surface-enhanced Raman spectroscopy (SERS). The electromagnetic fields of the particles can be investigated via mathematical model computing (for example in COMSOL). These methods may also reveal other explanations for this phenomenon.

9.3 Comparison of Colloidal Mixtures and Directly Synthesised Nanocomposites

Directly synthesised nanocomposites of hydrogenated nanodiamonds and silver nanoparticles supported by chitosan (HNDs-Chit-Ag) and oxidized nanodiamonds and silver nanoparticles supported by PVP (ONDs-PVP-Ag), prepared by Ing. Kateřina Kolářová, Ph.D., see Section 7.3, were characterised by the analysis of their optical absorbance, stability and morphology. These nanocomposites were compared to the colloidal mixtures of AgNPs (AgHNDs and AgONDs) investigated in the previous sections.

9.3.1 Optical Absorption

Directly synthesised nanocomposites were analysed using the spectrophotometry method explained in Section 8.3.1, and their spectra are depicted in Figure 9.21. The characteristic plasmonic peak of AgNPs was expected around 400 nm. However, in the spectrum of HNDs-Chit-Ag (A), there is no visible peak in this region. The peak located around 270 nm most likely belongs to the chitosan constituent of this nanocomposite. The plasmonic peak of AgNPs was most likely overshadowed by the optical absorbance of HND due to the low number of AgNPs and therefore, it is not detectable in the spectrum. The peak observed in the (B) graph of ONDs-PVP-Ag, located around 420 nm, could be the plasmonic peak of AgNPs, since PVP does not typically exhibit a prominent peak in its absorption spectrum. The plasmonic peak location at 420 nm may suggest larger silver particles in the colloid, leading to a shift in the plasmonic resonance towards higher wavelengths and a decrease of the OD of their plasmonic peak.

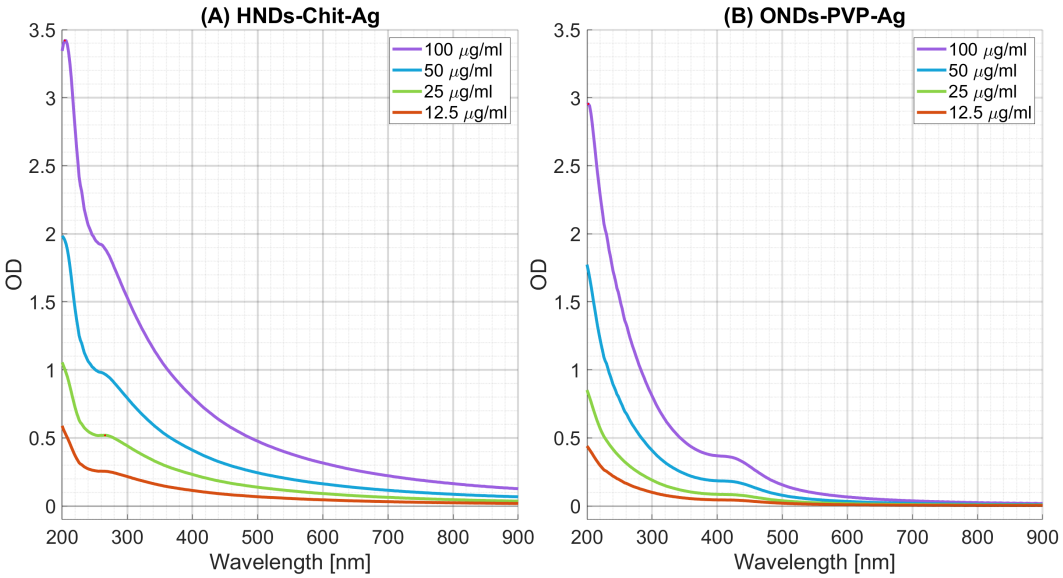

Figure 9.21: The optical absorption of directly synthesised nanocomposites (A) HNDs-Chit-Ag, (B) ONDs-PVP-Ag. The concentrations in the legend belong to the assumed concentration of NDs.

Both directly synthesised nanocomposites meet the Lambert-Beer Law stating that their OD is linearly dependent on their concentration as seen in Figure D.9 in Appendix D.

9.3.2 Stability

The stability experiment of synthesised nanocomposites is presented in Figure 9.22 and shows the change of the spectra after 24 hours. The experiment steps are explained in Section 8.3.2. The full line represents the spectrum at time zero, while the dashed line corresponds to the spectrum after 24 hours of incubation at 37 °C.

In graph (A), HNDs-Chit-Ag exhibits a decrease in OD. However, there is an abnormal increase in OD for the concentration 50 μg/ml of HNDs across the spectrum, which is unexpected compared to its other concentrations.

In graph (B), ONDs-PVP-Ag shows the expected decline in the spectrum, and the peak at 420 nm diminished too. Both directly synthesised nanocomposites, HNDs-Chit-Ag and ONDs-PVP-Ag, are considered unstable, as their total average standard deviations are 0.15 and 0.08, respectively, over the 24-hour period.

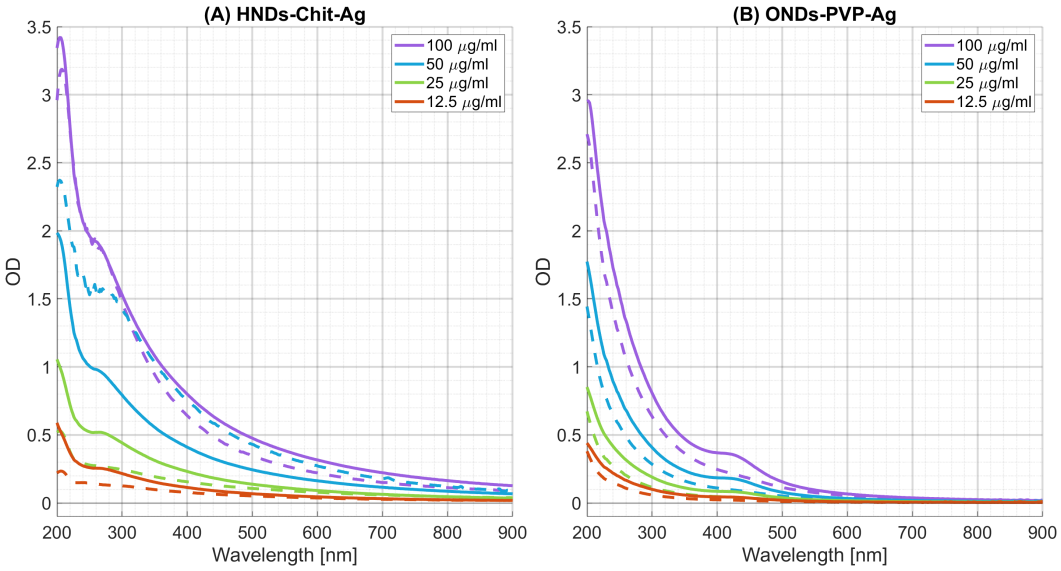

Figure 9.22: The stability of directly synthesised nanocomposites after 24 hours. (A) HNDs-Chit-Ag, (B) ONDs-PVP-Ag. The full line represents the spectrum at time zero, and the dashed line after 24 hours.

Zeta potential

ZP was measured for both HNDs-Chit-Ag and ONDs-PVP-Ag at an approximate ND concentration of 25 μg/ml according to the procedure described in Section 8.4. Both nanocomposites have absolute ZP values above the 30 mV limit indicating stability, although the spectrophotometry stability experiment suggested otherwise. The HNDs-Chit-Ag composite has a positive ZP, while the ONDs-PVP-Ag composite has a negative ZP. The specific values of ZP and their corresponding pH values are listed in Table 9.6.

In comparison with the colloidal mixtures, AgHND had negative ZP values. The positive value of HNDs-Chit-Ag can potentially be explained by the presence of chitosan or by a very low number of AgNP. Both measured directly synthesised nanocomposites had acidic pH.

Solution	ZP [mV]	pH
HNDs-Chit-Ag	45	5.0
ONDs-PVP-Ag	-34	5.8

Table 9.6: Zeta potential and pH of directly synthesised nanocomposites with an approximate ND concentration of 25 μg/ml.

9.3.3 Structure

Given the discrepancy between the spectrophotometric measurements and ZP measurements, suggesting a potentially low number of AgNPs in the directly synthesised nanocomposites, further investigation into the structural properties of these nanocomposites was deemed necessary. The morphology was investigated by DLS, SEM, and TEM.

DLS

Both directly synthesised nanocomposites were measured by the DLS method at an ND concentration of 25 μg/ml (according to Section 8.4). The volume distribution from the DLS measurement in Figure D.10 in Appendix D indicates that HNDs-Chit-Ag and ONDs-PVP-Ag form larger units around the mean size of 200 nm and 100 nm, respectively.

In the number distribution (Figure 9.23) HNDs-Chit-Ag shows particles with a mean size of 50 nm and a wider size distribution. ONDs-PVP-Ag appears to contain a single distribution of particles with a mean value of around 70 nm. Based on the results, the ONDs-PVP-Ag probably contains a significant amount of nanocomposites of ONDs and AgNPs, unlike HNDs-Chit-Ag.

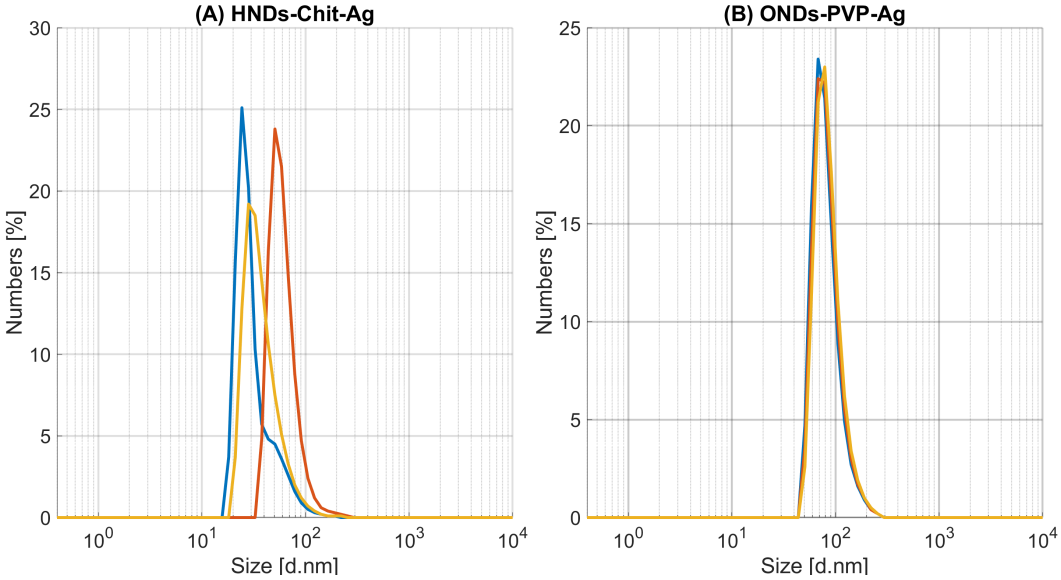

Figure 9.23: The number distribution of particle size of directly synthesised nanocomposites, (A) HNDs-Chit-Ag, (B) ONDs-PVP-Ag, with an approximate ND concentration of 25 μg/ml.

Conversely, according to the number distribution in Section 9.2.3, in colloidal mixtures, AgHNDs form larger structures (70 nm) than AgONDs (50 nm). ONDs in AgONDs could contain fewer AgNPs on the OND surface due to the same sign of their ZP and therefore their weaker interaction. On the other hand, AgNPs formed directly on the ONDs supported by PVP (ONDs-PVP-Ag) should exhibit stronger bonds. In AgHNDs, HNDs and AgNPs interact well, forming complexes. Contrarily, as it was observed in the absorption spectrum of HNDs-Chit-Ag, the number of AgNPs on the HNDs surface supported with chitosan is very low, therefore the nanocomposites reach smaller dimensions. To support these results and to see if HNDs-Chit-Ag form nanocomposites as well, SEM and TEM were performed.

SEM

SEM images, presented in Figure 9.24, were obtained according to Section 8.5. HNDs-Chit-Ag images show that ND particles combine into bigger units caused by agglomeration, most likely due to drop casting. BSE images of HNDs-Chit-Ag indicate very few AgNPs attached to HND, which explains the absence of the prominent plasmonic peak in the absorption spectrum. ONDs-PVP-Ag forms bigger units as well but the NDs contain more AgNPs on their surface. In both colloids, it seems that some NDs are without attached AgNPs, however, all AgNPs seem attached.

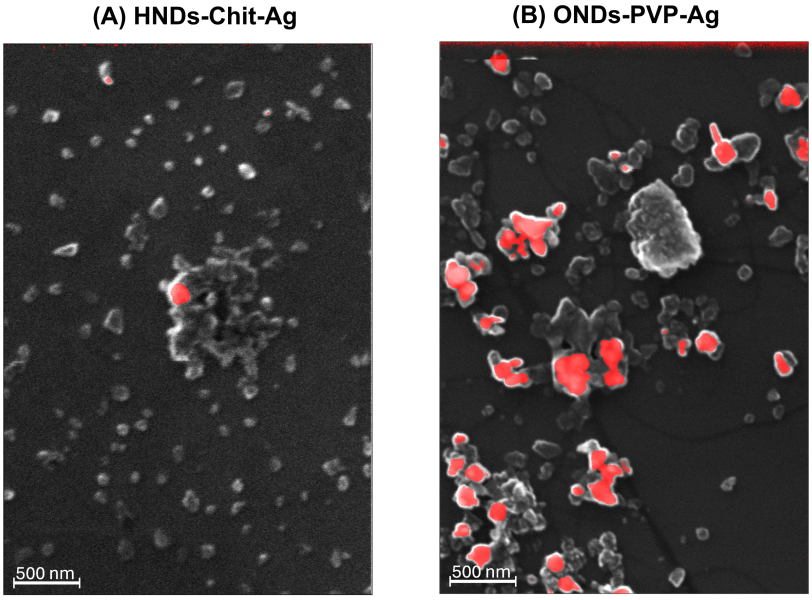

Figure 9.24: Images of directly synthesised nanocomposites from SEM. Images were processed followingly: metal NPs from BSEs were marked red and laid over the image formed by SEs. (A) HNDs-Chit-Ag, (B) ONDs-PVP-Ag

TEM

Due to the evidence of a low number of AgNPs in HNDs-Chit-Ag colloid, Ing. Kateřina Kolářová, Ph.D. from the Institute of Physics was asked to perform transmission electron microscopy (TEM) on the directly synthesised nanocomposites. She provided the images seen in Figure 9.25.

Darker AgNPs in the ONDs-PVP-Ag samples are visibly smaller but more numerous than in HNDs-Chit-Ag, which complements our findings so far. The AgNPs on HNDs also seem to form different shapes than just spherical ones. In contrast, the surface of ONDs contains spherical AgNPs and in a higher density.

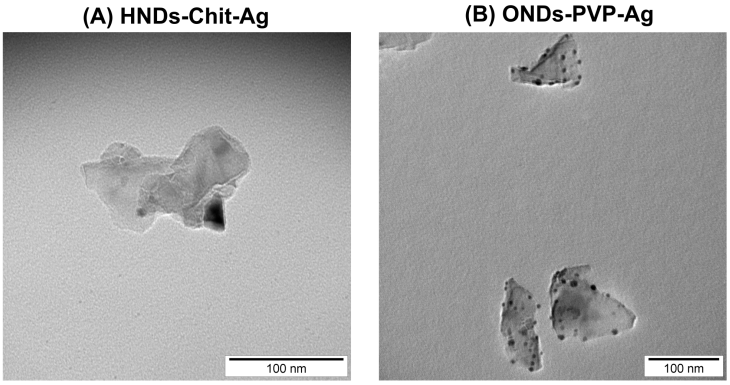

Figure 9.25: Images of synthesised nanocomposites from TEM provided by Ing. Kateřina Kolářová, Ph.D. from the Institute of Physics. (A) HNDs-Chit-Ag, (B) ONDs-PVP-Ag. AgNPs have darker colour compared to NDs.

9.3.4 Discussion

The comparison between colloidal mixtures and directly synthesised nanocomposites of NDs and AgNPs revealed differences in the structure and resulting properties.

Like colloidal mixtures, the directly synthesised nanocomposites followed the Lambert-Beer law. The absorption spectrum of ONDs-PVP-Ag showed a plasmonic peak located at 420 nm, compared to the peak of the AgOND mixture located at 396 nm. This implies that AgNPs should be bigger in ONDs-PVP-Ag than in AgOND. In HNDs-Chit-Ag, the plasmonic peak was not visible in the absorption spectrum, suggesting a low number of AgNP particles compared to the colloidal mixture of AgHNDs. SEM and TEM images confirmed a minimal amount of AgNPs on the surface of HNDs-Chit-Ag. Additionally, there were larger and non-spherical AgNPs present on the surface of NDs in HNDs-Chit-Ag than in ONDs-PVP-Ag which shows that the size and the shape of AgNPs was not controlled during the synthesis process. The variation in the number of AgNPs per ND was evident in the colour of the colloidal solutions as well. ONDs-PVP-Ag had a milky yellow coloration indicating the presence of sufficient amounts of AgNPs. However, HNDs-Chit-Ag had a pure milky grey colour (similar to that of pure ND colloids), which implies a smaller number of AgNPs in the colloid. The difference in the ZP polarity of HNDs-Chit-Ag with a positive sign and AgHNDs with a negative sign may also be caused by the low number of AgNPs in HNDs-Chit-Ag.

The stability of both colloidal mixtures and directly synthesised nanocomposites was negatively impacted by the presence of HNDs. However, both directly synthesised nanocomposites had ZP values indicating stability, contradicting the results of the spectrophotometry stability experiment, which implied instability of both nanocomposites. This shows that the role of ZP magnitude and sign should not be taken as the only determinative factor of stability. In the case of colloidal mixtures, AgHNDs showed instability through their ZP and absorption spectrum over time, and AgONDs were determined stable.

HNDs-Chit-Ag and ONDs-PVP-Ag exhibit an average size around 50 nm and 70 nm, respectively, with no observed free AgNPs out of NDs, contrary to the colloidal mixtures, which contained some free unbound AgNPs.

Considering the complexity and time required for creating the directly synthesised nanocomposites, colloidal mixtures appear to offer better control over particle size since the characteristics of pristine particles are defined beforehand. Moreover, the location of the plasmonic peak of metal NPs in the colloidal mixture is stable allowing better utilization in LSPR applications. The disadvantage of the colloidal mixture is certainly the fact that not all metal NPs attach to NDs and may remain free in the colloid. However, further experiments are needed to fully validate the advantages of colloidal mixture nanocomplexes over directly synthesised nanocomposites.

Chapter 10

Conclusion

This thesis studied the optical absorption of colloidal mixtures of surface modified nanodiamonds (hydrogenated nanodiamonds (HNDs) and oxidized nanodiamonds (ONDs) and plasmonic metal nanoparticles (silver nanoparticles (AgNPs) and gold nanoparticles (AuNPs)). The main parts of this work focused on becoming familiar with the field of nanoparticles and characterization methods, investigating the individual colloids, determining the appropriate ratio for their colloidal mixtures, and observing the optical properties of the mixtures based on their composition within an appropriate time range.

During the measurements, we observed the potential formation of nanocomplexes mainly in colloidal mixtures containing AgNPs. Therefore, these colloidal mixtures were compared with directly synthesized composites of nanodiamonds and silver (ND-Ag) to broaden our understanding of these nanocomplexes.

For studying the optical absorption and stability of colloids, spectrophotometry was performed. Stability was determined based on the average standard deviation of OD at specific time-points from OD at time zero. To meet the stability requirements, the average standard deviation should not exceed the 0.05 threshold determined from the accuracy of the spectrophotometer and considering possible evaporation. This method for stability determination was supported by measurements of zeta potential (ZP). The size distribution was determined through dynamic light scattering (DLS) measurements and the morphology of particles was observed using scanning electron microscopy (SEM).

Optical absorption analyses identified plasmonic peaks of AgNPs and AuNPs at stable wavelengths over various concentrations and showed prominent absorption of nanodiamonds (NDs) mainly in the UV region. Therefore, we assumed that NDs do not contain a considerable amount of NV or other colour centres. All individual colloids followed the Lambert-Beer law at the chosen wavelength of 450 nm except for the HND colloid, which exhibits some deviations from linearity at higher concentrations. HNDs were also determined unstable since the standard deviation of their absorption spectrum exceeded the stability limit at a 5-hour time-point, impacting the stability of all subsequent colloids derived from HNDs (colloidal mixtures and directly synthesized composites). Although, oxidized nanodiamonds (ONDs), AgNPs, and AuNPs were determined stable, all following experiments were performed within the first 5 hours after the preparation considering the agglomeration of HNDs in time.

Colloidal mixtures were prepared by combining ND colloid of a fixed concentration (25 μg/ml) with the four highest concentrations of metal nanoparticles (NPs) starting from their stock concentration (50 μg/ml of AuNPs and 20 μg/ml of AgNPs). In these ratios, the plasmonic peak of the metal NPs was not overshadowed by the absorption of NDs and the OD values were still high enough to gain information from absorption spectra. The investigation of the colloidal mixtures served three primary objectives: establishing an optimal time frame for studying optical phenomena, determining the presence of nanocomplexes, and studying the optical properties of these colloidal mixtures.

Compared to colloidal mixtures with ONDs, the presence of HNDs in the colloidal mixtures negatively affected their stability over a 24-hour period. Consequently, the optical properties of the colloidal mixtures were studied immediately after their preparation to ensure accurate and reliable results.

SEM images of colloidal mixtures showed metal NPs mainly over the surface of NDs. Despite some particles being unattached to ND surfaces, we assume that the metal NPs and NDs indeed form nanocomplexes. The formation of nanocomplexes of metal NPs and HNDs can be attributed to electrostatic attractive forces since they have opposite signs of ZP. However, both ONDs and metal NPs have negative ZP values, hence some force or chemical effect has to overcome the electrostatic repulsion between them. Based on the DLS measurements, nanocomplexes are more readily formed in colloidal mixtures containing AgNPs.

From spectrophotometric measurements, we see that colloidal mixtures adopt the plasmonic peak of their corresponding metal NPs and higher absorption in the UV region attributed to NDs. All colloidal mixtures followed the Lambert-Beer law outside the plasmonic peak region. Furthermore, the plasmonic peak of both types of metal NPs remained at its wavelength in the colloidal mixture, indicating that there was no increase in the size of metal NPs. Therefore, the agglomeration observed from DLS measurements is attributed to NDs. However, the spectra of present NDs and metal NPs did not simply add up and a new effect arose. It was expected that the potential difference between the mixtures would be mostly caused by different surface modifications of NDs and both metal NPs would behave similarly. Instead, we observed opposite behaviours. In colloidal mixtures containing AgNPs, the presence of NDs enhanced the absorption of the plasmonic peak at lower concentrations of AgNPs. However, as their concentration increased, this enhancement of OD faded, and the OD of the colloidal mixtures eventually decreased below that of AgNPs alone, and continued to decrease with increasing concentration. Conversely, colloidal mixtures containing AuNPs exhibited the opposite effect. Initially, the presence of NDs led to a decrease in the absorption of the plasmonic peak compared to pristine AuNPs, but as AuNP concentration increased, the gap between the OD of the colloidal mixture and AuNPs alone decreased.

As there was no observed shift of plasmonic peaks of colloidal mixtures compared to individual metal NP colloids, the optical effect is not influenced by the agglomeration or size change of metal NPs in the colloidal mixture. Additionally, the presence of colour centres, including NV centres, was not observed in the absorption spectra of NDs. Therefore the activity of colour centres in the colloidal mixtures cannot

be behind this effect. This behaviour could potentially be attributed to charge transfer between particles upon interaction which could take place in the colloidal mixtures with electrically conductive HNDs. Electrically resistive ONDs may interact with metal NPs due to polarization. Moreover, the constructive and destructive interference of electromagnetic fields of plasmonic NPs may influence the OD based on changes in concentration of the metal NPs. Other explanations and information about the NP interactions could be revealed through more characterization methods such as atomic force microscopy (AFM) or surface-enhanced Raman spectroscopy (SERS), or by mathematical computing.

To obtain more information about the optical properties of colloidal mixtures and their nanocomplexes, we compared colloidal mixture of silver nanoparticles and hydrogenated nanodiamonds (AgHNDs) and colloidal mixture of silver nanoparticles and oxidized nanodiamonds (AgONDs) (as they seem to contain most nanocomplexes and have more prominent behaviour of the observed optical phenomenon) with directly synthesised nanocomposites (HNDs-Chit-Ag and ONDs-PVP-Ag), derived from the same batch of NDs used for the colloidal mixtures. It was observed that colloidal mixtures provided better control over particle size, shape and distribution compared to directly synthesised nanocomposites since the characteristics of each constituent were defined before mixing. Both directly synthesised nanocomposites followed the Lambert-Beer law. However, the plasmonic peak in the absorption spectra of HNDs-Chit-Ag was completely overshadowed by the absorption of NDs. This was attributed to the lower number of present AgNPs in HNDs-Chit-Ag. In the case of ONDs-PVP-Ag, the peak was visible, but not very prominent and shifted to the longer wavelengths. Additionally, the plasmonic peaks seemed to diminish over time, as seen in the stability measurements. On the other hand, a disadvantage of the colloidal mixtures can be in the presence of free AgNPs, unbound to surfaces of NDs, contrasting with the directly synthesised nanocomposites, which had AgNPs firmly attached to NDs. Given the complexity and time required for creating the directly synthesised nanocomposites, colloidal mixtures may offer an alternative, potentially providing better control over particle size and utilisation of LSPR of metal NPs.

This study not only demonstrated the presence of nanocomplexes formed from NDs and metal NPs in colloidal mixtures but also revealed phenomena regarding their interactions, particularly ones dependent on the concentration of metal NPs. Therefore it would be beneficial to investigate their optical properties, stability and morphology for more concentration ratios of these colloidal mixtures and study the very causes of the formation of the nanocomplexes.

Bibliography

[1] S. M. Taghavi, M. Momenpour, M. Azarian, M. Ahmadian, F. Souri, S. A. Taghavi, M. Sadeghain, and M. Karchani, "Effects of nanoparticles on the environment and outdoor workplaces.," *Electronic physician*, vol. 5, pp. 706–12, Oct-Dec 2013.

[2] I. Khan, K. Saeed, and I. Khan, "Nanoparticles: Properties, applications and toxicities," *Arabian Journal of Chemistry*, vol. 12, no. 7, pp. 908–931, 2019.

[3] V. Mody, R. Siwale, A. Singh, and H. Mody, "Introduction to metallic nanoparticles," *Journal of Pharmacy And Bioallied Sciences*, vol. 2, no. 4, p. 282, 2010.

[4] E. A. Kumah, R. D. Fopa, S. Harati, P. Boadu, F. V. Zohoori, and T. Pak, "Human and environmental impacts of nanoparticles: a scoping review of the current literature," *BMC Public Health*, vol. 23, no. 1, p. 1059, 2023.

[5] H. M. Abuzeid, C. M. Julien, L. Zhu, and A. M. Hashem, "Green synthesis of nanoparticles and their energy storage, environmental, and biomedical applications," *Crystals*, vol. 13, no. 11, 2023.

[6] X. Hu, Y. Zhang, T. Ding, J. Liu, and H. Zhao, "Multifunctional gold nanoparticles: A novel nanomaterial for various medical applications and biological activities," *Frontiers in Bioengineering and Biotechnology*, vol. 8, 2020.

[7] X.-F. Zhang, Z.-G. Liu, W. Shen, and S. Gurunathan, "Silver nanoparticles: Synthesis, characterization, properties, applications, and therapeutic approaches," *International Journal of Molecular Sciences*, vol. 17, no. 9, 2016.

[8] M. A. Hassaan, M. A. El-Nemr, M. R. Elkatory, S. Ragab, V.-C. Niculescu, and A. El Nemr, "Principles of photocatalysts and their different applications: A review.," *Topics in current chemistry (Cham)*, vol. 381, p. 31, Oct 2023.

[9] C. Pfeiffer, C. Rehbock, D. Hühn, C. Carrillo-Carrion, D. J. de Aberasturi, V. Merk, S. Barcikowski, and W. J. Parak, "Interaction of colloidal nanoparticles with their local environment: the (ionic) nanoenvironment around nanoparticles is different from bulk and determines the physico-chemical properties of the nanoparticles.," *Journal of the Royal Society, Interface*, vol. 11, p. 20130931, Jul 2014.

[10] Y. Dahman, H. Javaheri, J. Chen, and B. AlChikh-Sulaiman, "Chapter 5 - nanoparticles," in *Nanotechnology and Functional Materials for Engineers* (Y. Dahman, ed.), Micro and Nano Technologies, pp. 93–119, Elsevier, 2017.

[11] M. A. Hayat, Y. Chen, M. Bevilacqua, L. Li, and Y. Yang, "Characteristics and potential applications of nano-enhanced phase change materials: A critical review on recent developments," *Sustainable Energy Technologies and Assessments*, vol. 50, p. 101799, 2022.

[12] K. L. Kelly, E. Coronado, L. L. Zhao, and G. C. Schatz, "The optical properties of metal nanoparticles: the influence of size, shape, and dielectric environment," *The Journal of Physical Chemistry B*, vol. 107, no. 3, pp. 668–677, 2003.

[13] S. Orlanducci, "Gold-decorated nanodiamonds: Powerful multifunctional materials for sensing, imaging, diagnostics, and therapy," *European Journal of Inorganic Chemistry*, vol. 2018, no. 48, pp. 5138–5145, 2018.

[14] Y.-S. Borghei, S. Hosseinkhani, and M. R. Ganjali, ""plasmonic nanomaterials": An emerging avenue in biomedical and biomedical engineering opportunities," *Journal of Advanced Research*, vol. 39, pp. 61–71, 2022.

[15] S. T. Galatage, A. S. Hebalkar, S. V. Dhobale, O. R. Mali, P. S. Kumbhar, S. V. Nikade, and S. G. Killedar, "Silver nanoparticles: Properties, synthesis, characterization, applications and future trends," in *Silver Micro-Nanoparticles* (S. Kumar, P. Kumar, and C. S. Pathak, eds.), ch. 4, Rijeka: IntechOpen, 2021.

[16] I. Hammami, N. M. Alabdallah, A. A. jomaa, and M. kamoun, "Gold nanoparticles: Synthesis properties and applications," *Journal of King Saud University - Science*, vol. 33, no. 7, p. 101560, 2021.

[17] J. Milan, K. Niemczyk, and M. Kus-Liśkiewicz, "Treasure on the earth—gold nanoparticles and their biomedical applications," *Materials*, vol. 15, no. 9, 2022.

[18] S. Chauhan, N. Jain, and U. Nagaich, "Nanodiamonds with powerful ability for drug delivery and biomedical applications: Recent updates on in vivo study and patents.," *Journal of pharmaceutical analysis*, vol. 10, pp. 1–12, Feb 2020.

[19] J.-X. Qin, X.-G. Yang, C.-F. Lv, Y.-Z. Li, K.-K. Liu, J.-H. Zang, X. Yang, L. Dong, and C.-X. Shan, "Nanodiamonds: Synthesis, properties, and applications in nanomedicine," *Materials & Design*, vol. 210, p. 110091, 2021.

[20] A. Thekkedath and K. Sridharan, "Nanodiamonds and its applications," in *Applications and Use of Diamond* (G. (David), ed.), ch. 3, Rijeka: IntechOpen, 2022.

[21] S. Stehlik, M. Mermoux, B. Schummer, O. Vanek, K. Kolarova, P. Stenclova, A. Vlk, M. Ledinsky, R. Pfeifer, O. Romanyuk, I. Gordeev, F. Roussel-Dherbey, Z. Nemeckova, J. Henych, P. Bezdicka, A. Kromka, and B. Rezek, "Size effects on surface chemistry and raman spectra of sub-5 nm oxidized high-pressure high-temperature and detonation nanodiamonds," *The Journal of Physical Chemistry C*, vol. 125, no. 10, pp. 5647–5669, 2021.

[22] R. Kaur and I. Badea, "Nanodiamonds as novel nanomaterials for biomedical applications: drug delivery and imaging systems.," *International journal of nanomedicine*, vol. 8, pp. 203–20, 2013.

[23] K. Kolarova, I. Bydzovska, O. Romanyuk, E. Shagieva, E. Ukraintsev, A. Kromka, B. Rezek, and S. Stehlik, "Hydrogenation of hpht nanodiamonds and their nanoscale interaction with chitosan," *Diamond and Related Materials*, vol. 134, p. 109754, 2023.

[24] V. Mochalin, O. Shenderova, D. Ho, and Y. Gogotsi, ""the properties and applications of nanodiamonds,"," *Nature nanotechnology*, vol. 7, pp. 11–23, 12 2011.

[25] I. I. Nikonova, V. F. Shkodich, N. E. Temnikova, M. V. Kolpakova, and O. V. Stoyanov, "Phenol-formaldehyde oligomers modified with carbon nanoparticles and their use in adhesives and prepregs," *Polymer Science, Series D*, vol. 14, no. 4, pp. 471–476, 2021.

[26] L. Basso, M. Cazzanelli, M. Orlandi, and A. Miotello, "Nanodiamonds: Synthesis and application in sensing, catalysis, and the possible connection with some processes occurring in space," *Applied Sciences*, vol. 10, no. 12, 2020.

[27] S. Stehlik, M. Varga, M. Ledinsky, V. Jirasek, A. Artemenko, H. Kozak, L. Ondic, V. Skakalova, G. Argentero, T. Pennycook, J. C. Meyer, A. Fejfar, A. Kromka, and B. Rezek, "Size and purity control of hpht nanodiamonds down to 1 nm," *The Journal of Physical Chemistry C*, vol. 119, no. 49, pp. 27708–27720, 2015. PMID: 26691647.

[28] S. Stehlik, O. Szabo, E. Shagieva, D. Miliaieva, A. Kromka, Z. Nemeckova, J. Henych, J. Kozempel, E. Ekimov, and B. Rezek, "Electrical and colloidal properties of hydrogenated nanodiamonds: Effects of structure, composition and size," *Carbon Trends*, vol. 14, p. 100327, 2024.

[29] K. Kolarova, D. Miliaieva, and S. Stehlik, "Polyvinylpyrrolidone coating fornanodiamond stabilization in saline solution and silver nanoparticle decoration," *in NANOCON 2020, 12th International Conference on Nanomaterials - Research & Application*, Dec. 2020.

[30] D. Miliaieva, A. S. Djoumessi, J. Čermák, K. Kolářová, M. Schaal, F. Otto, E. Shagieva, O. Romanyuk, J. Pangrác, J. Kuliček, V. Nádaždy, S. Stehlík, A. Kromka, H. Hoppe, and B. Rezek, "Absolute energy levels in nanodiamonds of different origins and surface chemistries," *Nanoscale Adv.*, vol. 5, pp. 4402–4414, 2023.

[31] J. Arnault and H. Girard, "Hydrogenated nanodiamonds: Synthesis and surface properties," *Current Opinion in Solid State and Materials Science*, vol. 21, no. 1, pp. 10–16, 2017. Nanodiamond Science and Technology.

[32] B. Woodhams, L. Ansel-Bollepalli, J. Surmacki, H. Knowles, L. Maggini, M. De Volder, M. Atatüre, and S. Bohndiek, "Graphitic and oxidised high

pressure high temperature (hpht) nanodiamonds induce differential biological responses in breast cancer cell lines," *Nanoscale*, vol. 10, 06 2018.

[33] T. Xu, L. Wu, Y. Yu, W. Li, and J. Zhi, "Synthesis and characterization of diamond–silver composite with anti-bacterial property," *Materials Letters*, vol. 114, pp. 92–95, 2014.

[34] M. Sen, "Nanocomposite materials," in *Nanotechnology and the Environment* (M. Sen, ed.), ch. 6, Rijeka: IntechOpen, 2020.

[35] D. Lee, S. H. Jeong, and E. Kang, "Nanodiamond/gold nanorod nanocomposites with tunable light-absorptive and local plasmonic properties," *Journal of Industrial and Engineering Chemistry*, vol. 65, pp. 205–212, 2018.

[36] Y.-C. Lin, E. Perevedentseva, Z.-R. Lin, C.-C. Chang, H.-H. Chen, S.-M. Yang, M.-D. Lin, A. Karmenyan, G. Speranza, L. Minati, C. Nebel, and C.-L. Cheng, "Multimodal bioimaging using nanodiamond and gold hybrid nanoparticles," *Scientific Reports*, vol. 12, no. 1, p. 5331, 2022.

[37] Z. Wang, F. Zhang, A. Ning, D. Lv, G. Jiang, and A. Song, "Nanosilver supported on inert nano-diamond as a direct plasmonic photocatalyst for degradation of methyl blue," *Journal of Environmental Chemical Engineering*, vol. 9, no. 1, p. 104912, 2021.

[38] L.-X. Su, Q. Lou, C.-X. Shan, D.-L. Chen, J.-H. Zang, and L.-J. Liu, "Ag/nanodiamond/g-c3n4 heterostructures with enhanced visible-light photocatalytic performance," *Applied Surface Science*, vol. 525, p. 146576, 2020.

[39] L. Liang, P. Zheng, S. Jia, K. Ray, Y. Chen, and I. Barman, "Plasmonic nanodiamonds," *Nano Letters*, vol. 23, no. 12, pp. 5746–5754, 2023. PMID: 37289011.

[40] Y. Akinay, U. Gunes, B. Çolak, and T. Cetin, "Recent progress of electromagnetic wave absorbers: A systematic review and bibliometric approach," *ChemPhysMater*, vol. 2, no. 3, pp. 197–206, 2023.

[41] H.-A. Kim, J.-K. Seo, T. Kim, and B.-T. Lee, "Nanometrology and its perspectives in environmental research," *Environmental health and toxicology*, vol. 29, 10 2014.

[42] M. L.C. Passos and M. L. M.F.S. Saraiva, "Detection in uv-visible spectrophotometry: Detectors, detection systems, and detection strategies," *Measurement*, vol. 135, pp. 896–904, 2019.

[43] L. Usoltseva, D. Volkov, D. Nedosekin, M. Korobov, M. Proskurnin, and V. Zharov, "Absorption spectra of nanodiamond aqueous dispersions by optical absorption and optoacoustic spectroscopies," *Photoacoustics*, vol. 12, pp. 55–66, 2018.

[44] Agilent, *BioTek Epoch 2 Microplate Spectrophotometer*, 2024.

[45] S. Bhattacharjee, "Dls and zeta potential – what they are and what they are not?," *Journal of Controlled Release*, vol. 235, pp. 337–351, 2016.

[46] Malvern Instruments Ltd. 2013, *Zetasizer Nano User Manual (Man0485-1.1)*, 2013.

[47] A. P. Ferreyra Maillard, J. C. Espeche, P. Maturana, A. C. Cutro, and A. Hollmann, "Zeta potential beyond materials science: Applications to bacterial systems and to the development of novel antimicrobials," *Biochimica et Biophysica Acta (BBA) - Biomembranes*, vol. 1863, no. 6, p. 183597, 2021.

[48] D. Rutherford, K. Kolářová, J. Čech, P. Haušild, J. Kuliček, E. Ukraintsev, Štěpán Stehlík, R. Dao, J. Neuman, and B. Rezek, "Correlative atomic force microscopy and scanning electron microscopy of bacteria-diamond-metal nanocomposites," *Ultramicroscopy*, vol. 258, p. 113909, 2024.

[49] D. Koga, S. Kusumi, M. Shibata, and T. Watanabe, "Applications of scanning electron microscopy using secondary and backscattered electron signals in neural structure," *Frontiers in Neuroanatomy*, vol. 15, 2021.

[50] NanoScience Instruments, *What is Scanning Electron Microscopy?*, 2024.

[51] D. Nečas and P. Klapetek, "Gwyddion: an open-source software for spm data analysis," *Open Physics*, vol. 10, Jan. 2012.

[52] H. Gonome, "Interference effect of localized surface plasmon resonance on radiative properties of plasmonic particle clusters in 3d assemblies," *Journal of Quantitative Spectroscopy and Radiative Transfer*, vol. 230, pp. 13–23, 2019.

Appendices

Appendix A

Laboratory Equipment, Scientific Instruments and Their Operators

- EPOCH2 Gen5 Microplate Reader,BioTek ..... Vendula Hrnčířová
- EVO SEM, ZEISS ..... Ing. Markéta Šlapal Bařinková, Vendula Hrnčířová
- Sonorex Digitec DT 31 Ultrasonic Bath, Bandelin ..... Vendula Hrnčířová
- Zetasizer Nano Series, Malvern ..... Vendula Hrnčířová
- MPT-2 AutoTitrator, Malvern ..... Ing. Markéta Šlapal Bařinková
- KL 2500 LED Fiber Optic Light Source, SCHOTT ..... Vendula Hrnčířová
- Tecnai G2 20 TEM, FEI ..... Ing. Kateřina Kolářová, Ph.D., FZU
- Incubator, Memmert ..... Vendula Hrnčířová
- Transillumination Panel, Reflecta ..... Vendula Hrnčířová

Appendix B

Materials

- HPLC grade water ..... ROTH
- Silver colloid ..... Sigma-Aldrich
- Gold colloid ..... BBI Solutions
- MSY HTHP Nanodiamonds ..... Pureon
- Hydrogenated Nanodiamonds ..... Ing. Kateřina Kolářová, Ph.D., FZU
- Oxidized Nanodiamonds ..... Ing. Kateřina Kolářová, Ph.D., FZU
- HNDs-Chit-Ag Nanocomposite ..... Ing. Kateřina Kolářová, Ph.D., FZU
- ONDs-PVP-Ag Nanocomposite ..... Ing. Kateřina Kolářová, Ph.D. FZU

Appendix C

Software

- Citation ..... JabRef
- Online LaTex Editor ..... Overleaf
- Translator ..... Seznam.cz Slovník
- Linguistic Adjustment ..... Grammarly
- Data Analysis ..... MATLAB R2023a, MathWorks
- Data Analysis ..... Microsoft Excel
- Data Analysis ..... Gen5 3.08, BioTek
- Graphic Design ..... Inkscape

Appendix D

Additional Graphs

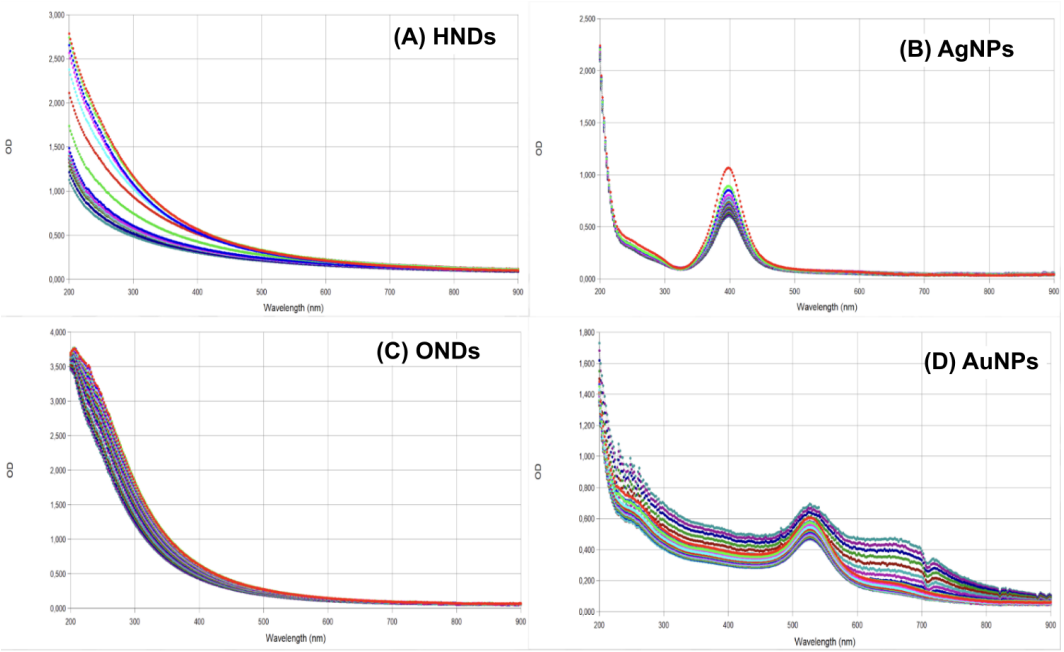

Figure D.1: Changes in absorbance spectra attributed to evaporation of samples in a 24-hour period at 37 °C.

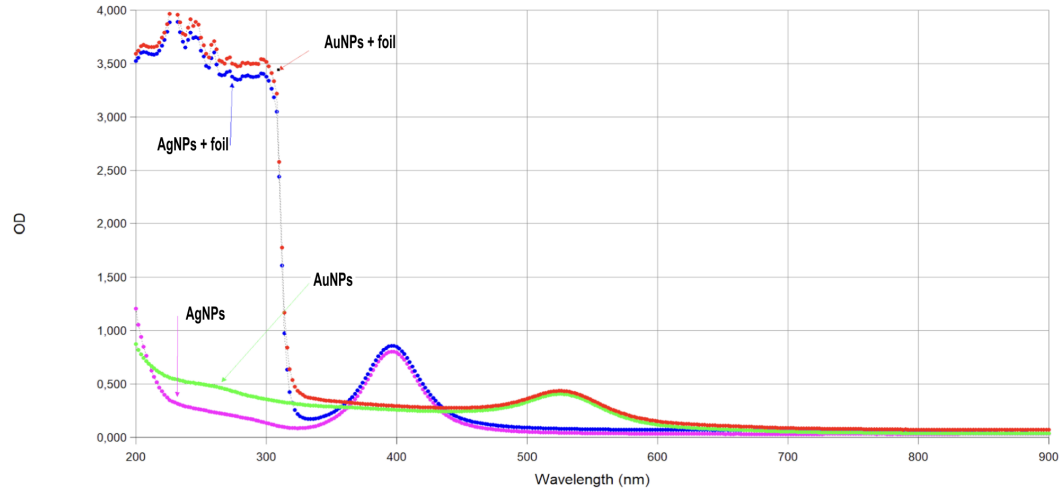

Figure D.2: Alteration of absorbance spectra in the UV region, when a plastic foil was used to prevent the evaporation of samples.

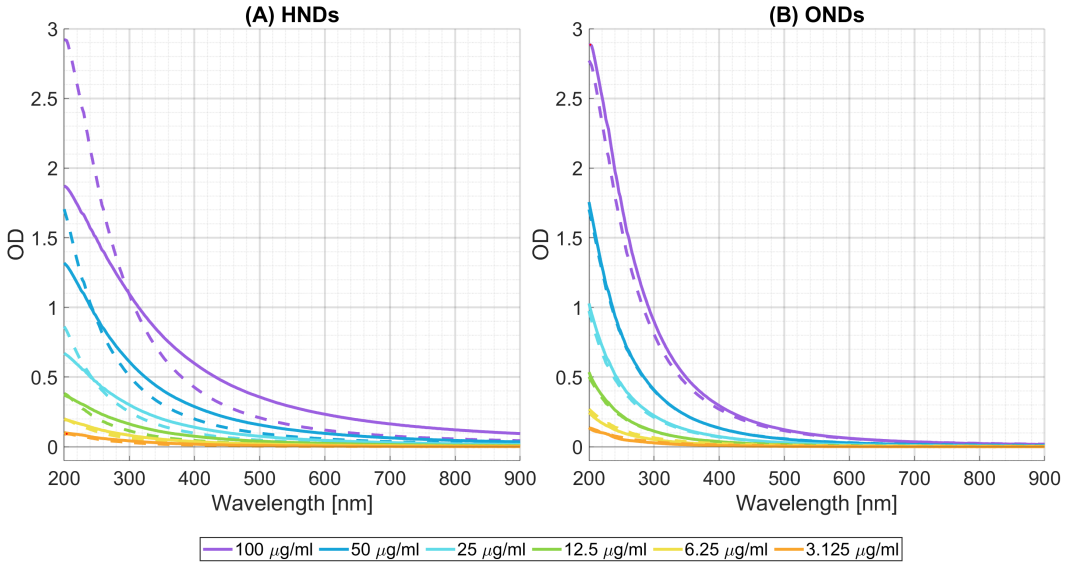

Figure D.3: Absorbance spectra of two batches of NDs. (A) HNDs, (B) ONDs. The full lines represent the spectra of the first batch from 27.7.2023 (absorption measured approximately four months after the synthesis - in November), while the dashed lines represent the spectra of the second batch prepared on 9.1.2024 (absorption measured a few days after preparation). OD values are blank corrected.

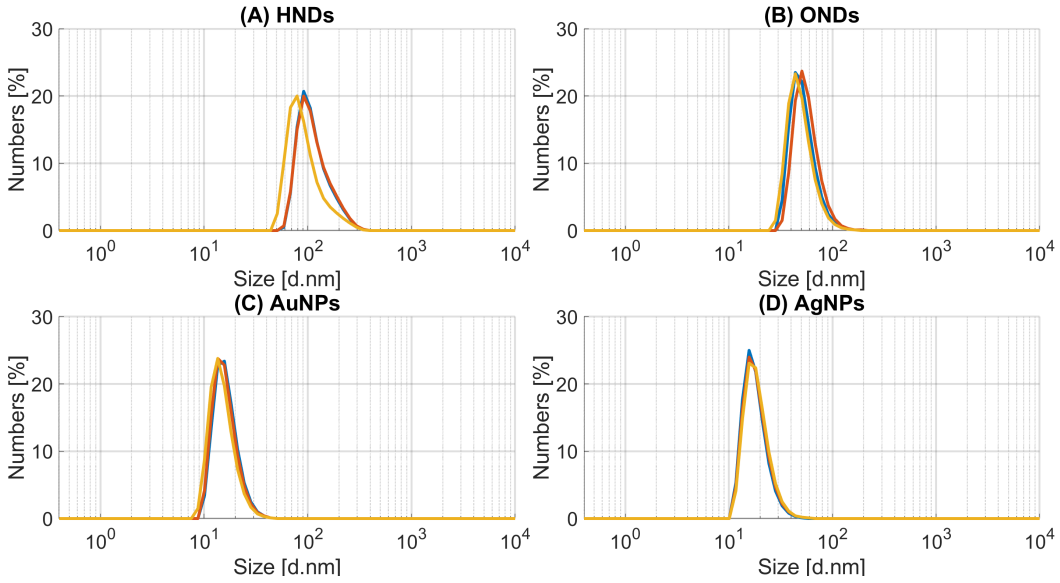

Figure D.4: Number distribution of DLS particle sizes in the colloid of (A) HND (25 μg/ml), (B) OND (25 μg/ml), (C) AuNP (6.25 μg/ml), (D) AgNP (2.5 μg/ml).

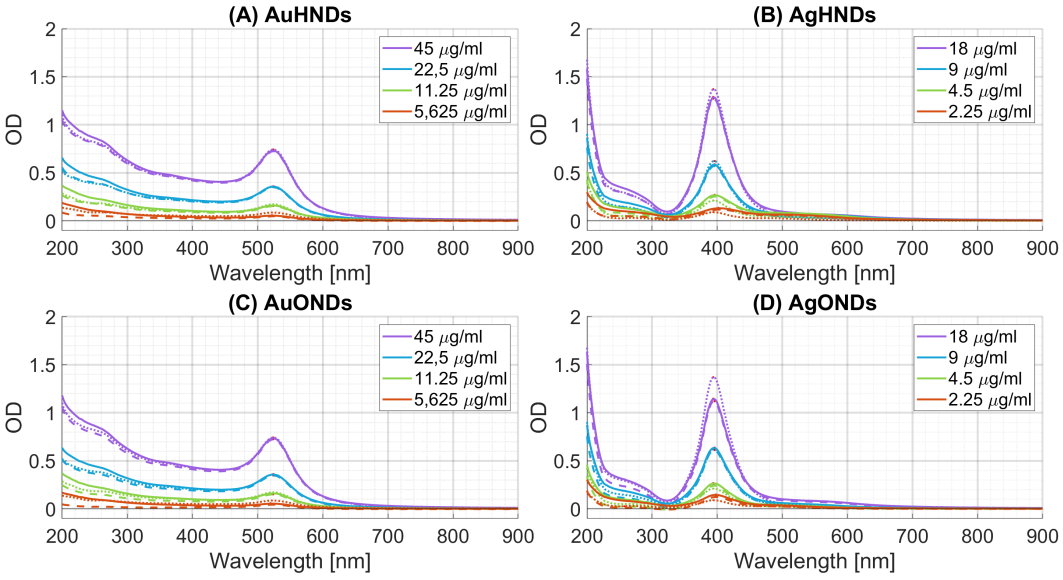

Figure D.5: Optical absorption of colloidal mixtures of metal NPs and NDs: (A) AuHNDs, (B) AgHNDs, (C) AuONDs, (D) AgONDs. The concentration of NDs is fixed at 6.25 μg/ml, and the concentrations of metal NPs are provided in the legends. The full lines represent the optical spectra of colloidal mixtures, the dashed lines the colloidal mixtures with subtracted ND spectra and the dotted lines the spectra of the metal NP. Mean OD values of triplicates are blank corrected.

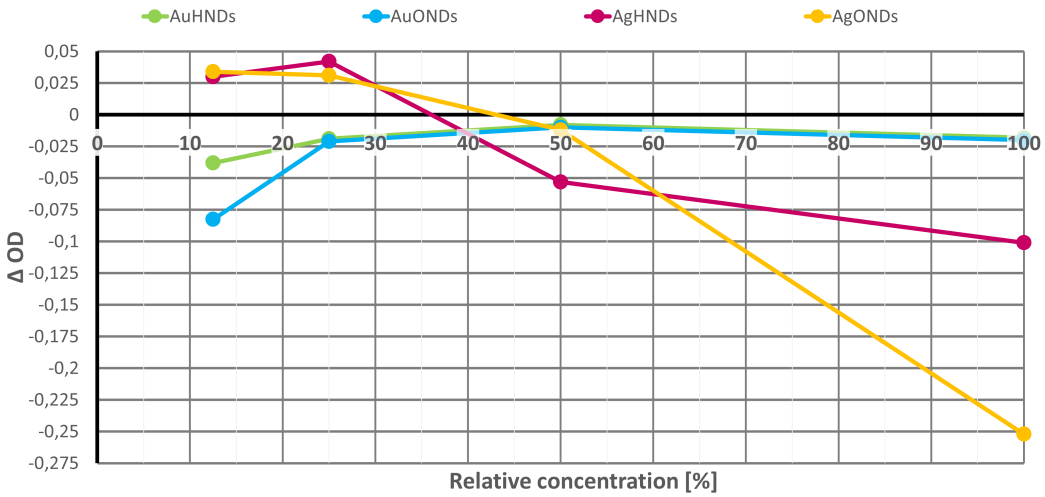

Figure D.6: Deviations of the plasmonic peak OD of colloidal mixtures after subtraction of 6.25 μg/ml ND spectra from the OD of pristine metal NP colloids depending on the relative concentration of metal NPs, represented in percentage of maximum values.

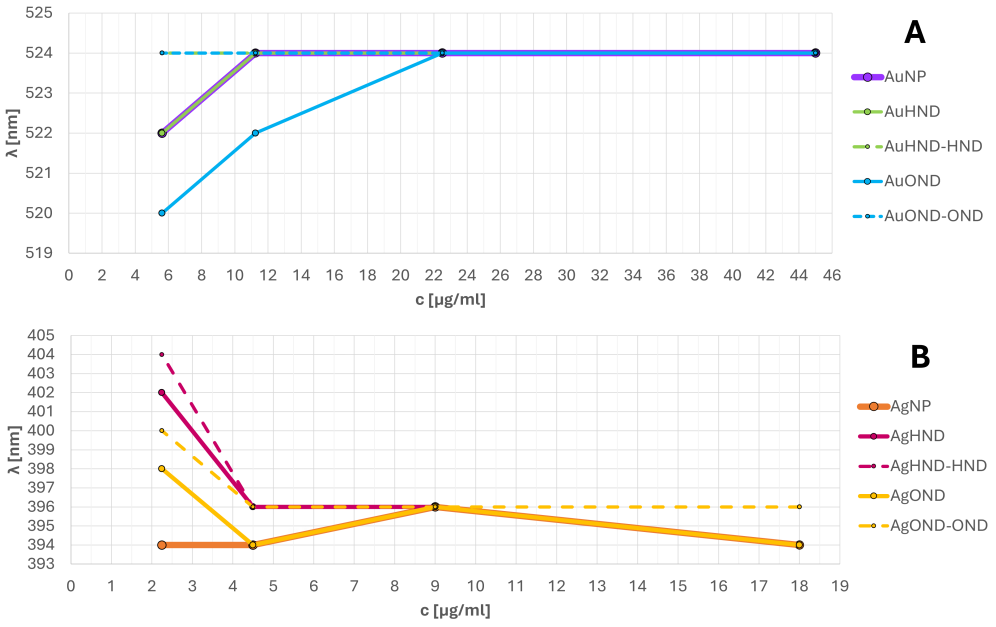

Figure D.7: Dependence of plasmonic peak location of colloidal mixtures (with ND concentration fixed at 6.25 μg/ml) on the concentration of metal NPs. (A) colloidal mixture containing AuNPs, and (B) AgNPs. Dashed lines represent spectrum of colloidal mixtures after subtraction of ND spectrum

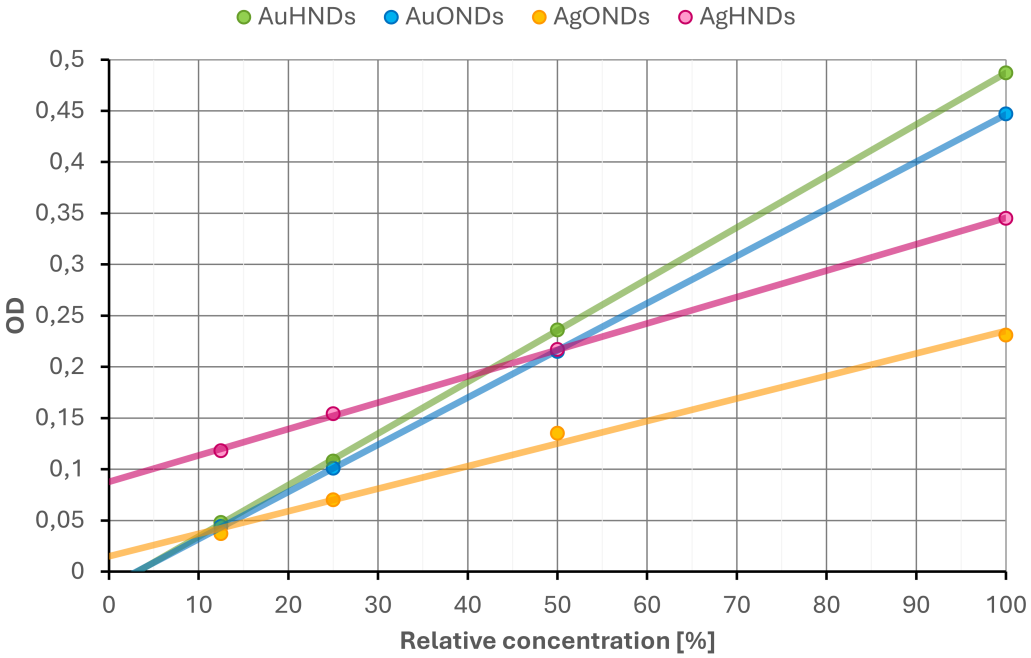

Figure D.8: Lambert-Beer law verification of the colloidal mixtures with OD measured at a wavelength of 450 nm. The horizontal axis is expressed as a percentage of the starting concentration of the NP present in the mixture. Points represent measured samples and full lines are linear trend lines of the corresponding colloidal mixtures. The concentration of NDs is 25 μg/ml.

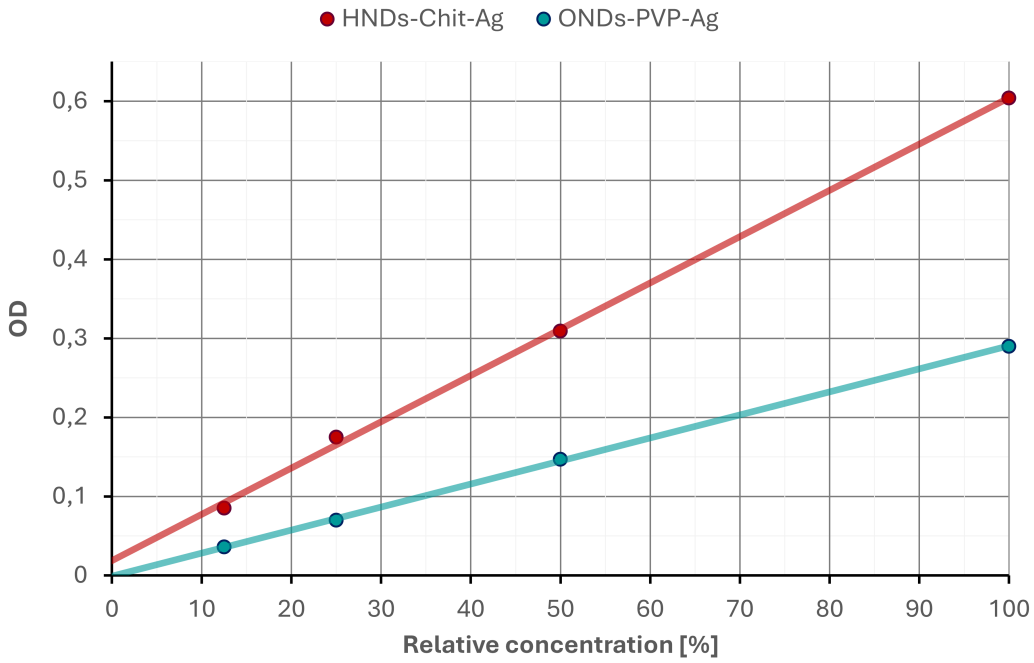

Figure D.9: Lambert-Beer law verification on the directly synthesized nanocomposites with OD measured at a wavelength of 450 nm. The horizontal axis is expressed as a percentage of the starting concentration. Points represent measured samples and full lines are linear trend lines of the corresponding directly synthesized nanocomposites.

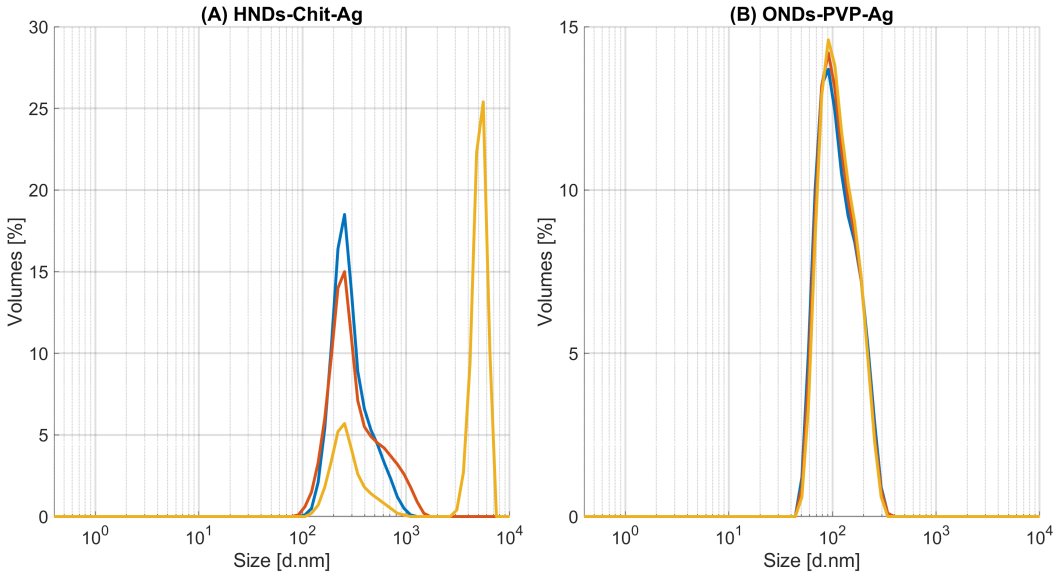

Figure D.10: Volume distribution of particle size of directly synthesised nanocomposites from DLS measurement, (A) HNDs-Chit-Ag, (B) ONDs-PVP-Ag, with an approximate ND concentration of 25 μg/ml.